

Long-Time Asymptotics for the Focusing Nonlinear Schrödinger Equation with Nonzero Boundary Conditions in the Presence of a Discrete Spectrum

Gino Biondini¹, Sitai Li², Dionyssios Mantzavinos³

- Department of Mathematics, State University of New York, Buffalo, NY 14260, USA. E-mail: biondini@buffalo.edu
- Department of Mathematics, University of Michigan, Ann Arbor, MI 48109, USA. E-mail: sitaili@umich.edu
 Department of Mathematics, University of Kansas, Lawrence, KS 66045, USA. E-mail: mantzavinos@ku.edu

Received: 18 September 2019 / Accepted: 15 January 2021 Published online: 9 March 2021 – © The Author(s), under exclusive licence to Springer-Verlag GmbH, DE part of Springer Nature 2021

Abstract: The long-time asymptotic behavior of solutions to the focusing nonlinear Schrödinger (NLS) equation on the line with symmetric, nonzero boundary conditions at infinity is studied in the case of initial conditions that allow for the presence of discrete spectrum. The results of the analysis provide the first rigorous characterization of the nonlinear interactions between solitons and the coherent oscillating structures produced by localized perturbations in a modulationally unstable medium. The study makes crucial use of the inverse scattering transform for the focusing NLS equation with nonzero boundary conditions, as well as of the nonlinear steepest descent method of Deift and Zhou for oscillatory Riemann-Hilbert problems. Previously, it was shown that in the absence of discrete spectrum the xt-plane decomposes asymptotically in time into two types of regions: a left far-field region and a right far-field region, where to leading order the solution equals the condition at infinity up to a phase shift, and a central region where the asymptotic behavior is described by slowly modulated periodic oscillations. Here, it is shown that in the presence of a conjugate pair of discrete eigenvalues in the spectrum a similar coherent oscillatory structure emerges but, in addition, three different interaction outcomes can arise depending on the precise location of the eigenvalues: (i) soliton transmission, (ii) soliton trapping, and (iii) a mixed regime in which the soliton transmission or trapping is accompanied by the formation of an additional, nondispersive localized structure akin to a soliton-generated wake. The soliton-induced position and phase shifts of the oscillatory structure are computed, and the analytical results are validated by a set of accurate numerical simulations.

1. Introduction

In this work, we characterize the long-time asymptotic behavior of solutions to the focusing nonlinear Schrödinger (NLS) equation formulated on the line with symmetric, nonzero boundary conditions at infinity and initial conditions that allow for the presence

of discrete spectrum. Specifically, we consider the initial value problem (IVP)

$$iq_t + q_{xx} + 2|q|^2 q = 0,$$
 $x \in \mathbb{R}, \ t > 0,$ (1.1a)

$$q(x,0) = f(x), x \in \mathbb{R}, (1.1b)$$

$$\lim_{x \to \pm \infty} q(x, t) = q_{\pm} e^{2iq_o^2 t}, \qquad t \geqslant 0,$$
 (1.1c)

where q_{\pm} are complex constants such that

$$|q_{\pm}| = q_o > 0, \tag{1.2}$$

and the initial datum f(x) generates a conjugate pair of discrete eigenvalues in the spectrum (as discussed in detail in Sect. 3). The nonzero boundary conditions (1.1c) are referred to as *symmetric* and imply that the initial datum also tends to nonzero values at infinity: $\lim_{x\to+\infty} f(x) = q_+$. In particular, throughout this work we assume that

$$e^{\pm q_0 x} (f - q_\pm) \in L^1(\mathbb{R}_\pm)$$
 (1.3)

with $L^1(\mathbb{R}_\pm)$ denoting the spaces of Lebesgue integrable functions over \mathbb{R}_\pm . This is a standard assumption when the long-time asymptotic analysis is performed via inverse scattering transform techniques. Well-posedness results for IVP (1.1) with rough initial data are available via harmonic analysis techniques, e.g. see the recent work [Mu] by Muñoz where local well-posedness is shown in Sobolev spaces H^s with $s > \frac{1}{2}$.

The boundary conditions (1.1c) motivate the transformation

$$q(x,t) \longmapsto q(x,t)e^{2iq_o^2t},$$
 (1.4)

which turns IVP (1.1) into the convenient form

$$iq_t + q_{xx} + 2(|q|^2 - q_o^2)q = 0,$$
 $x \in \mathbb{R}, t > 0,$ (1.5a)

$$q(x,0) = f(x), x \in \mathbb{R}, (1.5b)$$

$$\lim_{x \to +\infty} q(x, t) = q_{\pm}, \qquad t \geqslant 0, \tag{1.5c}$$

where importantly, the boundary conditions at infinity are now independent of time.

The focusing NLS equation (1.5a) is a prime example of a completely integrable system [ZS,AS]. As such, it can be written in the form of the compatibility condition $X_t - T_x + [X, T] = 0$ of the Lax pair

$$\Psi_x = X\Psi, \quad \Psi_t = T\Psi, \tag{1.6}$$

where $\Psi = \Psi(x, t, k)$ is a 2 × 2 matrix-valued function and

$$X = ik\sigma_3 + Q$$
, $T = -2ik^2\sigma_3 + i\sigma_3(Q_x - Q^2 - q_o^2I) - 2kQ$ (1.7)

with $k \in \mathbb{C}$ and

$$\sigma_3 = \begin{pmatrix} 1 & 0 \\ 0 & -1 \end{pmatrix}, \quad Q = \begin{pmatrix} 0 & q \\ -\bar{q} & 0 \end{pmatrix}.$$
 (1.8)

The Lax pair (1.6) can be used to analyze IVP (1.5) by means of the celebrated inverse scattering transform. For rapidly vanishing initial conditions, in which case $q_o = 0$, this task was accomplished by Zakharov and Shabat in 1972 [ZS]. For nonvanishing initial

conditions, however, which is the case relevant to the problem considered here, only partial results were available (e.g., [Ma]) until the recent work by Kovačič and the first author [BK]. There, the authors were able to develop the complete inverse scattering transform formalism for IVP (1.5) and, in particular, to associate its solution to that of a matrix Riemann–Hilbert problem. The work was then extended to asymmetric and one-sided boundary conditions in [DPVV] and [PV], respectively.

The results of [BK] provide a starting point for the *rigorous* analysis of the long-time asymptotic behavior of the solution of IVP (1.5). This task is far from trivial due to the fact that, in the case of nonvanishing initial conditions, the focusing NLS equation exhibits *modulational instability* (also known as Benjamin–Feir instability [BF]), namely, the instability of a constant background with respect to long-wavelength perturbations [ZO].

For example, in the special case of constant initial data $f(x) = q_o$ it is straightforward to verify that problem (1.5) admits the constant solution $q(x,t) = q_o$. Seeking a solution of (1.5) in the form of the localized perturbation $q(x,t) = q_o \left[1 + \varepsilon v(x,t)\right]$ with v = O(1) and $\varepsilon \ll 1$ yields to $O(\varepsilon)$ a linear equation with zero conditions at infinity, which can therefore be solved explicitly via Fourier transform. The associated dispersion relation is $\omega = k\sqrt{k^2 - 4q_o^2}$, which becomes purely imaginary for small wavenumbers (i.e. long wavelengths) characterized by $|k| < 2q_o$. Hence, v grows exponentially as $t \to \infty$, indicating instability. But, of course, the linearization becomes invalid once v grows to $O(\varepsilon^{-1})$. The question of what happens to the solution of the focusing NLS equation beyond this point is referred to as the nonlinear stage of modulational instability.

Despite interesting results concerning the behavior of solutions with periodic boundary conditions [AK,FL,TW], the nonlinear stage of modulational instability for the focusing NLS equation on the infinite line remained essentially open for more than fifty years. Recently, it was conjectured in [ZG,GZ] that the nonlinear stage of modulational instability is governed by the formation of certain breather pairs termed "super-regular solitons". However, this conjecture was disproved in [BF], where it was shown that solitons are not generically the main vehicle for the modulational instability; instead, the signature of the instability in the inverse scattering transform lies in the portion of the continuous spectrum associated with the nonlinearization of the unstable Fourier modes and manifests itself via exponentially growing jumps in the Riemann–Hilbert problem. The problem was then settled in [BM1,BM2]. First, the inverse scattering transform formalism of [BK] was suitably modified to yield a Riemann-Hilbert problem convenient for carrying out a long-time asymptotic analysis. The asymptotic behavior of the solutions of this Riemann-Hilbert problem was then studied using the Deift-Zhou nonlinear steepest descent method [DZ1,DZ2] and borrowing ideas from [BKS,BV,JM]. Eventually, it was shown in [BM2] that the solution of IVP (1.5) remains bounded at all times and, more specifically, at leading order it takes on the following asymptotic forms (see Fig. 2):

- (i) For $|x| > 4\sqrt{2}q_o t$, the solution is described by two plane waves, one for x < 0 and one for x > 0, whose amplitudes are equal to the "boundary data" q_- and q_+ respectively;
- (ii) For $|x| < 4\sqrt{2}q_o t$, the solution is described by slowly modulated periodic oscillations whose amplitude is given in terms of the well-known Jacobi elliptic snoidal solution of focusing NLS.

Importantly, in both of the above regions the spatial structure of the leading-order asymptotics is independent of the initial datum f. That is, within the class of initial data (1.3), generic localized perturbations of a constant background display the same

long-time behavior in *all* modulationally unstable media governed by the focusing NLS equation on the infinite line. In this sense, the results of [BM2] demonstrate that the asymptotic state of the nonlinear stage of modulational instability is *universal*. These analytical predictions were recently confirmed, and the resulting behavior was observed, in optical fiber experiments [KSER]. Moreover, it was shown in [BLMT] that this behavior is not limited to the focusing NLS equation, but instead it is a common feature of more general NLS-type systems. In this regard, we note that the focusing semilinear Schrödinger equation with power nonlinearity (which is not integrable besides the cubic case) and nonzero boundary conditions at infinity with perturbations in Sobolev spaces was recently studied via harmonic analysis techniques [Mu].

However, the analysis of [BM2] was carried out for initial data (1.3) such that *no discrete spectrum is present* in the Riemann–Hilbert problem emerging from the inverse scattering transform. This is a major assumption at the technical level (as will become evident while the analysis unfolds in the forthcoming sections) but, more importantly, a significant restriction from a physical point of view since, as is well-known, discrete spectrum is the mechanism generating *solitons*. Hence, in the case of IVP (1.5), an empty discrete spectrum excludes the possibility of describing solutions that contain solitons.

In this work, we perform the long-time asymptotic analysis of the focusing NLS IVP (1.5) without the assumption of an empty discrete spectrum that was used in [BM2]. Specifically, we consider initial data f satisfying (1.3) such that the analytic scattering coefficients arising in the inverse scattering transform have a single pair of conjugate simple poles in the complex spectral plane. This is clearly the simplest scenario that allows for the presence of solitons. As in the case of zero boundary conditions at infinity, each conjugate pair of discrete eigenvalues contributes a soliton to the solution of NLS. Hence, in the case considered here there is exactly one soliton present.

The simultaneous presence of a discrete spectrum and a nonvanishing reflection coefficient allows one to study the interactions between solitons and radiation (i.e. the components of the solution of the NLS equation arising from the reflection coefficient). In the case of zero boundary conditions at infinity, problems of this kind were first studied in the 1970s [SA1,SA2,ZM]. Those studies, however, employed formal methods. Moreover, and most importantly for our purposes, they were limited to the case of a zero background (i.e. $q_o=0$). In the context of the focusing NLS IVP (1.5), the presence of a discrete spectrum affords us the ability to rigorously study—for the first time—the interaction between solitons and radiation on a modulationally unstable background.

2. Overview of Results

Definitions and notation Before we can state our results precisely, we need to introduce some notation and provide definitions of various quantities that will appear throughout this work.

- For any complex-valued function f, we denote $f_{re} := Re(f)$ and $f_{im} := Im(f)$. Complex conjugation is denoted by an overbar.
- The complex square root $(k^2 + q_o^2)^{\frac{1}{2}}$, with $k \in \mathbb{C}$ being the spectral variable introduced through the Lax pair (1.6), is expressed in terms of a single-valued function $\lambda(k)$, which is uniquely defined by taking the branch cut along the segment

$$B := i[-q_o, q_o] (2.1)$$

of the complex k-plane and defining

$$\lambda(k) = \begin{cases} \sqrt{k^2 + q_o^2}, & k \in \mathbb{R}^+ \cup B, \\ -\sqrt{k^2 + q_o^2}, & k \in \mathbb{R}^-, \end{cases}$$
 (2.2)

so that $\lambda(k) \sim k$ as $k \to \infty$.

• The phase function $\theta(\xi, k)$ is defined by

$$\theta(\xi, k) = \lambda(k) (\xi - 2k), \qquad (2.3)$$

where ξ is the similarity variable

$$\xi = \frac{x}{t} \tag{2.4}$$

which, as usual, is the key independent parameter in the calculation of the long-time asymptotics. Importantly, θ is Schwarz-symmetric, i.e. $\theta(\xi, \bar{k}) = \overline{\theta(\xi, \bar{k})}$.

• As in [BM2], a key role in the analysis will be played by the function

$$h(\xi, k) = \frac{1}{2} \left(\int_{ia_0}^k + \int_{-ia_0}^k dh(\xi, z) \right)$$
 (2.5)

defined via the Abelian differential

$$dh(\xi, k) = -4 \frac{[k - k_o(\xi)][k - \alpha(\xi)][k - \bar{\alpha}(\xi)]}{\gamma(\xi, k)} dk, \tag{2.6}$$

with α and γ defined below and

$$k_o = -\alpha_{\rm re} + \frac{\xi}{4}.\tag{2.7}$$

Note that h is also Schwarz-symmetric, i.e. $h(\xi, \bar{k}) = \overline{h(\xi, k)}$.

• The complex quantity α and the elliptic parameter m of the slowly modulated genus-1 oscillations are uniquely determined by the solution of the modulation equations [EGKK, K1]

$$\frac{\xi}{2} = 2\alpha_{\rm re} + \frac{q_o^2 - \alpha_{\rm im}^2}{\alpha_{\rm re}}, \quad m^2 = \frac{4q_o\alpha_{\rm im}}{\alpha_{\rm re}^2 + (q_o + \alpha_{\rm im})^2},$$
 (2.8a)

$$\left[\alpha_{\rm re}^2 + (q_o - \alpha_{\rm im})^2\right] K(m) = \left(\alpha_{\rm re}^2 - \alpha_{\rm im}^2 + q_o^2\right) E(m), \tag{2.8b}$$

with K(m), E(m) being the complete elliptic integrals of the first and second kind respectively.

• The function

$$\gamma(\xi, k) := \left[\left(k^2 + q_o^2 \right) (k - \alpha) (k - \bar{\alpha}) \right]^{\frac{1}{2}}$$
 (2.9)

is uniquely defined by taking branch cuts along B as well as an appropriate contour \widetilde{B} connecting the points α , $\overline{\alpha}$ and k_0 . The dependence on the similarity variable ξ will often be suppressed from the arguments of α , $\overline{\alpha}$, k_o , γ and other quantities for brevity.

- We denote by p, \bar{p} the single pair of conjugate simple poles that form the discrete spectrum of the Riemann–Hilbert problem associated with the focusing NLS IVP (1.5) (see Sect. 3 for more details). The location of p will play a crucial role in the analysis. Thanks to the reflection invariance of the NLS equation (i.e. the fact that if q(x,t) is a solution then so is q(-x,t)) and the symmetry $k \mapsto \bar{k}$ of the spectrum of the scattering problem (see Sect. 3 for details), without loss of generality we may take p to lie in the third quadrant of the complex k-plane.
- Our analysis and the corresponding results are intimately related to the value of ξ relative to the following special values:

$$v_o = -4\sqrt{2}q_o$$
, $v_s = 2\left[p_{\text{re}} + \frac{\lambda_{\text{re}}(p)}{\lambda_{\text{im}}(p)}p_{\text{im}}\right]$. (2.10)

The velocity v_o defines the edge of the modulated elliptic wave region, whereas v_s is the unperturbed velocity of a soliton produced by a discrete eigenvalue located at k = p (see Fig. 2). Note that v_s is the value of ξ such that

$$\operatorname{Im}\left[\theta(\xi, p)\right] = 0 \tag{2.11}$$

and that $\operatorname{Im} [\theta(\xi, p)] = 0$ if and only if $\operatorname{Im} [\theta(v_s, \bar{p})] = 0$.

• Besides v_o and v_s , a key role will also be played by the solutions \widetilde{v}_s and v_w of the equation

$$\operatorname{Im}[h(\xi, p)] = 0, \quad \xi \in (v_0, 0).$$
 (2.12)

Note that Im $[h(\xi, p)] = 0$ if and only if Im $[h(\xi, \bar{p})] = 0$. The difference between \tilde{v}_s and v_w is explained below (see also Sects. 4 and 5 for more details).

• We will show in Sects. 4 and 5 that the third quadrant \mathbb{C}_{iii} of the complex k-plane is divided into the four regions D_1 , D_2^+ , D_2^- , D_3 defined as follows. Recall that, for a discrete eigenvalue at k = p, v_s is uniquely defined as the value of ξ such that $\text{Im}[\theta(\xi, p)] = 0$. Then, \mathbb{C}_{iii} can be decomposed into

$$D_1 \cup D_3 = \{k \in \mathbb{C}_{\text{iii}} : v_s < v_o < 0\},$$

 $D_2 = \{k \in \mathbb{C}_{\text{iii}} : 0 > v_s > v_o\}.$

These regions are shown in Fig. 1 with $D_1 \cup D_3$ in white and D_2 in gray. The solid blue curve separating them corresponds to the values of k for which $v_s = v_o$ or, equivalently, to $\text{Im}[\theta(v_o, k)] = 0$. The dashed green curve corresponds to the trace of the point $\bar{\alpha}$ as ξ increases from v_o to 0.

Note that:

- The region where $v_s < v_o < 0$ is divided by the blue curve $\text{Im}[\theta(V_o, k)] = 0$ into two disjoint domains. Among them, we take D_1 to be the infinite domain and D_3 the one adjacent to the imaginary axis.
- Similarly, the dashed green curve separates D_2 into two subdomains, D_2^+ and D_2^- , which we take as the portions of D_2 adjacent to D_1 and D_3 , respectively.
- We will show that D_1 and D_3 differ with respect to the number of solutions of Eq. (2.12) that arise in the interval $(v_o, 0)$. In particular, if $p \in D_1$ then (2.12) does not have a solution in $(v_o, 0)$, while if $p \in D_3$ then (2.12) possesses a unique solution $v_w \in (v_o, 0)$.
- Similarly, we will show that if $p \in D_2^+$ then Eq. (2.12) possesses a unique solution $\widetilde{v}_s \in (v_o, 0)$ while if $p \in D_2^-$ then (2.12) has two solutions $\widetilde{v}_s, v_w \in (v_o, 0)$ with $\widetilde{v}_s < v_w$.

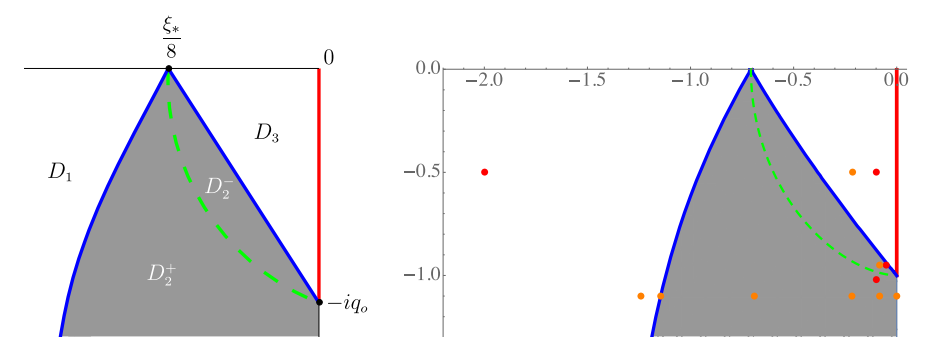


Fig. 1. Left: the third quadrant of the complex k-plane and the four regions D_1 , D_2^+ , D_2^- , D_3 . Solid blue curve: Im[$\theta(v_0, k)$] = 0; dashed green curve: the trace of the point $\bar{\alpha}$ [defined by (2.8)] as $\bar{\xi}$ increases from v_0 to 0. The case $p \in D_1$ corresponds to the transmission regime, the case $p \in D_2^+$ to the trap regime, the case $p \in D_2^-$ to the trap/wake regime, and the case $p \in D_3$ to the transmission/wake regime. Right: the different choices of the pole p used in the numerical simulations of Figs. 3, 4 (red dots) and 18 (orange dots)

The four interaction outcomes Placing p in each of the four regions D_1 , D_2^+ , D_2^- , D_3 gives rise to different, inequivalent asymptotic regimes, which we label as the *transmission regime*, the *trap regime*, the *trap/wake regime*, and the *transmission/wake regime* respectively.

Specifically, in Sects. 4 and 5 we show that, depending on its location in the complex k-plane (see Fig. 1), the presence of a discrete eigenvalue at k = p gives rise to the following leading-order contributions in addition to the portion of the solution generated by the continuous spectrum:

- (i) In the transmission regime, i.e. when $p \in D_1$, a soliton along the ray $x = v_s t$;
- (ii) In the trap regime, i.e. when $p \in D_2^+$, a soliton along the ray $x = \widetilde{v}_s t$;
- (iii) In the trap/wake regime, i.e. when $p \in D_2^-$, a soliton along $x = \tilde{v}_s t$ and a soliton wake along $x = v_w t$;
- (iv) In the transmission/wake regime, i.e. when $p \in D_3$, a soliton along $x = v_s t$ and a soliton wake along $x = v_w t$.

In particular, we will see that the above outcomes are determined by whether there exist solutions of Eq. (2.11) for $\xi \in (-\infty, v_o)$ and of equation (2.12) for $\xi \in (v_o, 0)$.

Long-time asymptotic results We are now ready to give the precise form of the leading-order long-time asymptotics of the solution of the focusing NLS IVP (1.5) in each of the four inequivalent regimes described above. Numerical simulations with the discrete eigenvalue chosen in each of the four regions of Fig. 1, illustrating the asymptotic results, are shown in Figs. 3 and 4. For comparison purposes, Figs. 3 and 4 also show the difference between q(x, t) and the solution $q_{\text{wedge}}(x, t)$ produced by an initial condition that generates the same reflection coefficient as f(x) but no discrete spectrum. The numerical methods used in the numerical simulations were described in [BLM2]. Recall that, since we are taking Re(p) < 0, all relevant velocities and all values of ξ considered in Theorems 2.1–2.4 below are negative.

Theorem 2.1 (Transmission regime). Suppose $p \in D_1$ and let $v_s < v_o < 0$ be defined by (2.10). Then the solution q(x, t) of the focusing NLS IVP (1.5) exhibits the following asymptotic behavior as $t \to \infty$.

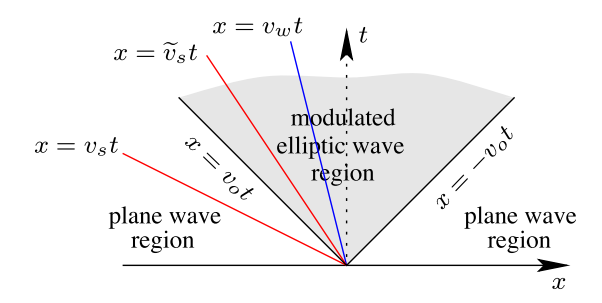


Fig. 2. Asymptotically in time, the xt-plane is divided into the plane wave regions $|x| > |v_0|t$ and the modulated elliptic wave region $|x| < |v_0|t$. Also shown are the locations of the O(1) contributions generated by a discrete eigenvalue at k = p in the four inequivalent cases corresponding to the regions of Fig. 1

(i) If $\xi < v_s$, then the leading-order asymptotics is described by the plane wave

$$q(x,t) = q_{pw}(\xi) + O(t^{-\frac{1}{2}}), \quad t \to \infty,$$
 (2.13)

where

$$q_{pw}(\xi) := q_- e^{2ig_{\infty}(\xi)}$$
 (2.14)

and the real, constant phase $g_{\infty}(\xi)$ is given by (4.16).

(ii) If $\xi = v_s$, then the leading-order asymptotics is equal to a soliton on top of a nonzero plane-wave background, i.e.

$$q(x,t) = q_{pw}(v_s) + q_s(t) e^{2ig_{\infty}(v_s)} + O(t^{-\frac{1}{2}}), \quad t \to \infty,$$
 (2.15)

with q_{pw} given by (2.14), $g_{\infty}(v_s)$ defined by (4.16), and the soliton q_s given by

$$q_{s}(t) = \frac{\left|R_{p}\left[\left(\bar{\mathcal{A}}\Lambda_{1}^{2}\bar{q}_{-} + \mathcal{A}\Lambda_{2}^{2}q_{-} - 2\mathcal{B}\Lambda_{1}\Lambda_{2}q_{o}\right) + e^{i\left[2\theta(v_{s},p)t + \arg(R_{p})\right]}\Lambda_{1}^{2}\bar{q}_{-} + e^{-i\left[2\theta(v_{s},p)t + \arg(R_{p})\right]}\Lambda_{2}^{2}q_{-}}{4i\bar{q}_{-}\left\{\sqrt{|\mathcal{A}|^{2} - \mathcal{B}^{2}}\cosh\left[\ln\left(|R_{p}|\sqrt{|\mathcal{A}|^{2} - \mathcal{B}^{2}}\right)\right] + \operatorname{Re}\left(\mathcal{A}e^{i\left[2\theta(v_{s},p)t + \arg(R_{p})\right]}\right)\right\}}$$

$$(2.16)$$

with the constants R_p , (A, B) and (Λ_1, Λ_2) given by (4.34), (4.47) and (4.55) respectively.

(iii) If $v_s < \xi < v_o$, then the leading-order asymptotics is given by the plane wave (2.13) up to a constant phase shift, namely

$$q(x,t) = q_{pw}(\xi) e^{4i \arg[p+\lambda(p)]} + O(t^{-\frac{1}{2}}), \quad t \to \infty.$$
 (2.17)

(iv) Finally, if $v_o < \xi < 0$, then the asymptotic behavior of the solution is described at leading order by the phase-shifted modulated elliptic wave

$$q(x,t) = \widetilde{q}_{mew}(x,t) e^{4i \arg[p+\lambda(p)]} + O\left(t^{-\frac{1}{2}}\right), \quad t \to \infty, \tag{2.18}$$

where

$$\widetilde{q}_{mew}(x,t) = \frac{q_o\left(q_o + \alpha_{im}\right)}{\bar{q}_-} \frac{\Theta\left(\frac{\sqrt{q_o\alpha_{im}}}{mK(m)}\left(x - 2\alpha_{re}t\right) - X_o + 2\nu_{\infty} - \frac{1}{2} - \frac{\widetilde{\omega}}{2\pi}\right)\Theta\left(\frac{1}{2}\right)}{\Theta\left(\frac{\sqrt{q_o\alpha_{im}}}{mK(m)}\left(x - 2\alpha_{re}t\right) - X_o - \frac{1}{2} - \frac{\widetilde{\omega}}{2\pi}\right)\Theta\left(2\nu_{\infty} - \frac{1}{2}\right)} e^{2i\left[g_{\infty}(\xi) - G_{\infty}(\xi)t\right]}$$
(2.19)

with the Jacobi function Θ defined by (4.120), the complex quantity v_{∞} given by (4.125), and the real quantities G_{∞} , g_{∞} , X_o and $\widetilde{\omega}$ defined by Eqs. (4.79), (4.87), (4.134) and (4.99) respectively. Importantly, all of these quantities depend on x and t only through the similarity variable ξ .

Theorem 2.2 (Trap regime). Suppose $p \in D_2^+$ and let \widetilde{v}_s be the unique solution of Eq. (2.12) in the interval $(v_o, 0)$. Then the solution q(x, t) of the focusing NLS IVP (1.5) exhibits the following asymptotic behavior as $t \to \infty$.

- (i) If $\xi < v_0$, then the leading-order asymptotics is given by the plane wave (2.13).
- (ii) If $v_o < \xi < \widetilde{v}_s$, then the leading-order asymptotics is described by the modulated elliptic wave

$$q(x,t) = q_{mew}(x,t) + O(t^{-\frac{1}{2}}), \quad t \to \infty,$$
 (2.20)

where q_{mew} is obtained from (2.19) after setting $\widetilde{\omega} = 0$, i.e.

$$q_{mew}(x,t) = \frac{q_o\left(q_o + \alpha_{im}\right)}{\bar{q}_-} \frac{\Theta\left(\frac{\sqrt{q_o\alpha_{im}}}{mK(m)}\left(x - 2\alpha_{re}t\right) - X_o + 2\nu_{\infty} - \frac{1}{2}\right)\Theta\left(\frac{1}{2}\right)}{\Theta\left(\frac{\sqrt{q_o\alpha_{im}}}{mK(m)}\left(x - 2\alpha_{re}t\right) - X_o - \frac{1}{2}\right)\Theta\left(2\nu_{\infty} - \frac{1}{2}\right)}$$

$$e^{2i\left[g_{\infty}(\xi) - G_{\infty}(\xi)t\right]}.$$
(2.21)

(iii) If $\xi = \tilde{v}_s$, then at leading order the asymptotics is equal to a soliton on top of a nonzero modulated-elliptic-wave background, i.e.

$$q(x,t) = q_{mew}(\widetilde{v}_s t, t) + q_p(t) + O\left(t^{-\frac{1}{2}}\right), \quad t \to \infty, \tag{2.22}$$

where the modulated elliptic wave q_{mew} is defined by (2.21) and the soliton q_p is given by

$$q_{p}(t) = 2i \frac{2\mathcal{B}\rho_{p}\rho_{\bar{p}}W_{11}(p)W_{12}(\bar{p}) - \left(1 + \mathcal{C}\rho_{\bar{p}}\right)\rho_{p}W_{11}(p)^{2} + \left(1 + \mathcal{A}\rho_{p}\right)\rho_{\bar{p}}W_{12}(\bar{p})^{2}}{\mathcal{B}^{2}\rho_{p}\rho_{\bar{p}} + \left(1 + \mathcal{C}\rho_{\bar{p}}\right)\left(1 + \mathcal{A}\rho_{p}\right)} \tag{2.23}$$

with $(\rho_p, \rho_{\bar{p}})$, W and $(\mathcal{A}, \mathcal{B}, \mathcal{C})$ given by (5.17), (5.21) and (5.28) respectively.

(iv) Finally, if $\tilde{v}_s < \xi < 0$, then the asymptotics is given by the phase-shifted modulated elliptic wave (2.18).

Theorem 2.3 (Trap/wake regime). Suppose $p \in D_2^-$ and let $\widetilde{v}_s < v_w$ be the two solutions of Eq. (2.12) in the interval $(v_o, 0)$. Then, the solution q(x, t) of the focusing NLS IVP (1.5) exhibits the following asymptotic behavior as $t \to \infty$.

- (i) If $\xi < v_o$, then the leading-order asymptotics is described by the plane wave (2.13).
- (ii) If $v_o < \xi < \widetilde{v}_s$, then the leading-order asymptotics is given by the modulated elliptic wave (2.20).
- (iii) If $\xi = \widetilde{v}_s$, then the asymptotics is characterized by (2.22), namely at leading order it is equal to the sum of the modulated elliptic wave (2.21) evaluated at $x = \widetilde{v}_s t$ and the soliton (2.23).
- (iv) If $\tilde{v}_s < \xi < v_w$, then the leading-order asymptotics is given by the phase-shifted modulated elliptic wave (2.18).
- (v) If $\xi = v_w$, then at leading order the asymptotics is equal to a soliton wake on top of a nonzero modulated-elliptic-wave background, i.e.

$$q(x,t) = q_{mew,w}(t) + q_w(t) + O(t^{-\frac{1}{2}}), \quad t \to \infty,$$
 (2.24)

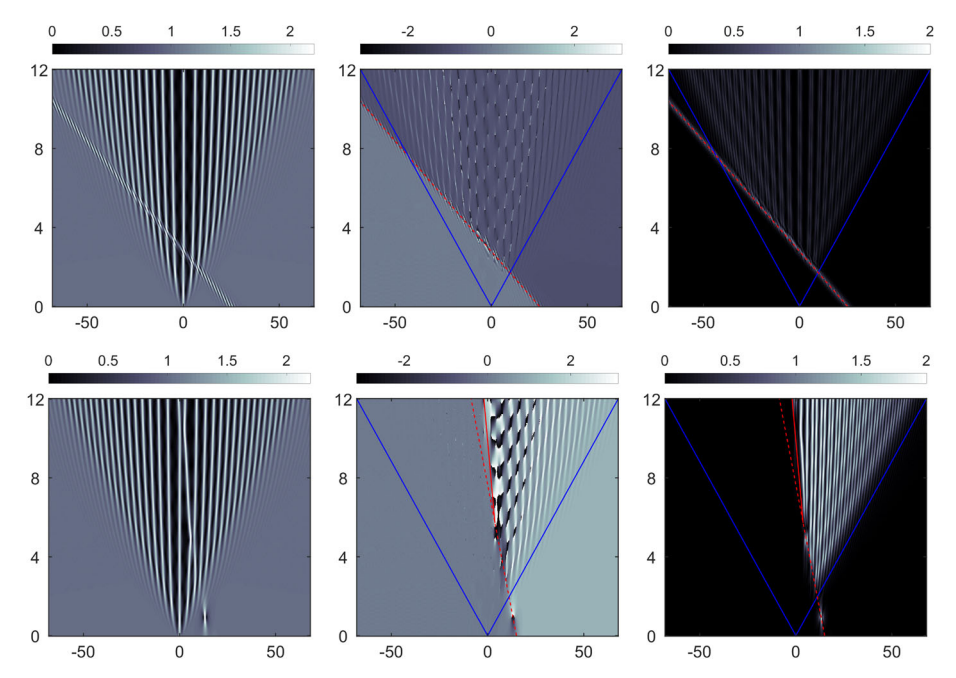


Fig. 3. Numerical solutions of the IVP (1.5) with $q_0 = 1$ and different choices of p for the two pure asymptotic regimes (red dots in Fig. 1). Top row: Transmission regime (Theorem 2.1) with $p = -2 - 0.5i \in D_1$. Bottom row: Trap regime (Theorem 2.2) with $p = -0.1 - 1.02i \in D_2^+$. In all cases, the horizontal axis corresponds to x and the vertical axis to t. The grayscale used in the plots is shown in the top inserts. Left column: Density plots of the solution amplitude |q(x,t)|. Center column: The complex phase difference between the solution in the left column and the solution $q_{\text{wedge}}(x,t)$ generated just by the localized disturbance (i.e. without the soliton), illustrating the asymptotic phase shift as $x \to \pm \infty$ induced by the soliton. Right column: The amplitude difference between the solution in the left column and $q_{\text{wedge}}(x,t)$, illustrating the asymptotic position shift introduced by the soliton. Blue lines: The boundary $x = \pm v_0 t$ between the wedge of modulated periodic oscillations from the left and right plane wave regions. Dashed red lines: The original soliton trajectory (velocity v_s). Solid red lines: The final soliton trajectory (which is either v_s or \widetilde{v}_s depending on the regime). The position shift is very small in the transmission regime but becomes more noticeable in the trap regime. In both cases, the position shift is confined to the portion of the wedge lying above the soliton, in agreement with Theorems 2.1 and 2.2

where the modulated elliptic wave $q_{mew,w}(t)$ is given by (2.21) evaluated at $x = v_w t$ but with ω in X_o replaced by ω_w of (6.9) and with g_∞ replaced by $g_{w,\infty}$ of (6.13), and the soliton wake q_w is defined by

$$q_{w}(t) := 2i \frac{2\mathcal{B}_{w}\rho_{p_{w}}\rho_{\bar{p}_{w}}W_{w11}(\bar{p})W_{w12}(p) - \left(1 + \mathcal{C}_{w}\rho_{p_{w}}\right)\rho_{\bar{p}_{w}}W_{w11}(\bar{p})^{2} + \left(1 + \mathcal{A}_{w}\rho_{\bar{p}_{w}}\right)\rho_{p_{w}}W_{w12}(p)^{2}}{\mathcal{B}_{w}^{2}\rho_{p_{w}}\rho_{\bar{p}_{w}} + \left(1 + \mathcal{C}_{w}\rho_{p_{w}}\right)\left(1 + \mathcal{A}_{w}\rho_{\bar{p}_{w}}\right)},$$

$$(2.25)$$

with $(\rho_{p_w}, \rho_{\bar{p}_w})$, W_w and $(\mathcal{A}_w, \mathcal{B}_w, \mathcal{C}_w)$ given by (6.22), (6.27) and (6.33) respectively.

(vi) Finally, if $v_w < \xi < 0$, then the leading-order asymptotics is the same with the one in the range $\widetilde{v}_s < \xi < v_w$, namely it is given by the phase-shifted modulated elliptic wave (2.18).

Theorem 2.4 (Transmission/wake regime). Suppose $p \in D_3$, let $v_s < v_o < 0$ be defined by (2.10), and let v_w be the unique solution of Eq. (2.12) in the interval $(v_o, 0)$. Then, the

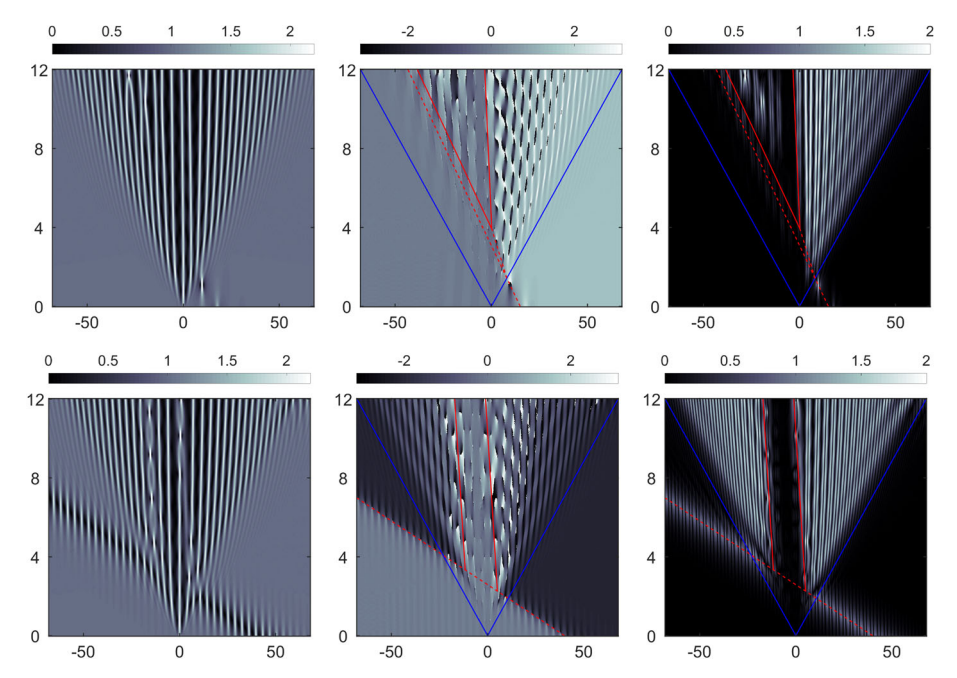


Fig. 4. The analogue of Fig. 3 for p corresponding to the two mixed asymptotic regimes (orange dots in Fig. 1). Here, the solid red lines also identify the soliton wakes, propagating with velocity v_w , where $|v_w| < |\widetilde{v}_s| < |v_s|$. Top row: Trap/wake regime (Theorem 2.3) with $p = -0.05 - 0.95i \in D_2^-$. Bottom row: Transmission/wake regime (Theorem 2.4) with $p = -0.1 - 0.5i \in D_3$. Note that the choice of p in the trap/wake regime is very close to the boundary between D_2^- and D_3 and, as a result, the dashed and solid red lines corresponding respectively to the original and modified soliton velocities are almost identical. Moreover, note that the two wakes seen in the transmission/wake regime have the same speed, and hence are detected as a single wake in the asymptotic analysis, which is why no wake-induced phase or position shift is observed in the asymptotics for $\xi > v_w$

solution q(x, t) of the focusing NLS IVP (1.5) exhibits the following asymptotic behavior as $t \to \infty$.

- (i) If $\xi < v_s$, then the leading-order asymptotics is given by the plane wave (2.13).
- (ii) If $\xi = v_s$, then the asymptotics is characterized by (2.15), namely at leading order it is given by the superposition of the plane wave (2.14) and the soliton (2.16).
- (iii) If $v_s < \xi < v_o$, then the leading-order asymptotics is described by the phase-shifted plane wave (2.17).
- (iv) If $v_o < \xi < v_w$, then the leading-order asymptotics is given by the phase-shifted modulated elliptic wave (2.18).
- (v) If $\xi = v_w$, then the asymptotics is characterized by (2.24), i.e. at leading order it is equal to the sum of the modulated elliptic wave $q_{mew,w}(t)$ and the soliton wake (2.25).
- (vi) Finally, if $v_w < \xi < 0$, then the leading-order asymptotics is the same with the one in the range $v_o < \xi < v_w$, namely it is given by the phase-shifted modulated elliptic wave (2.18).

Remark 2.1 (Leading-order asymptotics for x > 0). Since the pole p lies in the third quadrant of the complex k-plane, it has no effect on the asymptotics for x > 0 (equivalently, $\xi > 0$; see Fig. 6). In particular, for x > 0 the leading-order asymptotics of

IVP (1.5) is described by Theorems 1.1 and 1.2 of [BM2], the only difference being that now one must also include the constant phase shift $4\arg [p + \lambda(p)]$ and the position shift induced by the soliton arising for x < 0.

Remark 2.2. In the appendix, we explicitly verify that the expression (2.16) for the soliton obtained in the long-time asymptotics agrees with the long-time asymptotics of the standard soliton solution of the focusing NLS with nonzero background.

Remark 2.3 (Soliton vs. soliton wake). The soliton arising either at $\xi = v_s$ or at $\xi = \widetilde{v}_s$ induces a constant phase shift (equal to 4arg $[p + \lambda(p)]$) as well as a position shift (related to the presence of $\widetilde{\omega}$ in (2.19) as opposed to (2.21)) in the leading-order asymptotics for subsequent values of ξ . On the contrary, the soliton wake arising at $\xi = v_w$ has no effect on the leading-order asymptotics for $\xi > v_w$. The numerical simulations of Figs. 3 and 4 illustrate these remarks.

Remark 2.4 (Multiple leading-order contributions from the poles). We find it quite remarkable that in the two mixed regimes a single pair of complex conjugate poles produces O(1) contributions to the solution at two different velocities: the soliton velocity and the wake velocity, as specified in Theorems 2.3 and 2.4. (These predictions are validated by the numerical results in Figs. 3 and 4.) To the best of our knowledge, this is the first time that such a phenomenon has been observed in the long-time asymptotic analysis of an integrable system, and is perhaps one of the main novelties in the results of the present work. Moreover, the numerical results in the bottom row of Fig. 4 suggest that the soliton-generated wake may comprise itself two different localized structures. We emphasize however that, since these two structures propagate with the same velocity, in order to be able to differentiate between them one would have to compute the asymptotics by taking $x = \xi t + y$. Such a calculation is outside the scope of this work.

Structure of the paper In Sect. 3, the solution of IVP (1.5) for the focusing NLS equation is associated with the solution of a matrix Riemann–Hilbert problem via the inverse scattering transform. Furthermore, the four different long-time asymptotic patterns, namely the transmission, trap, trap/wake, and transmission/wake regimes, are motivated through the behavior of the jump matrices of this Riemann–Hilbert problem. The transmission regime is analyzed in Sect. 4, resulting in the proof of Theorem 2.1. The proof of Theorem 2.2 for the trap regime is provided in Sect. 5. The two mixed regimes are discussed in Sect. 6, leading to the proofs of Theorems 2.3 and 2.4. Finally, some concluding remarks are given in Sect. 7.

3. The Riemann–Hilbert Problem and Outline of the Asymptotic Analysis

The implementation of the inverse scattering transform method for IVP (1.5) begins with the integration of the Lax pair (1.6) for the 2×2 matrix-valued function Ψ assuming as usual that the solution q of problem (1.5) is given. This task is known as the direct problem. Then, q is expressed in terms of a sectionally meromorphic function M which is defined via appropriate combinations of the two column vectors Ψ_1 and Ψ_2 of Ψ , and which satisfies a certain matrix Riemann–Hilbert problem. This portion of the analysis is known as the inverse problem. Specifically, the discussion of the direct problem in Sect. 2 of [BM2] motivates the following definition for the sectionally meromorphic

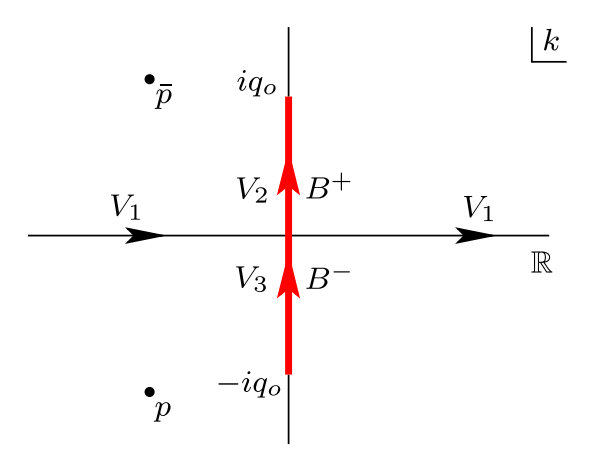


Fig. 5. The branch cut $B = B^+ \cup B^-$, the jumps V_1 , V_2 , V_3 of Riemann–Hilbert problem (3.7), and the conjugate pair of simple poles p, \bar{p}

matrix-valued function M:

$$M(x,t,k) = \begin{cases} \left(\frac{\Psi_{+1}(x,t,k)}{\bar{a}(k)d(k)}, \Psi_{-2}(x,t,k)\right) e^{-i\theta(\xi,k)t\sigma_3}, k \in \mathbb{C}^+ \backslash B^+, \\ \left(\Psi_{-1}(x,t,k), \frac{\Psi_{+2}(x,t,k)}{a(k)d(k)}\right) e^{-i\theta(\xi,k)t\sigma_3}, k \in \mathbb{C}^- \backslash B^-. \end{cases}$$
(3.1)

In the above definition, we use the notation

$$\mathbb{C}^{\pm} := \{k \in \mathbb{C} : \mathrm{Im}(k) \geq 0\} \,, \quad B^{+} := i \, [0, q_{o}] \,, \quad B^{-} := i \, [-q_{o}, 0] \,$$

and denote by Ψ_{\pm} the so-called Jost solutions, namely the simultaneous solutions of the Lax pair (1.6) with prescribed normalizations as $x \to \pm \infty$:

$$\Psi_{\pm}(x,t,k) = \begin{pmatrix} 1 & i(\lambda - k)/\bar{q}_{\pm} \\ i(\lambda - k)/q_{\pm} & 1 \end{pmatrix} e^{i\theta(\xi,k)t\sigma_3} [1 + o(1)], \quad x \to \pm \infty. \quad (3.2)$$

(Recall that the quantities λ , θ and ξ are defined by (2.2), (2.3) and (2.4) respectively.) Furthermore, we define the spectral function a(k) along with its Schwarz conjugate $\bar{a}(k)$ by

$$a(k) = \frac{\operatorname{wr}\left[\Psi_{-1}(x,t,k), \Psi_{+2}(x,t,k)\right]}{d(k)}, \quad \bar{a}(k) := \overline{a(\bar{k})} = \frac{\operatorname{wr}\left[\Psi_{+1}(x,t,k), \Psi_{-2}(x,t,k)\right]}{d(k)},$$
(3.3)

where "wr" denotes the Wronskian determinant and

$$d(k) := \frac{2\lambda(k)}{\lambda(k) + k}. (3.4)$$

Importantly, the Wronskian determinants appearing in (3.3) are independent of x and t, and hence the functions a and \bar{a} depend only on k.

The definition (3.1) of M, in combination with the analyticity properties of Ψ_{\pm} (see [BM2] for more details), implies that the only sources of nonanalyticity of M are

(i) the continuous spectrum

$$\Sigma := \mathbb{R} \cup B, \tag{3.5}$$

along which M exhibits jump discontinuities, and

(ii) the possible zeros of the spectral function a(k), which form the *discrete spectrum* of the Riemann–Hilbert problem satisfied by M.

It was shown in [BM2] that, if there is no discrete spectrum, namely, if

$$a(k) \neq 0 \quad \forall k \in \mathbb{C}^- \cup \Sigma,$$
 (3.6)

then the function M(x, t, k) satisfies the following Riemann–Hilbert problem:

$$M^+ = M^- V_1, \qquad k \in \mathbb{R}, \tag{3.7a}$$

$$M^+ = M^- V_2, \qquad k \in B^+,$$
 (3.7b)

$$M^+ = M^- V_3, \qquad k \in B^-,$$
 (3.7c)

$$M = I + O\left(\frac{1}{k}\right), \quad k \to \infty,$$
 (3.7d)

where the jump matrices along the three contours \mathbb{R} , B^+ , B^- comprising the continuous spectrum Σ are given by (see Fig. 5)

$$V_{1}(x,t,k) = \begin{pmatrix} \frac{1}{d(k)} [1 + r(k)\bar{r}(k)] \bar{r}(k)e^{2i\theta(\xi,k)t} \\ r(k)e^{-2i\theta(\xi,k)t} \end{pmatrix},$$
(3.8a)

$$V_{2}(x,t,k) = \begin{pmatrix} -\frac{\lambda(k) - k}{iq_{-}} \bar{r}(k) e^{2i\theta(\xi,k)t} & \frac{2\lambda(k)}{i\bar{q}_{-}} \\ \frac{\bar{q}_{-}}{2i\lambda(k)} [1 + r(k)\bar{r}(k)] & -\frac{\lambda(k) + k}{i\bar{q}_{-}} r(k) e^{-2i\theta(\xi,k)t} \end{pmatrix}, \quad (3.8b)$$

$$V_{3}(x,t,k) = \begin{pmatrix} \frac{\lambda(k) + k}{iq_{-}} \bar{r}(k) e^{2i\theta(\xi,k)t} & \frac{q_{-}}{2i\lambda(k)} [1 + r(k)\bar{r}(k)] \\ \frac{2\lambda(k)}{iq_{-}} & \frac{\lambda(k) - k}{i\bar{q}_{-}} r(k) e^{-2i\theta(\xi,k)t} \end{pmatrix},$$
(3.8c)

with the reflection coefficient r defined by

$$r(k) = -\frac{b(k)}{\bar{a}(k)}, \quad b(k) := \frac{\text{wr}\left[\Psi_{+1}(x, t, k), \Psi_{-1}(x, t, k)\right]}{d(k)}.$$
 (3.9)

Removing the assumption (3.6), i.e. allowing the spectral function a(k) to vanish in \mathbb{C}^- , results in a Riemann–Hilbert problem with a *nonempty* discrete spectrum. In this work, we consider the simplest such scenario, according to which the initial data f(x) of IVP (1.5) is such that a(k) has a *unique*, *simple zero* in $\mathbb{C}^- \setminus \Sigma$. That is, we assume that there exists a unique $p \in \mathbb{C}^- \setminus \Sigma$ such that a(p) = 0 and, furthermore, $a'(p) \neq 0$. Correspondingly, the Schwarz conjugate $\bar{a}(k)$ of a(k) possesses a *unique*, *simple zero* $\bar{p} \in \mathbb{C}^+ \setminus \Sigma$ and, by definition (3.1), M is meromorphic in $\mathbb{C} \setminus \Sigma$ with two simple poles, at k = p and at $k = \bar{p}$. Therefore, in addition to the jumps V_1, V_2, V_3 along the continuous spectrum Σ , the Riemann–Hilbert problem for M must be supplemented by suitable residue conditions at p and \bar{p} . These can be computed as follows.

Since a(p) = 0, by expression (3.3) we have that wr $\left[\Psi_{-1}(x, t, p), \Psi_{+2}(x, t, p)\right] = 0$ for all $x, t \in \mathbb{R}$. In turn, since neither $\Psi_{-1}(x, t, p)$ nor $\Psi_{+2}(x, t, p)$ can be identically

zero due to the normalization (3.2), we infer that there exists a constant $C_p \neq 0$ such that

$$\Psi_{+2}(x, t, p) = C_p \Psi_{-1}(x, t, p) \quad \forall x, t \in \mathbb{R}.$$
 (3.10a)

Similarly, evaluating (3.3) at $k = \bar{p}$ we obtain

$$\Psi_{+1}(x, t, \bar{p}) = C_{\bar{p}}\Psi_{-2}(x, t, \bar{p}) \quad \forall x, t \in \mathbb{R}$$
 (3.10b)

for some constant $C_{\bar{p}} \neq 0$. Thus,

$$\operatorname{Res}_{k=p} \frac{\Psi_{+2}(x,t,k)}{a(k)d(k)} = \frac{\Psi_{+2}(x,t,p)}{a'(p)d(p)} = c_p \Psi_{-1}(x,t,p) \quad \forall x,t \in \mathbb{R}, \quad c_p := \frac{C_p}{a'(p)d(p)}.$$
(3.11a)

$$\operatorname{Res}_{k=\bar{p}} \frac{\Psi_{+1}(x,t,k)}{\bar{a}(k)d(k)} = \frac{\Psi_{+1}(x,t,\bar{p})}{\bar{a}'(\bar{p})d(\bar{p})} = c_{\bar{p}}\Psi_{-2}(x,t,\bar{p}) \quad \forall x,t \in \mathbb{R}, \quad c_{\bar{p}} := \frac{C_{\bar{p}}}{\bar{a}'(\bar{p})d(\bar{p})}.$$
(3.11b)

Relations (3.11a) and (3.11b) imply the following residue conditions for M:

$$\operatorname{Res}_{k=p} M(x,t,k) = M(x,t,p) \begin{pmatrix} 0 & c_p e^{2i\theta(\xi,p)t} \\ 0 & 0 \end{pmatrix} \qquad \forall x,t \in \mathbb{R},$$
 (3.12a)

$$\operatorname{Res}_{k=\bar{p}} M(x,t,k) = M(x,t,\bar{p}) \begin{pmatrix} 0 & 0 \\ c_{\bar{p}} e^{-2i\theta(\xi,\bar{p})t} & 0 \end{pmatrix} \qquad \forall x,t \in \mathbb{R}.$$
 (3.12b)

The Riemann–Hilbert problem for the focusing NLS IVP (1.5) in the presence of the discrete spectrum $\{p, \bar{p}\}$ comprises the empty-discrete-spectrum problem (3.7) augmented with the residue conditions (3.12). To ensure uniqueness of solutions of the above Riemann–Hilbert problem, one must also supplement it with suitable growth conditions at the branch points [BMi].

The x-part of the Lax pair (1.6) together with the definition (3.1) and the asymptotic condition (3.16f) yield the solution of the IVP (1.5) via the reconstruction formula

$$q(x,t) = -2i \lim_{k \to \infty} k M_{12}(x,t,k).$$
 (3.13)

For the purpose of computing the long-time asymptotics, it is convenient to convert the residue conditions (3.12) into jump discontinuities. In particular, following [Mi], we let $\partial D_p^{\varepsilon}$ and $\partial D_{\bar{p}}^{\varepsilon}$ be the positively oriented boundaries of the disks D_p^{ε} and $D_{\bar{p}}^{\varepsilon}$ of radius ε centered at p and \bar{p} respectively, and define the function N by

$$N(x,t,k) = \begin{cases} M(x,t,k)V_{p}(x,t,k), & k \in D_{p}^{\varepsilon}, \\ M(x,t,k), & k \in \mathbb{C}^{-} \setminus \left(B^{-} \cup \overline{D_{p}^{\varepsilon}}\right), \\ M(x,t,k)V_{\bar{p}}(x,t,k), & k \in D_{\bar{p}}^{\varepsilon}, \\ M(x,t,k), & k \in \mathbb{C}^{+} \setminus \left(B^{+} \cup \overline{D_{p}^{\varepsilon}}\right), \end{cases}$$
(3.14)

where the matrices V_p and $V_{\bar{p}}$ are given by

$$V_{p}(x,t,k) = \begin{pmatrix} 1 - \frac{c_{p}}{k-p} e^{2i\theta(\xi,p)t} \\ 0 & 1 \end{pmatrix}, \quad V_{\bar{p}}(x,t,k) = \begin{pmatrix} 1 & 0 \\ -\frac{c_{\bar{p}}}{k-\bar{p}} e^{-2i\theta(\xi,\bar{p})t} & 1 \end{pmatrix}.$$
(3.15)

Note that the residue conditions (3.12) imply that N is analytic at p and \bar{p} . Furthermore, the jumps of N along the continuous spectrum Σ are the same with those of M since N=M outside the disks D_p^ε and $D_{\bar{p}}^\varepsilon$. Therefore, N(x,t,k) is analytic for $k \in \mathbb{C} \setminus \left(\Sigma \cup \partial D_p^\varepsilon \cup \partial D_{\bar{p}}^\varepsilon\right)$ and satisfies the following Riemann–Hilbert problem:

$$N^+ = N^- V_1, \qquad k \in \mathbb{R}, \tag{3.16a}$$

$$N^{+} = N^{-}V_{2}, \qquad k \in B^{+}, \tag{3.16b}$$

$$N^{+} = N^{-}V_{3}, \qquad k \in B^{-}, \tag{3.16c}$$

$$N^{+} = N^{-}V_{p}, \qquad k \in \partial D_{p}^{\varepsilon}, \tag{3.16d}$$

$$N^{+} = N^{-}V_{\bar{p}}, \qquad k \in \partial D_{\bar{p}}^{\varepsilon}, \tag{3.16e}$$

$$N = I + O(1/k), \qquad k \to \infty, \tag{3.16f}$$

with the jumps V_1 , V_2 , V_3 given by (3.8) and the jumps V_p , $V_{\bar{p}}$ defined by (3.15). Note that the transformation (3.14) does not affect the normalization as $k \to \infty$. Thus, the long-time asymptotic behavior of the solution q of the IVP (1.5) for the focusing NLS equation can equivalently be obtained by determining the corresponding behavior of the solution N of the Riemann–Hilbert problem (3.16).

Overview of the long-time asymptotic analysis The time dependence of the jumps of Riemann–Hilbert problem (3.16) is dictated by the exponentials $e^{\pm i\theta t}$, which become highly oscillatory in the limit $t \to \infty$. Thus, a delicate analysis via the nonlinear steepest descent method of Deift and Zhou [DZ1,DZ2] is required in order to extract the leading-order asymptotic contribution to the solution. Like in the classical steepest descent method, the main idea behind the Deift-Zhou method is to deform the contours associated with the oscillatory jumps to appropriate regions of the complex k-plane where the exponentials $e^{\pm i\theta t}$ decay to zero as $t \to \infty$. Hence, the first step in the asymptotic analysis of problem (3.16) consists of studying the sign structure of $Re(i\theta)$ in the complex k-plane. Recall, however, that the controlling phase function θ depends parametrically on the similarity variable ξ . Thus, similarly to the use of the steepest descent method for computing the long-time asymptotics of solutions of linear equations (e.g., see [AS, W]), the analysis begins by studying how the sign structure of $Re(i\theta)$ changes as ξ increases from $-\infty$ to ∞ .

Let us first focus on the sign structure of $\text{Re}(i\theta)$ for $\xi < 0$ (i.e. x < 0), which is depicted in the first four frames of Fig. 6. Observe that, as ξ increases from $-\infty$ to 0, the sign of $\text{Re}(i\theta)$ switches from negative to positive in the third quadrant and from positive to negative in the second quadrant, while it remains the same in the first and the fourth quadrant. More specifically, two regions of positive sign emerge in the third quadrant: an unbounded region on the left of the point k_1 , and a bounded region on the right of the point k_2 and on the left of the branch cut B, where

$$k_1(\xi) := \frac{1}{8} \left(\xi - \sqrt{\xi^2 - v_o^2} \right), \quad k_2(\xi) := \frac{1}{8} \left(\xi + \sqrt{\xi^2 - v_o^2} \right)$$
 (3.17)

are the two stationary points of θ with v_o defined by (2.10). The two regions of positive sign grow continuously and remain disjoint until $\xi = v_o$ (third frame in Fig. 6) where $k_1(v_o) = k_2(v_o) = \frac{v_o}{8}$. Note that for $\xi \leq v_o$ the stationary points k_1, k_2 are real. Subsequently, however, for $v_o < \xi < 0$, the two stationary points become complex, and the two regions of positive sign merge to a *single* region that eventually grows to occupy

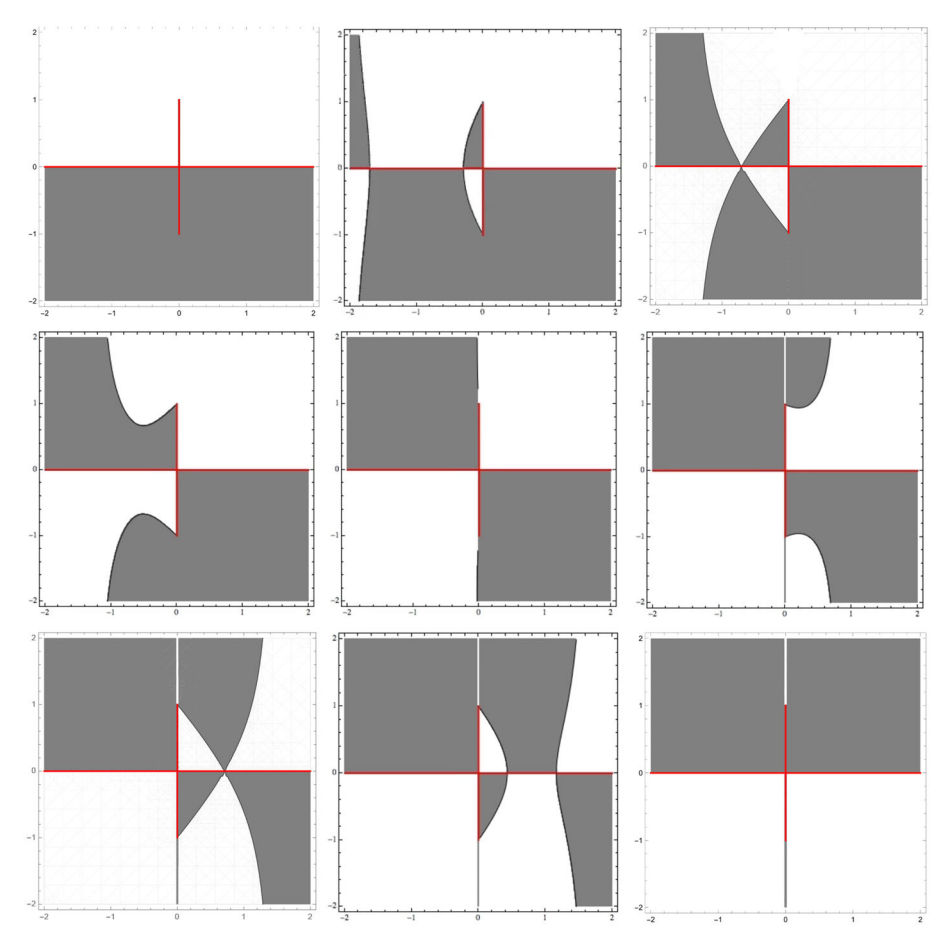


Fig. 6. The sign of $\operatorname{Re}(i\theta)$ as ξ increases from $-\infty$ to $+\infty$. *Gray*: $\operatorname{Re}(i\theta) < 0$; *White*: $\operatorname{Re}(i\theta) > 0$. *Top row*: $\xi = -\infty$, $\xi \in (-\infty, v_o)$, $\xi = v_o$; *Middle row*: $\xi \in (v_o, 0)$, $\xi = 0$, $\xi \in (0, -v_o)$; *Bottom row*: $\xi = -v_o$, $\xi = (-v_o, \infty)$, and $\xi = +\infty$

all of the third quadrant (fourth and fifth frames in Fig. 6). As a result, the value $\xi = v_o$ is a bifurcation point in the analysis of the problem via the Deift-Zhou method.

More specifically, for $\xi < v_o$, the sign structure of $\text{Re}(i\theta)$ allows for two different factorizations of the jump V_1 along the real axis, both of which result in exponentially decaying contributions, as will be explained in detail in Sects. 4 and 5. On the other hand, for $v_o < \xi < 0$ it turns out that only one of the aforementioned factorizations can be employed. This results in an exponentially growing jump along a certain portion of the deformed jump contour, which is corrected by introducing a so-called g-function [DVZ1,DVZ2] (see also Chapter 4 of [KMM] in the context of semiclassical analysis). The corresponding transformation of the Riemann–Hilbert problem replaces the original controlling phase function from θ to the Abelian integral h defined by (2.5), and is the reason why the asymptotics change dramatically as ξ crosses v_o . The sign structure of Re(ih) in the third quadrant of the complex k-plane as ξ decreases from v_o to 0 is shown in Fig. 7.

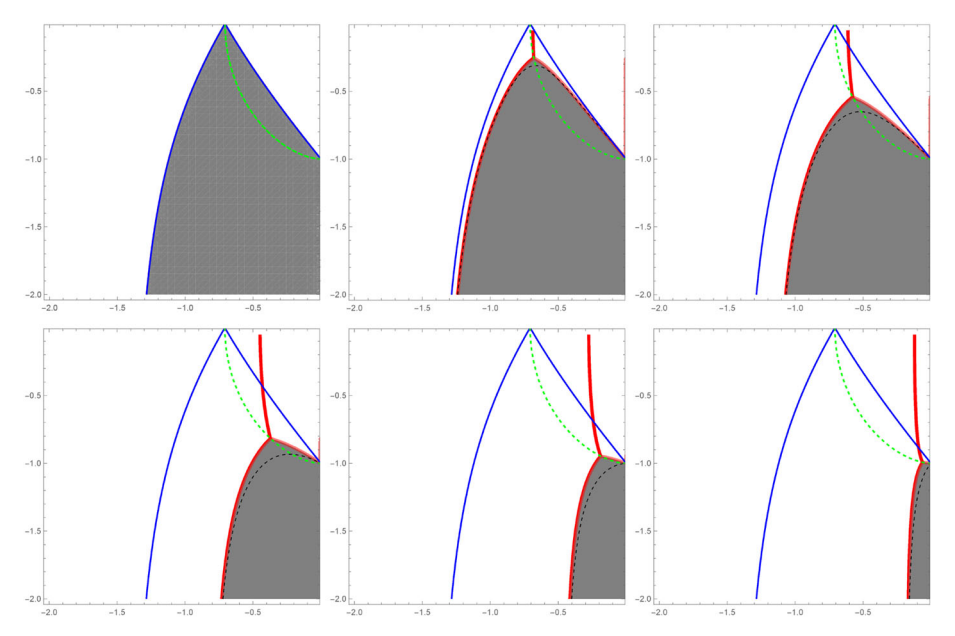


Fig. 7. The sign of Re(ih) as ξ increases gradually from v_0 (top left plot) to just below $\xi=0$ (bottom right plot). Gray: Re(ih) < 0; White: Re(ih) > 0. Note $h \equiv \theta$ when $\xi=v_0$. Red curves: The contours Im(h) = 0. Green curve: The path described by $\bar{\alpha}$ (defined by (2.8)), the intersection point of the contours Im(h) = 0. Black curve: The contour Im[$\theta(v_0, k)$] = 0

Of course, apart from the jumps V_1 , V_2 , V_3 along the continuous spectrum, the Riemann–Hilbert problem (3.16) also involves the jumps V_p , $V_{\bar{p}}$ originating from the poles p, \bar{p} . Thus, another crucial value of ξ now emerges, namely the value v_s for which $\text{Re}(i\theta)$ vanishes at p and \bar{p} . Observe that v_s is the same for p and \bar{p} , since $\text{Re}\left[i\theta(\xi,p)\right]=0 \Leftrightarrow \text{Re}\left[i\theta(\xi,\bar{p})\right]=0$ due to the symmetry $\theta(\xi,\bar{k})=\theta(\xi,k)$. Solving either of these equations, we obtain v_s in the explicit form (2.10). Note that in the third quadrant, where p lies, we have λ_{re} , $\lambda_{\text{im}} \leqslant 0$, thus $v_s < 0$.

In the range $(-\infty, v_o)$, we shall see that the jumps V_p , $V_{\bar{p}}$ (equivalently, the poles p, \bar{p}) contribute to the leading-order asymptotics only when $\xi = v_s$, provided that p is such that $v_s \in (-\infty, v_o)$. On the other hand, as explained above, in the range $(v_o, 0)$ the phase function θ is replaced by the Abelian integral h defined by (2.5). Thus, the role of v_s is now played by the solutions of the equation

$$\text{Re}[ih(\xi, p)] = 0.$$
 (3.18)

The complicated form of h does not allow us to solve Eq. (3.18) explicitly. It turns out, however, that, depending on the location of p inside the third quadrant, Eq. (3.18) has either zero, one or two solutions in the interval $(v_o, 0)$. More specifically, as already noted in Sect. 2, the third quadrant is divided into the four regions D_1 , D_2^+ , D_2^- , D_3 of Fig. 1, where for $\xi \in (v_o, 0)$ equation (3.18) has no solutions in D_1 , a unique solution \widetilde{v}_s in D_2^+ , two solutions $\widetilde{v}_s < v_w$ in D_2^- , and a unique solution v_w in D_3 . The mathematical description of the long-time asymptotic regimes that arise in these four regions is given in Theorems 2.1–2.4. Before proceeding to the proofs of these results, we give a brief outline of the way in which the asymptotics unravels in each regime.

 $p \in D_1$: The transmission regime. In this case, $v_s < v_o$ and, furthermore, Eq. (3.18) has no solution in the interval $(v_o, 0)$ —in fact, $Re(ih)(\xi, p) > 0$ for all $v_o < \xi < 0$. For $\xi < v_s$, the jumps V_p , $V_{\bar{p}}$ decay exponentially and hence do not yield leading-order contributions. Thus, the dominant component of Riemann–Hilbert problem (3.16) in the limit $t \to \infty$ involves only the jumps along the continuous spectrum Σ , giving rise to the plane wave (2.13). At $\xi = v_s$, the jumps V_p , $V_{\bar{p}}$ switch from exponentially decaying to purely oscillatory. Consequently, they are now part of the dominant Riemann-Hilbert problem, generating the soliton (2.15). Observe that this soliton propagates with velocity v_s and, since $|v_s| > |v_o|$, it eventually escapes to infinity outside the wedge $|\xi| < |v_o|$ of Fig. 2. For $v_s < \xi < v_o$, the jumps V_p , $V_{\bar{p}}$ grow exponentially. Nevertheless, it turns out that this growth can be converted into decay via an appropriate transformation. Hence, similarly to the range $\xi < v_s$, the leading-order asymptotic behavior does not depend on V_p , $V_{\bar{p}}$ and is characterized by the plane wave (2.13), but now with a phase shift generated by the soliton that has arisen at $\xi = v_s$. Finally, for $v_o < \xi < 0$ the phase function switches from θ to h. Then, since Re(ih)(ξ , p) > 0 for all $v_0 < \xi < 0$, the jumps V_p , $V_{\bar{p}}$ do not contribute to the leading-order asymptotics. Hence, no soliton is present in the range $v_o < \xi < 0$ and the solution is asymptotically equal to the modulated elliptic wave (2.19) with the phase shift already generated by the soliton at $\xi = v_s$ in the range $v_s < \xi < v_o$.

 $p \in D_2^+$: The trap regime. In this case, $v_s > v_o$ and, in addition, Eq. (3.18) has a unique solution \widetilde{v}_s in the interval $(v_o,0)$ —in fact, it turns out that $v_s < \widetilde{v}_s$. Thus, for $\xi < \widetilde{v}_s$ the jumps V_p , $V_{\bar{p}}$ are not significant at leading order. In particular, for $\xi < v_o$ the leading-order asymptotics is given by the plane wave (2.13), while for $v_o < \xi < \widetilde{v}_s$ the solution is asymptotically equal to the modulated elliptic wave (2.21). At $\xi = \widetilde{v}_s$, however, the jumps V_p , $V_{\bar{p}}$ become purely oscillatory and hence do contribute to the leading-order asymptotics, which is now given by the soliton (2.22). Observe that, since $|\widetilde{v}_s| < |v_o|$, this soliton is trapped forever inside the wedge $|\xi| < |v_o|$ of Fig. 2. Furthermore, the fact that $|\widetilde{v}_s| < |v_s|$ indicates that the soliton is delayed by its interaction with the modulated elliptic wave. Finally, since \widetilde{v}_s is the only solution of Eq. (3.18) in $(v_o,0)$, for $\widetilde{v}_s < \xi < 0$ the jumps V_p , $V_{\bar{p}}$ do not affect the leading-order asymptotics, which is now equal to the modulated elliptic wave (2.19) with an additional phase shift generated by the soliton at $\xi = \widetilde{v}_s$.

 $p \in D_2^-$: The trap/wake regime. This case is similar to the trap regime apart from the fact that now Eq. (3.18) has two (as opposed to one) solutions in the interval $(v_o, 0)$, namely \widetilde{v}_s and v_w with $\widetilde{v}_s < v_w$. Therefore, for $\xi < v_w$ the asymptotics is the same with the one in the trap regime, including the soliton that arises at $\xi = \widetilde{v}_s$. However, at $\xi = v_w$ a new phenomenon emerges, namely the soliton wake (2.24). Importantly, contrary to the soliton (which induces a phase shift for $\xi > \widetilde{v}_s$), the soliton wake does not affect the leading-order asymptotics in the range $v_w < \xi < 0$.

 $p \in D_3$: The transmission/wake regime. This case is similar to the transmission regime apart from the fact that Eq. (3.18) now has a unique solution v_w in the interval $(v_o, 0)$ (as opposed to no solution). Thus, the leading-order asymptotics is the same with the one in the transmission regime except for $\xi = v_w$, where the soliton wake (2.24) arises. Importantly, contrary to the soliton at $\xi = v_s$ (which generates a phase shift for $\xi > v_s$), the leading-order asymptotics for $v_w < \xi < 0$ are not affected by the soliton wake.

4. The Transmission Regime: Proof of Theorem 2.1

This regime arises when p lies in the region D_1 of Fig. 1, in which case $v_s < v_o$ and $\operatorname{Re}(ih)(\xi, p)$ does not vanish in the interval $(v_0, 0)$. Thus, we split the interval $(-\infty, 0)$ into the following ranges: $\xi < v_s$; $\xi = v_s$; $v_s < \xi < v_o$; and $v_o < \xi < 0$.

4.1. The range $\xi < v_s$: plane wave. In this range, we have $Re(i\theta)(\xi, p) < 0$ and $Re(i\theta)(\xi,\bar{p}) > 0$. Hence, the jumps V_p and $V_{\bar{p}}$ given by (3.15) tend to the identity as $t \to \infty$ and therefore are not expected to be part of the dominant component of Riemann-Hilbert problem (3.16) in the limit $t \to \infty$. Next, we shall show that this is indeed the case by performing several deformations of problem (3.16) in the spirit of the Deift-Zhou nonlinear steepest descent method. We emphasize that although some of these deformations are similar to those of the no-discrete-spectrum analysis of [BM2], one now needs to carefully handle the jumps around the poles p, \bar{p} , which were not present in [BM2].

First deformation This deformation is carried out in four stages. In each of these stages, a new function $N^{(1)}$ is defined in terms of the solution $N = N^{(0)}$ of Riemann–Hilbert problem (3.16), as shown in Figs. 8, 9, 10 and 11. Importantly, the jumps $V_p = V_p^{(0)}$ and $V_{\bar p}=V_{\bar p}^{(0)}$ are not affected by this deformation. In its final form, the function $N^{(1)}$ is analytic in $\mathbb{C}\setminus (\bigcup_{i=0}^4 L_i \cup B \cup \partial D_p^{\varepsilon} \cup \partial D_{\bar{p}}^{\varepsilon})$, satisfies the asymptotic condition

$$N^{(1)} = I + O\left(\frac{1}{k}\right), \quad k \to \infty, \tag{4.1}$$

and possesses the following jump discontinuities along the contours $\bigcup_{i=0}^4 L_i \cup B \cup B$ $\partial D_p^{\varepsilon} \cup \partial D_{\bar{p}}^{\varepsilon}$, as shown in Fig. 11:

$$V_{B}^{(1)} = V_{B} = \begin{pmatrix} 0 & \frac{q_{-}}{iq_{o}} \\ \frac{\bar{q}_{-}}{iq_{o}} & 0 \end{pmatrix}, \quad V_{0}^{(1)} = \begin{pmatrix} 1 + r\bar{r} & 0 \\ 0 & \frac{1}{1 + r\bar{r}} \end{pmatrix}, \quad V_{1}^{(1)} = \begin{pmatrix} d^{-\frac{1}{2}} & \frac{d^{\frac{1}{2}}\bar{r}e^{2i\theta t}}{1 + r\bar{r}} \\ 0 & d^{\frac{1}{2}} \end{pmatrix},$$

$$V_{2}^{(1)} = \begin{pmatrix} d^{-\frac{1}{2}} & 0 \\ \frac{d^{\frac{1}{2}}re^{-2i\theta t}}{1 + r\bar{r}} & d^{\frac{1}{2}} \end{pmatrix}, \quad V_{3}^{(1)} = \begin{pmatrix} d^{-\frac{1}{2}} & 0 \\ d^{-\frac{1}{2}}re^{-2i\theta t} & d^{\frac{1}{2}} \end{pmatrix}, \quad V_{4}^{(1)} = \begin{pmatrix} d^{-\frac{1}{2}} & d^{-\frac{1}{2}}\bar{r}e^{2i\theta t} \\ 0 & d^{\frac{1}{2}} \end{pmatrix},$$

$$V_{p}^{(1)} = V_{p}^{(0)}, \quad V_{\bar{p}}^{(1)} = V_{\bar{p}}^{(0)}. \tag{4.2}$$

Second deformation The jump $V_0^{(1)}$ along the contour $L_0 := (-\infty, k_1)$ shown in Fig. 11 can be removed by means of the transformation

$$N^{(2)}(x,t,k) = N^{(1)}(x,t,k)\delta(\xi,k)^{-\sigma_3},$$
(4.3)

where the scalar function $\delta(\xi, k)$ is analytic in $\mathbb{C}\setminus(-\infty, k_1)$ and satisfies the Riemann– Hilbert problem

$$\delta^{+} = \delta^{-} (1 + r\bar{r}), \qquad k \in (-\infty, k_1),$$
 (4.4a)

$$\delta^{+} = \delta^{-} (1 + r\bar{r}), \qquad k \in (-\infty, k_{1}),$$

$$\delta = 1 + O\left(\frac{1}{k}\right), \qquad k \to \infty.$$
(4.4a)

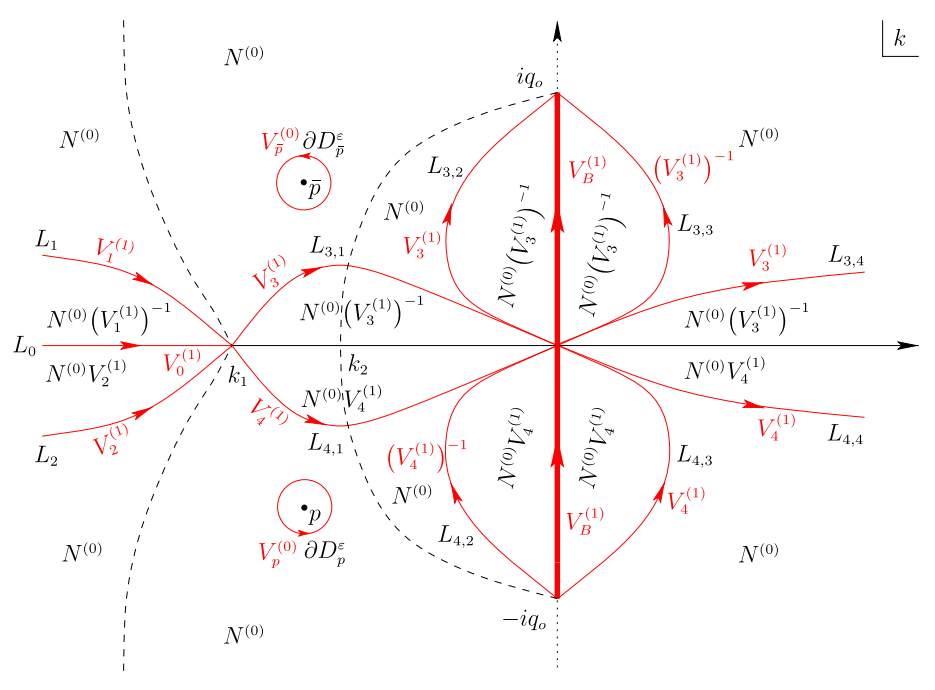


Fig. 8. Plane wave region in the transmission regime: the first stage of the first deformation. A new function $N^{(1)}$ is defined in terms of the solution $N^{(0)}$ of Riemann–Hilbert problem (3.16) via different expressions in different regions of the complex k-plane. This allows us to eliminate the jump of (3.16) along (k_1, ∞) . The jumps $V_p = V_p^{(0)}$ and $V_{\bar{p}} = V_{\bar{p}}^{(0)}$ along the circles $\partial D_{\bar{p}}^{\varepsilon}$ and $\partial D_{\bar{p}}^{\varepsilon}$ are not affected at this stage

In fact, problem (4.4) can be solved explicitly via the Plemeli formulae to yield

$$\delta(\xi, k) = \exp\left\{\frac{1}{2i\pi} \int_{-\infty}^{k_1(\xi)} \frac{\ln\left[1 + r(\nu)\bar{r}(\nu)\right]}{\nu - k} \, d\nu\right\}, \quad k \notin (-\infty, k_1). \tag{4.5}$$

Through transformation (4.3), the jumps of $N^{(1)}$ give rise to corresponding jumps for $N^{(2)}$. As shown in Fig. 12, these jumps occur along the contours $\bigcup_{j=1}^4 L_j \cup B$ and are given by

$$V_{B}^{(2)} = \begin{pmatrix} 0 & \frac{q_{-}}{iq_{o}} \delta^{2} \\ \frac{\bar{q}_{-}}{iq_{o}} \delta^{-2} & 0 \end{pmatrix}, \quad V_{1}^{(2)} = \begin{pmatrix} d^{-\frac{1}{2}} & \frac{d^{\frac{1}{2}} \bar{r} e^{2i\theta t}}{1 + r\bar{r}} \delta^{2} \\ 0 & d^{\frac{1}{2}} \end{pmatrix},$$

$$V_{2}^{(2)} = \begin{pmatrix} d^{-\frac{1}{2}} & 0 \\ \frac{d^{\frac{1}{2}} r e^{-2i\theta t}}{1 + r\bar{r}} \delta^{-2} & d^{\frac{1}{2}} \end{pmatrix},$$

$$V_{3}^{(2)} = \begin{pmatrix} d^{-\frac{1}{2}} & 0 \\ d^{-\frac{1}{2}} r e^{-2i\theta t} \delta^{-2} & d^{\frac{1}{2}} \end{pmatrix}, \quad V_{4}^{(2)} = \begin{pmatrix} d^{-\frac{1}{2}} d^{-\frac{1}{2}} \bar{r} e^{2i\theta t} \delta^{2} \\ 0 & d^{\frac{1}{2}} \end{pmatrix}, \quad (4.6)$$

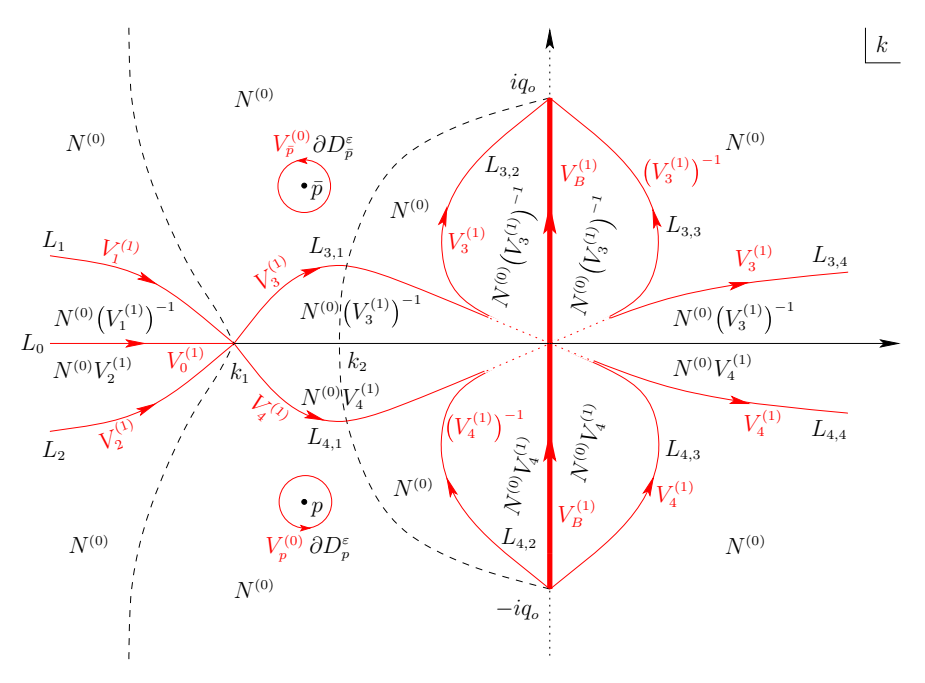


Fig. 9. Plane wave region in the transmission regime: the second stage of the first deformation. In the second quadrant, the function $N^{(1)}$ is defined in terms of $N^{(0)}$ by the same expression both below the contour $L_{3,1}$ and to the right of the contour $L_{3,2}$. Thus, $N^{(1)}$ does not have a jump along the overlapping portion between these two contours (dotted line), allowing one to lift them away from the origin. The same is true for the contour pairs $\{L_{3,3}, L_{3,4}\}$, $\{L_{4,1}, L_{4,2}\}$ and $\{L_{4,3}, L_{4,4}\}$. The jumps along $\partial D_p^{\tilde{\nu}}$ remain unchanged

as well as along the disks $\partial D_p^{\varepsilon}$ and $\partial D_{\bar{p}}^{\varepsilon}$, where they read (modified for the first time)

$$V_{p}^{(2)} = \begin{pmatrix} 1 - \frac{c_{p} \delta^{2}(\xi, k)}{k - p} e^{2i\theta(\xi, p)t} \\ 0 & 1 \end{pmatrix}, \quad V_{\bar{p}}^{(2)} = \begin{pmatrix} 1 & 0 \\ -\frac{c_{\bar{p}} \delta^{-2}(\xi, k)}{k - \bar{p}} e^{-2i\theta(\xi, \bar{p})t} & 1 \end{pmatrix}. \tag{4.7}$$

Finally, the normalization condition (4.5) for $N^{(1)}$ is also satisfied by $N^{(2)}$.

Third deformation The function d(k) can be eliminated from the jump matrices along $\bigcup_{j=1}^4 L_j$ by introducing a new function $N^{(3)}$ defined in terms of $N^{(2)}$ according to Fig. 13. In particular, the jumps of $N^{(3)}$ along the contours $\bigcup_{j=1}^4 L_j \cup B$ are given by

$$V_{B}^{(3)} = \begin{pmatrix} 0 & \frac{q_{-}}{iq_{o}} \delta^{2} \\ \frac{\bar{q}_{-}}{iq_{o}} \delta^{-2} & 0 \end{pmatrix}, \quad V_{1}^{(3)} = \begin{pmatrix} 1 & \frac{\bar{r}e^{2i\theta t}}{1 + r\bar{r}} \delta^{2} \\ 0 & 1 \end{pmatrix}, \quad V_{2}^{(3)} = \begin{pmatrix} 1 & 0 \\ \frac{re^{-2i\theta t}}{1 + r\bar{r}} \delta^{-2} & 1 \end{pmatrix},$$

$$V_{3}^{(3)} = \begin{pmatrix} 1 & 0 \\ re^{-2i\theta t} \delta^{-2} & 1 \end{pmatrix}, \quad V_{4}^{(3)} = \begin{pmatrix} 1 & \bar{r}e^{2i\theta t} \delta^{2} \\ 0 & 1 \end{pmatrix}.$$

$$(4.8)$$

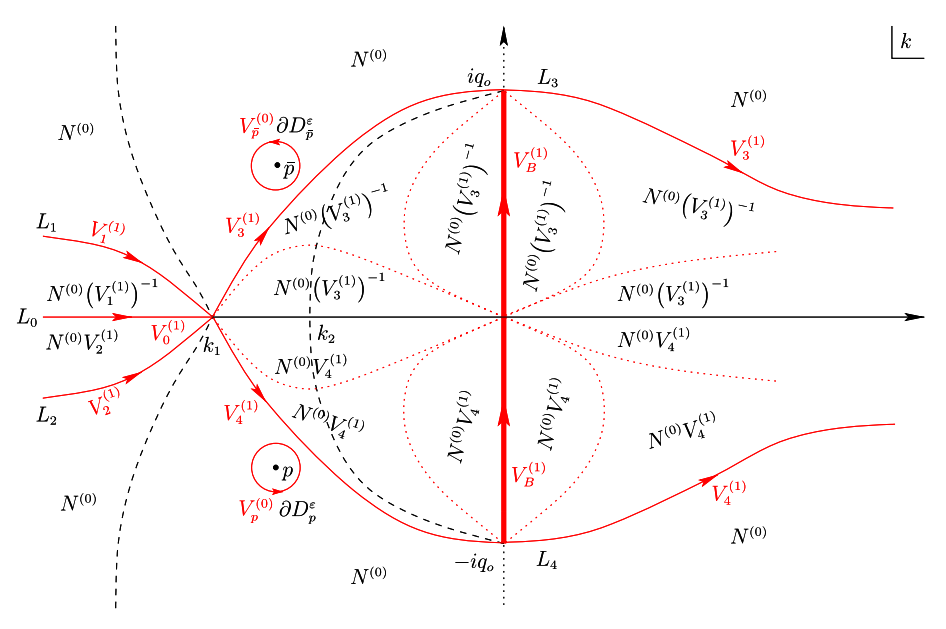


Fig. 10. Plane wave region in the transmission regime: the third stage of the first deformation. Having lifted the jump contours away from the origin as shown in Fig. 9, one can now adjust the definition of $N^{(1)}$ according to the present figure in order to move these jump contours outside the finite region defined by the branch cut B and the dashed line through the stationary point k_2 . This ensures that the relevant jumps occur along contours of appropriate sign for $Re(i\theta)$. The jumps along ∂D_p^E and ∂D_p^E are as before

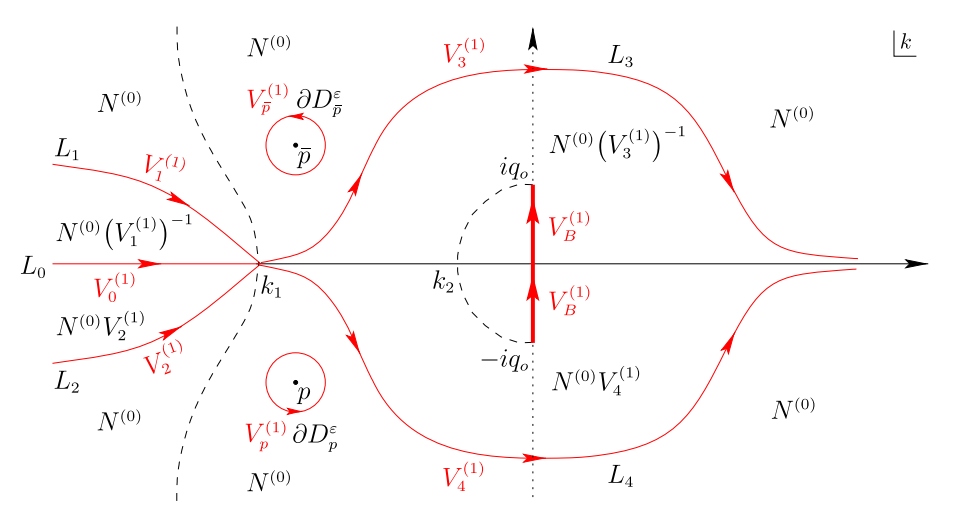


Fig. 11. Plane wave region in the transmission regime: the fourth and final stage of the first deformation. The jump contours L_3 and L_4 have been lifted away from the branch points $\pm iq_o$ similarly to [BM2]. Overall, the jumps along $\partial D_p^{\varepsilon}$ and $\partial D_{\bar{p}}^{\varepsilon}$ have not changed in the transition from $N^{(0)}$ to $N^{(1)}$, i.e. $V_p^{(1)} = V_p^{(0)}$ and $V_{\bar{p}}^{(1)} = V_{\bar{p}}^{(0)}$

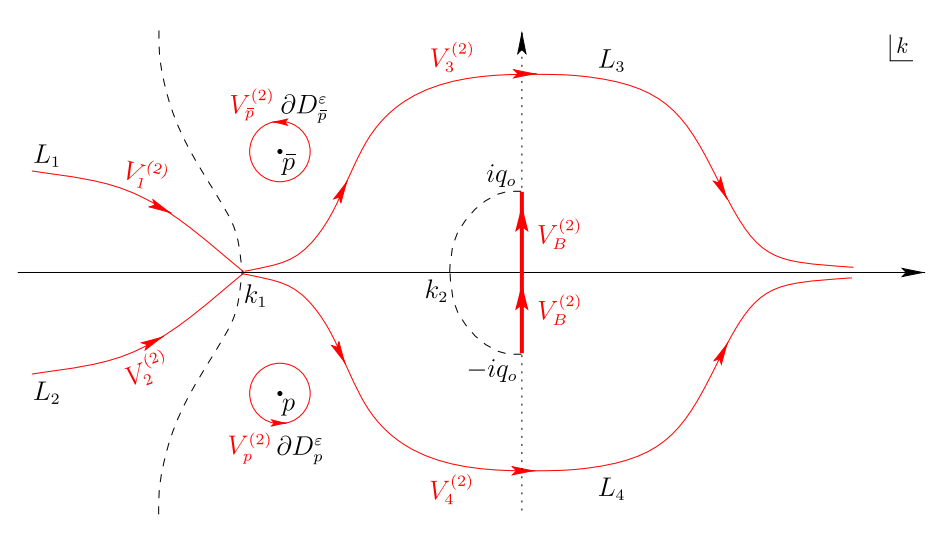


Fig. 12. Plane wave region in the transmission regime: the second deformation

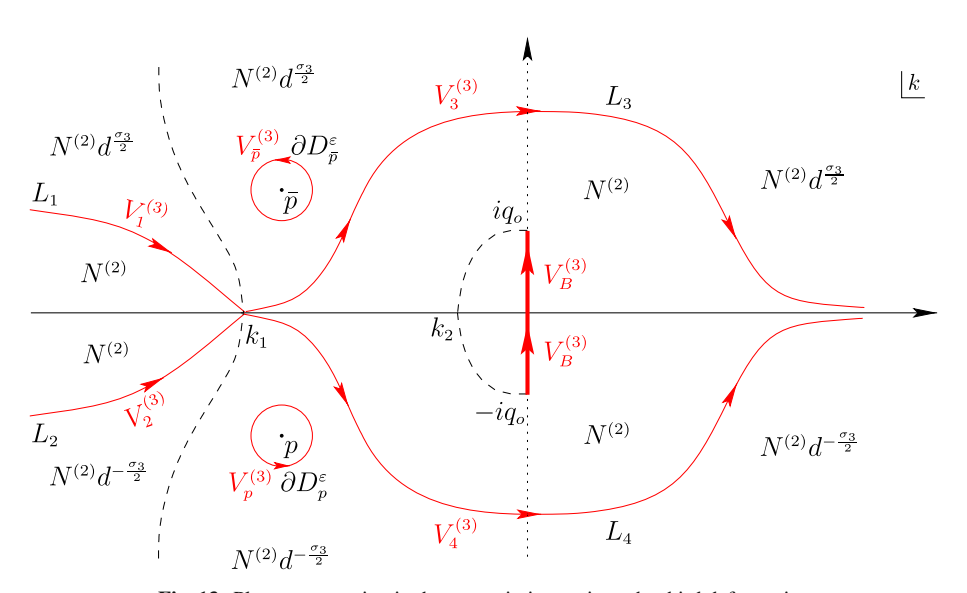


Fig. 13. Plane wave region in the transmission regime: the third deformation

Moreover, noting that $N^{(3)}=N^{(2)}d^{-\frac{\sigma_3}{2}}$ for $k\in D_p^{\varepsilon}$ and $N^{(3)}=N^{(2)}d^{\frac{\sigma_3}{2}}$ for $k\in D_{\vec{p}}^{\varepsilon}$, we obtain

$$V_{p}^{(3)} = \begin{pmatrix} 1 - \frac{c_{p} \delta^{2}(\xi, k) d(k)}{k - p} e^{2i\theta(\xi, p)t} \\ 0 & 1 \end{pmatrix}, V_{\bar{p}}^{(3)} = \begin{pmatrix} 1 & 0 \\ -\frac{c_{\bar{p}} \delta^{-2}(\xi, k) d(k)}{k - \bar{p}} e^{-2i\theta(\xi, \bar{p})t} & 1 \end{pmatrix}.$$

$$(4.9)$$

Fourth deformation Our final goal is to convert the jump along the branch cut B into the *constant* matrix V_B given by (4.2). This can be achieved by means of the global

transformation

$$N^{(4)}(x,t,k) = N^{(3)}(x,t,k)e^{ig(\xi,k)\sigma_3},$$
(4.10)

where the function $g(\xi, k)$ is analytic in $\mathbb{C}\backslash B$ and satisfies the jump condition

$$e^{i(g^++g^-)} = \delta^2, \quad k \in B,$$
 (4.11)

and the normalization condition

$$\frac{g}{\lambda} = O\left(\frac{1}{k}\right), \quad k \to \infty.$$
 (4.12)

Indeed, the jump condition (4.11) implies that the jump of $N^{(4)}$ along B is precisely V_B . Equations (4.11) and (4.12) formulate a Riemann–Hilbert problem for g, which can be solved explicitly to yield

$$g(\xi,k) = \frac{\lambda(k)}{2i\pi^2} \int_{\zeta \in B} \frac{1}{\lambda(\zeta)(\zeta - k)} \int_{-\infty}^{k_1(\xi)} \frac{\ln\left[1 + r(\nu)\bar{r}(\nu)\right]}{\nu - \zeta} d\nu d\zeta, \quad k \notin B. \quad (4.13)$$

Under transformation (4.10), the Riemann–Hilbert problem for $N^{(3)}$ turns into the following Riemann–Hilbert problem for $N^{(4)}$:

$$N^{(4)+} = N^{(4)-}V_B, k \in B, (4.14a)$$

$$N^{(4)+} = N^{(4)-}V_j^{(4)}, \qquad k \in L_j, \ j = 1, 2, 3, 4,$$
 (4.14b)

$$N^{(4)+} = N^{(4)-}V_p^{(4)}, \qquad k \in \partial D_p^{\varepsilon},$$
 (4.14c)

$$N^{(4)+} = N^{(4)-}V_{\bar{p}}^{(4)}, \qquad k \in \partial D_{\bar{p}}^{\varepsilon},$$
 (4.14d)

$$N^{(4)} = \left[I + O\left(\frac{1}{k}\right)\right] e^{ig_{\infty}(\xi)\sigma_3}, \qquad k \to \infty, \tag{4.14e}$$

with the jump V_B given by (4.2) and

$$\begin{split} V_{1}^{(4)} &= \begin{pmatrix} 1 \, \frac{\bar{r} e^{2i(\theta t - g)}}{1 + r\bar{r}} \, \delta^{2} \\ 0 \, & 1 + r\bar{r} \end{pmatrix}, \quad V_{2}^{(4)} = \begin{pmatrix} 1 & 0 \\ \frac{r e^{-2i(\theta t - g)}}{1 + r\bar{r}} \, \delta^{-2} \, 1 \end{pmatrix}, \\ V_{3}^{(4)} &= \begin{pmatrix} 1 & 0 \\ r e^{-2i(\theta t - g)} \delta^{-2} \, 1 \end{pmatrix}, \\ V_{4}^{(4)} &= \begin{pmatrix} 1 \, \bar{r} e^{2i(\theta t - g)} \delta^{2} \\ 0 & 1 \end{pmatrix}, \quad V_{p}^{(4)} &= \begin{pmatrix} 1 - \frac{c_{p} \, \delta^{2}(\xi, k) \, d(k) \, e^{-2ig(\xi, k)}}{k - p} \, e^{2i\theta(\xi, p)t} \\ 0 & 1 \end{pmatrix}, \\ V_{\bar{p}}^{(4)} &= \begin{pmatrix} 1 & 0 \\ -\frac{c_{\bar{p}} \, \delta^{-2}(\xi, k) \, d(k) \, e^{2ig(\xi, k)}}{k - \bar{p}} \, e^{-2i\theta(\xi, \bar{p})t} \, 1 \end{pmatrix}, \end{split}$$

$$(4.15)$$

where the associated jump contours are shown in Fig. 13 and $g_{\infty}(\xi)$ is the limit of $g(\xi, k)$ as $k \to \infty$, i.e.

$$g_{\infty}(\xi) := \lim_{k \to \infty} g(\xi, k) = -\frac{1}{2i\pi^2} \int_{\zeta \in B} \frac{1}{\lambda(\zeta)} \int_{-\infty}^{k_1(\xi)} \frac{\ln\left[1 + r(\nu)\bar{r}(\nu)\right]}{\nu - \zeta} d\nu d\zeta. \quad (4.16)$$

Importantly, expressing g_{∞} in terms of δ and using the symmetries $\overline{\lambda(k)} = \lambda(\overline{k})$ and $\overline{\delta(\xi, k)} = \left[\delta(\xi, \overline{k})\right]^{-1}$, we have that $\overline{g_{\infty}(\xi)} = g_{\infty}(\xi)$, i.e. that $g_{\infty} \in \mathbb{R}$.

Observe that all the jumps of $N^{(4)}$ apart from V_B tend to the identity exponentially fast in the limit $t \to \infty$. Hence, proceeding as in the appendix of [BM2], we find that the contribution of these jumps is of order $O(t^{-1/2})$. Then, starting from the reconstruction formula (3.13) and applying the four successive deformations that lead to $N^{(4)}$, we eventually obtain

$$q(x,t) = -2i \lim_{k \to \infty} \left[k N_{12}^{\mathrm{dom}}(x,t,k) \right] e^{ig_{\infty}(\xi)} + O\left(t^{-\frac{1}{2}}\right), \quad t \to \infty, \tag{4.17}$$

where $N^{\text{dom}}(x, t, k)$ satisfies the dominant component of Riemann–Hilbert problem (4.14), that is

$$N^{\text{dom+}} = N^{\text{dom-}} V_B, \qquad k \in B, \tag{4.18a}$$

$$N^{\text{dom}} = \left[I + O\left(\frac{1}{k}\right)\right] e^{ig_{\infty}(\xi)\sigma_3}, \qquad k \to \infty.$$
 (4.18b)

The dominant problem (4.18) has been extracted from problem (4.14) in a similar way with problem (4.23) of Sect. 4.2. In fact, it is straightforward to verify that N^{dom} is given by the explicit formula

$$N^{\text{dom}} = \frac{1}{2} e^{ig_{\infty}(\xi)\sigma_{3}} \begin{pmatrix} \Lambda(k) + \Lambda^{-1}(k) & -\frac{q_{o}}{\bar{q}_{-}} \left[\Lambda(k) - \Lambda^{-1}(k) \right] \\ -\frac{q_{o}}{q_{-}} \left[\Lambda(k) - \Lambda^{-1}(k) \right] & \Lambda(k) + \Lambda^{-1}(k) \end{pmatrix}, \quad (4.19)$$

where

$$\Lambda(k) := \left(\frac{k - iq_o}{k + iq_o}\right)^{\frac{1}{4}}.\tag{4.20}$$

Expressions (4.17) and (4.19) yield the leading-order asymptotics (2.13) in the range $\xi < v_s$ of the transmission regime $p \in D_1$. We note that, as expected from the fact that the discrete spectrum does not contribute at leading order for $\xi < v_s$, (2.13) is consistent with the result obtained for $\xi < v_o$ in the case of no discrete spectrum analyzed in [BM2].

4.2. The case $\xi = v_s$: soliton on top of a plane wave. The same four deformations that were performed for $\xi < v_s$ yield once again Riemann–Hilbert problem (4.14). In particular, the jumps along $\partial D_p^{\varepsilon}$ and $\partial D_{\bar{p}}^{\varepsilon}$ read

$$V_p^{(4)} = \begin{pmatrix} 1 - \frac{c_p \, \delta^2(v_s, k) \, d(k) \, e^{-2ig(v_s, k)}}{k - p} \, e^{2i\theta(v_s, p)t} \\ 0 & 1 \end{pmatrix},\tag{4.21a}$$

$$V_{\bar{p}}^{(4)} = \begin{pmatrix} 1 & 0 \\ -\frac{c_{\bar{p}} \delta^{-2}(v_s, k) d(k) e^{2ig(v_s, k)}}{k - \bar{p}} e^{-2i\theta(v_s, \bar{p})t} 1 \end{pmatrix}.$$
(4.21b)

However, since $\text{Re}(i\theta)(v_s, p) = \text{Re}(i\theta)(v_s, \bar{p}) = 0$, the time-dependent exponentials involved in the jumps (4.21) are purely oscillatory (as opposed to decaying). That is, contrary to the range $\xi < v_s$, the jumps $V_p^{(4)}$ and $V_{\bar{p}}^{(4)}$ no longer tend to the identity

as $t \to \infty$. Hence, $V_p^{(4)}$ and $V_{\bar{p}}^{(4)}$ are now expected to contribute to the leading-order asymptotics (together, of course, with the jump V_B along the branch cut B, which is constant) and, therefore, they must be included in the dominant component of problem (4.14). Next, we extract the dominant component from the rest of the problem.

Decomposition into dominant and error problems Let $D_{k_1}^{\epsilon}$ be a disk centered at k_1 with radius ϵ sufficiently small so that $D_{k_1}^{\epsilon} \cap \left(B \cup \overline{D_p^{\epsilon} \cup D_{\bar{p}}^{\epsilon}}\right) = \emptyset$. Then, write the solution $N^{(4)}$ of problem (4.14) in the form

$$N^{(4)} = N^{\text{err}} N^{\text{asymp}}, \quad N^{\text{asymp}} = \begin{cases} N^{\text{dom}}, & k \in \mathbb{C} \backslash D_{k_1}^{\epsilon}, \\ N^{k_1}, & k \in D_{k_1}^{\epsilon}, \end{cases}$$
(4.22)

where the components N^{dom} , N^{k_1} and N^{err} are defined as follows:

• The function $N^{\mathrm{dom}}(v_s t, t, k)$ is analytic in $\mathbb{C} \setminus \left(B \cup \partial D_p^{\varepsilon} \cup \partial D_{\bar{p}}^{\varepsilon} \right)$ and satisfies the Riemann–Hilbert problem

$$N^{\text{dom+}} = N^{\text{dom-}} V_B, \qquad k \in B, \tag{4.23a}$$

$$N^{\text{dom+}} = N^{\text{dom-}} V_p^{(4)}, \qquad k \in \partial D_p^{\varepsilon}, \tag{4.23b}$$

$$N^{\mathrm{dom+}} = N^{\mathrm{dom-}} V_{\bar{p}}^{(4)}, \qquad \qquad k \in \partial D_{\bar{p}}^{\varepsilon}, \tag{4.23c}$$

$$N^{\text{dom}} = \left[I + O\left(\frac{1}{k}\right)\right] e^{ig_{\infty}(v_s)\sigma_3}, \qquad k \to \infty, \tag{4.23d}$$

with V_B given by (4.2) and $V_p^{(4)}$, $V_{\bar{p}}^{(4)}$ given by (4.21).

• The function $N^{k_1}(v_s t, t, k)$ is analytic in $D_{k_1}^{\epsilon} \setminus \bigcup_{j=1}^4 L_j$ with jumps

$$N^{k_1+} = N^{k_1-}V_j^{(4)}, \quad k \in \widehat{L}_j := L_j \cap D_{k_1}^{\epsilon}, \quad j = 1, 2, 3, 4.$$
 (4.24)

Note that nothing has been specified about N^{k_1} outside the disk $D_{k_1}^{\epsilon}$.

• The function $N^{\text{err}}(v_s, t, k)$ is analytic in $\mathbb{C}\setminus (\bigcup_{j=1}^4 \widecheck{L}_j \cup \partial D_{k_1}^{\epsilon})$, where $\widecheck{L}_j := L_j \setminus \widehat{L}_j$, and satisfies the Riemann–Hilbert problem

$$N^{\text{err+}} = N^{\text{err-}} V^{\text{err}}, \qquad k \in \bigcup_{j=1}^{4} \widecheck{L}_{j} \cup \partial D_{k_{1}}^{\epsilon},$$
 (4.25a)

$$N^{\text{err}} = I + O\left(\frac{1}{k}\right), \qquad k \to \infty,$$
 (4.25b)

where

$$V^{\text{err}} = \begin{cases} N^{\text{dom}} V_j^{(4)} (N^{\text{dom}})^{-1}, & k \in \widecheck{L}_j, \\ N^{\text{asymp}-} (V_D^{\text{asymp}})^{-1} (N^{\text{asymp}-})^{-1}, & k \in \partial D_{k_1}^{\epsilon}, \end{cases}$$
(4.26)

and V_D^{asymp} is the yet unknown jump of N^{asymp} along the circle $\partial D_{k_1}^\epsilon$.

Under the four successive deformations that lead to problem (4.14), the reconstruction formula (3.13) becomes

$$q(x,t) = -2i \lim_{k \to \infty} k N_{12}^{(4)}(v_s t, t, k) e^{ig_{\infty}(v_s)}, \tag{4.27}$$

where we have also used the fact that δ , $d \to 1$ as $k \to \infty$. This formula combined with the decomposition (4.22) and the asymptotic conditions (4.23d) and (4.25b) implies

$$q(x,t) = -2i \lim_{k \to \infty} k \left[N_{12}^{\text{dom}}(v_s t, t, k) e^{ig_{\infty}(v_s)} + N_{12}^{\text{err}}(v_s t, t, k) \right]. \tag{4.28}$$

The error problem (4.25) is precisely that of the plane wave region in [BM2], since the jumps around p and \bar{p} are not part of this problem. Hence, as shown in [BM2], $\lim_{k\to\infty} kN_{12}^{\rm err} = O(t^{-1/2})$. In turn, we obtain

$$q(x,t) = -2i \lim_{k \to \infty} k N_{12}^{\text{dom}}(v_s t, t, k) e^{ig_{\infty}(v_s)} + O(t^{-\frac{1}{2}}), \quad t \to \infty.$$
 (4.29)

It remains to determine N^{dom} , i.e. to solve the dominant Riemann–Hilbert problem (4.23).

Solution of the dominant problem We begin by converting the jumps along the circles $\partial D_p^{\varepsilon}$ and $\partial D_{\bar{p}}^{\varepsilon}$ back to residue conditions at p and \bar{p} . This is done by reverting transformation (3.14), i.e. by letting

$$M^{\text{dom}} = \begin{cases} N^{\text{dom}} (V_p^{(4)})^{-1}, & k \in D_p^{\varepsilon}, \\ N^{\text{dom}}, & k \in \mathbb{C}^- \setminus \left(B^- \cup \overline{D_p^{\varepsilon}} \right), \\ N^{\text{dom}} (V_{\bar{p}}^{(4)})^{-1}, & k \in D_{\bar{p}}^{\varepsilon}, \\ N^{\text{dom}}, & k \in \mathbb{C}^+ \setminus \left(B^+ \cup \overline{D_p^{\varepsilon}} \right). \end{cases}$$
(4.30)

Then, M^{dom} is the solution of the Riemann–Hilbert problem

$$M^{\text{dom+}} = M^{\text{dom-}} V_B, \qquad k \in B, \tag{4.31a}$$

$$M^{\text{dom}} = \left[I + O\left(\frac{1}{k}\right)\right] e^{ig_{\infty}(v_s)\sigma_3}, \qquad k \to \infty, \tag{4.31b}$$

$$\operatorname{Res}_{k=p} M^{\operatorname{dom}} = \left(0, \rho_p \, M_1^{\operatorname{dom}}(p)\right),\tag{4.31c}$$

$$\operatorname{Res}_{k=\bar{p}} M^{\operatorname{dom}} = \left(\rho_{\bar{p}} M_2^{\operatorname{dom}}(\bar{p}), 0 \right), \tag{4.31d}$$

where M_1^{dom} , M_2^{dom} denote the two columns of M^{dom} and

$$\rho_p = c_p \delta^2(v_s, p) d(p) e^{2i[\theta(v_s, p)t - g(v_s, p)]}, \tag{4.32a}$$

$$\rho_{\bar{p}} = c_{\bar{p}} \delta^{-2}(v_s, \bar{p}) d(\bar{p}) e^{-2i[\theta(v_s, \bar{p})t - g(v_s, \bar{p})]}. \tag{4.32b}$$

In fact, the expressions for ρ_p and $\rho_{\bar{p}}$ can be simplified after noting that the symmetry (see [BM2])

$$\overline{\Psi_{\pm}(x,t,\bar{k})} = -\sigma_* \Psi_{\pm}(x,t,k) \sigma_*, \quad \sigma_* := \begin{pmatrix} 0 & 1 \\ -1 & 0 \end{pmatrix},$$

together with relations (3.10a) and (3.10b) imply $C_{\bar{p}} = -\overline{C_p}$. Then, recalling the Schwarz symmetries $\bar{a}'(\bar{k}) = \overline{a'(k)}$, $d(\bar{k}) = \overline{d(k)}$ and the definitions (3.11a) and (3.11b) of c_p and $c_{\bar{p}}$, we obtain

$$c_{\bar{p}} = -\overline{c_p}. (4.33)$$

Hence, noting in addition that $\theta(\xi, \bar{k}) = \overline{\theta(\xi, k)}$, $g(\xi, \bar{k}) = \overline{g(\xi, k)}$, $\delta(\xi, \bar{k}) = \overline{\delta^{-1}(\xi, k)}$, and since $\theta(v_{\delta}, \bar{p}) \in \mathbb{R}$, we have

$$\rho_{p} = R_{p} e^{2i\theta(v_{s}, p)t}, \quad \rho_{\bar{p}} = -\overline{R_{p}} e^{-2i\theta(v_{s}, p)t}, \quad R_{p} := C_{p} \frac{\delta^{2}(v_{s}, p)e^{-2ig(v_{s}, p)}}{a'(p)}, \quad (4.34)$$

which shows that $\rho_{\bar{p}} = -\overline{\rho_p}$.

We will solve problem (4.31) by decomposing it into discrete and continuous spectrum components via the substitution

$$M^{\text{dom}} = \mathcal{M}^{\text{dom}} W. \tag{4.35}$$

Here, W is the solution of the continuous spectrum component problem

$$W^+ = W^- V_B, \qquad k \in B,$$
 (4.36a)

$$W = \left[I + O\left(\frac{1}{k}\right)\right] e^{ig_{\infty}(v_s)\sigma_3}, \quad k \to \infty, \tag{4.36b}$$

which is nothing but problem (4.18) evaluated at $\xi = v_s$. Therefore,

$$W = \frac{1}{2} e^{ig_{\infty}(v_s)\sigma_3} \begin{pmatrix} \Lambda(k) + \Lambda^{-1}(k) & -\frac{q_o}{q_-} \left[\Lambda(k) - \Lambda^{-1}(k) \right] \\ -\frac{q_o}{q_-} \left[\Lambda(k) - \Lambda^{-1}(k) \right] & \Lambda(k) + \Lambda^{-1}(k) \end{pmatrix}$$
(4.37)

with Λ given by (4.20).

Since det $W \equiv 1 \neq 0$, we can rearrange (4.35) to

$$\mathcal{M}^{\text{dom}} = M^{\text{dom}} W^{-1} \tag{4.38}$$

and hence deduce that \mathcal{M}^{dom} does not have a jump along B, i.e. \mathcal{M}^{dom} is indeed the discrete spectrum component of M^{dom} . Moreover, since M_1^{dom} and W are analytic at p, formula (4.38) and the residue condition (4.31c) imply

$$\operatorname{Res}_{k=p} \mathcal{M}_{1}^{\text{dom}} = -W_{21}(p)\rho_{p} M_{1}^{\text{dom}}(p). \tag{4.39a}$$

Similarly, we find

$$\operatorname{Res}_{k=p} \mathcal{M}_{2}^{\text{dom}} = W_{11}(p)\rho_{p} M_{1}^{\text{dom}}(p), \tag{4.39b}$$

$$\operatorname{Res}_{k=\bar{p}} \mathcal{M}_{1}^{\text{dom}} = W_{22}(\bar{p})\rho_{\bar{p}} M_{2}^{\text{dom}}(\bar{p}) = \overline{W_{11}(p)}\rho_{\bar{p}} M_{2}^{\text{dom}}(\bar{p}), \tag{4.39c}$$

$$\operatorname{Res}_{k=\bar{p}} \mathcal{M}_{2}^{\text{dom}} = -W_{12}(\bar{p})\rho_{\bar{p}} M_{2}^{\text{dom}}(\bar{p}) = \overline{W_{21}(p)}\rho_{\bar{p}} M_{2}^{\text{dom}}(\bar{p}), \tag{4.39d}$$

where in the last two conditions we have also made use of the symmetries

$$W_{22}(\bar{p}) = \overline{W_{11}(p)}, \quad W_{12}(\bar{p}) = -\overline{W_{21}(p)}.$$
 (4.40)

Furthermore, (4.38) in combination with the asymptotic conditions for M^{dom} and W as $k \to \infty$ yield the following asymptotic condition for \mathcal{M}^{dom} :

$$\mathcal{M}^{\text{dom}} = \left(\left[I + O\left(\frac{1}{k}\right) \right] e^{ig_{\infty}(v_s)\sigma_3} \right) \left(\left[I + O\left(\frac{1}{k}\right) \right] e^{ig_{\infty}(v_s)\sigma_3} \right)^{-1}$$
$$= \left[I + O\left(\frac{1}{k}\right) \right] \left[I + O\left(\frac{1}{k}\right) \right]^{-1} = I + O\left(\frac{1}{k}\right), \quad k \to \infty, \tag{4.41}$$

where we note that the $O(\frac{1}{k})$ term possibly involves in some form the exponential $e^{ig_{\infty}(v_s)\sigma_3}$.

In summary, \mathcal{M}^{dom} is analytic for $k \in \mathbb{C} \setminus \{p, \bar{p}\}$, has simple poles at p and \bar{p} with associated residues satisfying (4.39), and satisfies the asymptotic condition (4.41) as $k \to \infty$. Thus, Liouville's theorem implies

$$\mathcal{M}^{\text{dom}} = I + \frac{\underset{k=p}{\text{Res } \mathcal{M}^{\text{dom}}}}{k-p} + \frac{\underset{k=\bar{p}}{\text{Res } \mathcal{M}^{\text{dom}}}}{k-\bar{p}}, \tag{4.42}$$

and hence it only remains to determine the residues of \mathcal{M}^{dom} at p and \bar{p} . In fact, thanks to (4.39) this amounts to computing the corresponding residues of M^{dom} . Combining (4.38), (4.39), (4.40) and (4.42), we find

$$M_{1}^{\text{dom}} = W_{1} + W_{11} \left[-\frac{W_{21}(p)\rho_{p} M_{1}^{\text{dom}}(p)}{k - p} + \frac{\overline{W_{11}(p)}\rho_{\bar{p}} M_{2}^{\text{dom}}(\bar{p})}{k - \bar{p}} \right]$$

$$+ W_{21} \left[\frac{W_{11}(p)\rho_{p} M_{1}^{\text{dom}}(p)}{k - p} + \frac{\overline{W_{21}(p)}\rho_{\bar{p}} M_{2}^{\text{dom}}(\bar{p})}{k - \bar{p}} \right]$$

$$(4.43a)$$

and

$$M_{2}^{\text{dom}} = W_{2} + W_{12} \left[-\frac{W_{21}(p)\rho_{p} M_{1}^{\text{dom}}(p)}{k - p} + \frac{\overline{W_{11}(p)}\rho_{\bar{p}} M_{2}^{\text{dom}}(\bar{p})}{k - \bar{p}} \right]$$

$$+ W_{22} \left[\frac{W_{11}(p)\rho_{p} M_{1}^{\text{dom}}(p)}{k - p} + \frac{\overline{W_{21}(p)}\rho_{\bar{p}} M_{2}^{\text{dom}}(\bar{p})}{k - \bar{p}} \right].$$
 (4.43b)

Since M_1^{dom} is analytic at p, we can evaluate (4.43a) at k = p to obtain

$$M_{1}^{\text{dom}}(p) = W_{1}(p) + \rho_{p} \left[-W_{11}'(p)W_{21}(p) + W_{11}(p)W_{21}'(p) \right] M_{1}^{\text{dom}}(p)$$

$$+ \rho_{\bar{p}} \frac{|W_{11}(p)|^{2} + |W_{21}(p)|^{2}}{p - \bar{p}} M_{2}^{\text{dom}}(\bar{p}).$$

$$(4.44a)$$

Similarly, since M_2^{dom} is analytic at \bar{p} , evaluating (4.43b) at $k = \bar{p}$ and using the symmetries (4.40) (which also apply for W'), we have

$$M_2^{\text{dom}}(\bar{p}) = W_2(\bar{p}) - \rho_p \frac{|W_{11}(p)|^2 + |W_{21}(p)|^2}{p - \bar{p}} M_1^{\text{dom}}(p) + \rho_{\bar{p}} \left[\overline{W'_{11}(p)W_{21}(p) - W'_{21}(p)W_{11}(p)} \right] M_2^{\text{dom}}(\bar{p}).$$
(4.44b)

Equations (4.44) form a system for $M_1^{\text{dom}}(p)$ and $M_2^{\text{dom}}(\bar{p})$, which can be solved to yield

$$M_1^{\text{dom}}(p) = \frac{\mathcal{B}\rho_{\bar{p}}W_2(\bar{p}) + (1 - \bar{\mathcal{A}}\rho_{\bar{p}})W_1(p)}{\mathcal{B}^2\rho_p\rho_{\bar{p}} + (1 - \bar{\mathcal{A}}\rho_{\bar{p}})(1 + \mathcal{A}\rho_p)},$$
(4.45a)

$$M_2^{\text{dom}}(\bar{p}) = \frac{\left(1 + \mathcal{A}\rho_p\right)W_2(\bar{p}) - \mathcal{B}\rho_pW_1(p)}{\mathcal{B}^2\rho_p\rho_{\bar{p}} + \left(1 - \bar{\mathcal{A}}\rho_{\bar{p}}\right)\left(1 + \mathcal{A}\rho_p\right)},\tag{4.45b}$$

where

$$\mathcal{A} = W'_{11}(p)W_{21}(p) - W_{11}(p)W'_{21}(p), \quad \mathcal{B} = \frac{|W_{11}(p)|^2 + |W_{21}(p)|^2}{p - \bar{p}}.$$
 (4.46)

Actually, using formula (4.37), we can simplify A and B to the constants

$$\mathcal{A} = \frac{i\bar{q}_{-}}{2(p^{2} + q_{o}^{2})}, \quad \mathcal{B} = \frac{|p - iq_{o}| + |p + iq_{o}|}{2|p^{2} + q_{o}^{2}|^{\frac{1}{2}}(p - \bar{p})}.$$
 (4.47)

Expressions (4.45) combined with (4.39) yield the residues of \mathcal{M}^{dom} at p and \bar{p} , and hence \mathcal{M}^{dom} itself via formula (4.42).

Having determined \mathcal{M}^{dom} , we return to the reconstruction formula (4.29) and note that transformations (4.30) and (4.38) imply

$$q(x,t) = -2i \lim_{k \to \infty} k \left(\mathcal{M}^{\text{dom}} W \right)_{12} e^{ig_{\infty}(v_s)} + O\left(t^{-\frac{1}{2}}\right), \quad t \to \infty.$$
 (4.48)

Furthermore, by the asymptotic conditions (4.36b) and (4.41) we have

$$W = e^{ig_{\infty}(v_s)\sigma_3} + \frac{w}{k} + O\left(\frac{1}{k^2}\right), \quad \mathcal{M}^{\text{dom}} = I + \frac{\mu}{k} + O\left(\frac{1}{k^2}\right), \quad k \to \infty, \quad (4.49)$$

where the matrix-valued functions w and μ may depend on x and t but not on k. Thus,

$$\left(\mathcal{M}^{\text{dom}}W\right)_{12} = \frac{w_{12} + \mu_{12} e^{-ig_{\infty}(v_s)}}{k} + O\left(\frac{1}{k^2}\right), \quad k \to \infty.$$
 (4.50)

Hence, noting that $w_{12} = \frac{iq_-}{2} e^{ig_\infty(v_s)}$ by formula (4.37), we obtain

$$q(x,t) = e^{2ig_{\infty}(v_s)}q_{-} - 2i\mu_{12} + O(t^{-\frac{1}{2}}), \quad t \to \infty.$$
 (4.51)

Moreover, matching the second expansion in (4.49) with the large-k expansion of (4.42), we infer

$$\mu_{12} = \left(\underset{k=p}{\text{Res }} \mathcal{M}_2^{\text{dom}}\right)^{(1)} + \left(\underset{k=\bar{p}}{\text{Res }} \mathcal{M}_2^{\text{dom}}\right)^{(1)}.$$
 (4.52)

Thus, using successively (4.39), (4.45) and (4.40), we find

$$\mu_{12} = \frac{\left(1 - \bar{\mathcal{A}}\rho_{\bar{p}}\right)\rho_{p}W_{11}(p)^{2} - \left(1 + \mathcal{A}\rho_{p}\right)\rho_{\bar{p}}\overline{W_{21}(p)}^{2} - 2\mathcal{B}\rho_{p}\rho_{\bar{p}}W_{11}(p)\overline{W_{21}(p)}}{\mathcal{B}^{2}\rho_{p}\rho_{\bar{p}} + \left(1 - \bar{\mathcal{A}}\rho_{\bar{p}}\right)\left(1 + \mathcal{A}\rho_{p}\right)}.$$
(4.53)

Substituting for W via (4.37) and inserting the resulting expression in (4.51), we conclude that

$$q(x,t) = q_{pw}(v_s) - \frac{i}{2} e^{2ig_{\infty}(v_s)} \left[\mathcal{B}^2 \rho_p \rho_{\bar{p}} + \left(1 - \bar{\mathcal{A}} \rho_{\bar{p}} \right) \left(1 + \mathcal{A} \rho_p \right) \right]^{-1}$$

$$\left\{ \left(1 - \bar{\mathcal{A}} \rho_{\bar{p}} \right) \rho_p \left[\Lambda(p) + \Lambda^{-1}(p) \right]^2$$

$$- \left(1 + \mathcal{A} \rho_p \right) \rho_{\bar{p}} \frac{q_-}{\bar{q}_-} \left[\overline{\Lambda(p) - \Lambda^{-1}(p)} \right]^2$$

$$+ 2\mathcal{B} \rho_p \rho_{\bar{p}} \frac{q_o}{\bar{q}_-} \left[\Lambda(p) + \Lambda^{-1}(p) \right] \left[\overline{\Lambda(p) - \Lambda^{-1}(p)} \right] \right\}$$

$$+ O(t^{-\frac{1}{2}}), \quad t \to \infty, \tag{4.54}$$

where $q_{\mathrm{pw}}(v_s)$ is the plane wave (2.14) evaluated at $\xi = v_s$, the quantities Λ , \mathcal{A} , \mathcal{B} , ρ_p , $\rho_{\bar{p}}$ are given by (4.20), (4.47), (4.34) and the real constant $g_{\infty}(v_s)$ is obtained by evaluating (4.16) at $\xi = v_s$. In fact, setting

$$\Lambda_1 := \Lambda(p) + \Lambda^{-1}(p), \quad \Lambda_2 := \overline{\Lambda(p) - \Lambda^{-1}(p)}, \tag{4.55}$$

and substituting for ρ_p , $\rho_{\bar{p}}$ via (4.34) turns the leading-order asymptotics (4.54) into the form (2.15)–(2.16) given in Theorem 2.1.

4.3. The range $v_s < \xi < v_o$: plane wave with a phase shift. The analysis in this range is similar to the one for $\xi < v_s$. Indeed, under the same series of deformations as in Sect. 4.1, Riemann–Hilbert problem (3.16) can be transformed once again into Riemann–Hilbert problem (4.14). We note, in particular, that, since $p \in D_1$, for $v_s < \xi < v_o$ the point p lies inside the *unbounded* region of positive sign to the left of the stationary point k_1 (the unbounded region in white inside the third quadrant of the second frame of Fig. 6). Thus, all four stages of the first deformation for $\xi < v_s$ can be repeated for $v_s < \xi < v_o$ in a way that leaves the jump along $\partial D_p^{\varepsilon}$ invariant. By symmetry, the same is true for the jump along $\partial D_p^{\varepsilon}$. Importantly, we shall see later that this is not the case for $p \in D_3$ (transmission/wake regime).

An important difference between the ranges $(-\infty, v_s)$ and (v_s, v_o) , however, is that in the latter case the jumps $V_p^{(4)}$ and $V_{\bar{p}}^{(4)}$ defined by (4.15) grow exponentially as $t \to \infty$, since $\text{Re}(i\theta)(\xi,p)>0$ and $\text{Re}(i\theta)(\xi,\bar{p})<0$ for all $\xi>v_s$. This is to be contrasted with the range $(-\infty,v_s)$, where we recall that these jumps decayed exponentially to the identity and hence could be immediately neglected from the dominant Riemann–Hilbert problem. Nevertheless, it turns out that the jumps along $\partial D_{\bar{p}}^{\varepsilon}$ and $\partial D_{\bar{p}}^{\varepsilon}$ still do not contribute to the leading-order asymptotics. Along the lines of [DKKZ], this can be seen by applying the following additional transformation to problem (4.14):

$$\widetilde{N}^{(4)} = \begin{cases} N^{(4)} n^{\sigma_3}, & k \in \mathbb{C} \setminus \left(\overline{D_p^{\varepsilon}} \cup \overline{D_{\bar{p}}^{\varepsilon}} \right), \\ N^{(4)} J_p n^{\sigma_3}, & k \in D_p^{\varepsilon}, \\ N^{(4)} J_{\bar{p}} n^{\sigma_3}, & k \in D_{\bar{p}}^{\varepsilon}, \end{cases}$$

$$(4.56a)$$

where n(k) is the piecewise-defined function

$$n(k) = \begin{cases} \frac{k - \bar{p}}{k - p}, & k \in \mathbb{C} \setminus \left(\overline{D_p^{\varepsilon}} \cup \overline{D_{\bar{p}}^{\varepsilon}}\right), \\ k - \bar{p}, & k \in D_p^{\varepsilon}, \\ \frac{1}{k - p}, & k \in D_{\bar{p}}^{\varepsilon}, \end{cases}$$
(4.56b)

and the matrices $J_p(\xi, k)$ and $J_{\bar{p}}(\xi, k)$ are given by

$$J_{p}(\xi,k) = \begin{pmatrix} \frac{1 - \frac{n^{2}(p)}{n^{2}(k)}}{k - p} & c_{p} d(k)\delta^{2}(\xi,k)e^{2i[\theta(\xi,p)t - g(\xi,k)]} \\ - \frac{n^{2}(p) e^{-2i[\theta(\xi,p)t - g(\xi,k)]}}{c_{p} d(k)\delta^{2}(\xi,k) (k - \bar{p})^{2}} & k - p \end{pmatrix},$$

$$(4.56c)$$

$$J_{\bar{p}}(\xi,k) = \begin{pmatrix} k - \bar{p} & -\frac{e^{2i[\theta(\xi,\bar{p})t - g(\xi,k)]}}{n^2(\bar{p})c_{\bar{p}}d(k)\delta^{-2}(\xi,k)(k-p)^2} \\ c_{\bar{p}}d(k)\delta^{-2}(\xi,k)e^{-2i[\theta(\xi,\bar{p})t - g(\xi,k)]} & \frac{1 - \frac{n^2(k)}{n^2(\bar{p})}}{k - \bar{p}} \end{pmatrix}.$$

$$(4.56d)$$

Note importantly that J_p is analytic in D_p^{ε} since the singularity of its 11-element at k=p is removable. Similarly, $J_{\bar{p}}$ is analytic in $D_{\bar{p}}^{\varepsilon}$. Therefore, $\widetilde{N}^{(4)}$ inherits the analyticity of $N^{(4)}$ and satisfies the following Riemann–Hilbert problem:

$$\widetilde{N}^{(4)+} = \widetilde{N}^{(4)-} \widetilde{V}_R^{(4)}, \qquad k \in B,$$
(4.57a)

$$\widetilde{N}^{(4)+} = \widetilde{N}^{(4)-} \widetilde{V}_{j}^{(4)}, \qquad k \in L_{j}, \ j = 1, 2, 3, 4,$$
 (4.57b)

$$\widetilde{N}^{(4)+} = \widetilde{N}^{(4)-} \widetilde{V}_p^{(4)}, \qquad k \in \partial D_p^{\varepsilon}, \tag{4.57c}$$

$$\widetilde{N}^{(4)+} = \widetilde{N}^{(4)-} \widetilde{V}_{\bar{p}}^{(4)}, \qquad k \in \partial D_{\bar{p}}^{\varepsilon}, \tag{4.57d}$$

$$\widetilde{N}^{(4)} = \left[I + O\left(\frac{1}{k}\right)\right] e^{ig_{\infty}(\xi)\sigma_3}, \qquad k \to \infty, \tag{4.57e}$$

with g_{∞} defined by (4.16) and

$$\widetilde{V}_{B}^{(4)} = \begin{pmatrix} 0 & \frac{q_{-}}{iq_{o}} n^{-2} \\ \frac{\bar{q}_{-}}{iq_{o}} n^{2} & 0 \end{pmatrix},
\widetilde{V}_{1}^{(4)} = \begin{pmatrix} 1 & \frac{\bar{r}}{\delta^{2} n^{-2} e^{-2ig}} e^{2i\theta t} \\ 0 & 1 + r\bar{r} & 1 \end{pmatrix}, \quad \widetilde{V}_{2}^{(4)} = \begin{pmatrix} 1 & 0 \\ \frac{r\delta^{-2} n^{2} e^{2ig}}{1 + r\bar{r}} e^{-2i\theta t} & 1 \end{pmatrix},
\widetilde{V}_{3}^{(4)} = \begin{pmatrix} 1 & 0 \\ r\delta^{-2} n^{2} e^{2ig} e^{-2i\theta t} & 1 \end{pmatrix}, \widetilde{V}_{4}^{(4)} = \begin{pmatrix} 1 & \bar{r}\delta^{2} n^{-2} e^{-2ig} e^{2i\theta t} \\ 0 & 1 \end{pmatrix},
\widetilde{V}_{p}^{(4)} = \begin{pmatrix} 1 & 0 \\ -\frac{n^{2}(p)\delta^{-2}(\xi, k)e^{2ig(\xi, k)}}{c_{p} d(k) (k - p)} e^{-2i\theta(\xi, p)t} & 1 \end{pmatrix},
\widetilde{V}_{\bar{p}}^{(4)} = \begin{pmatrix} 1 & -\frac{n^{-2}(\bar{p})\delta^{2}(\xi, k)e^{-2ig(\xi, k)}}{c_{\bar{p}} d(k) (k - \bar{p})} e^{2i\theta(\xi, \bar{p})t} \\ 0 & 1 \end{pmatrix}.$$

$$(4.58)$$

All the jumps of $\widetilde{N}^{(4)}$ with the exception of $\widetilde{V}_B^{(4)}$ tend to the identity exponentially fast as $t\to\infty$. Importantly, as a result of transformation (4.56), this includes the jumps $\widetilde{V}_p^{(4)}$ and $\widetilde{V}_{\bar{p}}^{(4)}$. Hence, we anticipate that the leading-order contribution of problem (4.57)

comes from the jump $\widetilde{V}_{B}^{(4)}$. As this jump depends on k through the function n, prior to decomposing problem (4.57) into dominant and error components we employ yet one more transformation that converts $\widetilde{V}_{B}^{(4)}$ into the constant jump V_{B} . Specifically, we let

$$\widetilde{N}^{(5)}(x,t,k) = \widetilde{N}^{(4)}(x,t,k)e^{i\widetilde{g}(k)\sigma_3},$$
(4.59)

where the function $\widetilde{g}(k)$ is analytic in $\mathbb{C}\backslash B$ and satisfies the Riemann–Hilbert problem

$$e^{i(\widetilde{g}^+ + \widetilde{g}^-)} = n^{-2}, \qquad k \in B, \tag{4.60a}$$

$$\frac{\widetilde{g}}{\lambda} = O\left(\frac{1}{k}\right), \qquad k \to \infty. \tag{4.60b}$$

The above problem can be solved explicitly via Plemelj's formulae to yield

$$\widetilde{g}(k) = -\frac{\lambda(k)}{\pi} \int_{\zeta \in B} \frac{\ln\left(\frac{\zeta - \overline{p}}{\zeta - p}\right)}{\lambda(\zeta) \left(\zeta - k\right)} d\zeta, \quad k \notin B.$$
(4.61)

Note that \widetilde{g} does not depend on ξ . Combining problems (4.57) and (4.60), we obtain the following Riemann–Hilbert problem for $\widetilde{N}^{(5)}$:

$$\widetilde{N}^{(5)+} = \widetilde{N}^{(5)-} V_B, \qquad k \in B, \tag{4.62a}$$

$$\widetilde{N}^{(5)+} = \widetilde{N}^{(5)-} \widetilde{V}_i^{(5)}, \qquad k \in L_j, \ j = 1, 2, 3, 4,$$
 (4.62b)

$$\widetilde{N}^{(5)+} = \widetilde{N}^{(5)-} \widetilde{V}_p^{(5)}, \qquad k \in \partial D_p^{\varepsilon}, \tag{4.62c}$$

$$\widetilde{N}^{(5)+} = \widetilde{N}^{(5)-} \widetilde{V}_{\bar{p}}^{(5)}, \qquad k \in \partial D_{\bar{p}}^{\varepsilon}, \tag{4.62d}$$

$$\widetilde{N}^{(5)} = \left[I + O\left(\frac{1}{k}\right)\right] e^{i\left[g_{\infty}(\xi) + \widetilde{g}_{\infty}\right]\sigma_{3}}, \qquad k \to \infty, \tag{4.62e}$$

where V_B is defined by (4.2), the remaining jumps are given by

$$\widetilde{V}_{1}^{(5)} = \begin{pmatrix} 1 & \frac{\bar{r} \, \delta^{2} n^{-2} e^{-2i(g+\tilde{g})}}{1 + r\bar{r}} \, e^{2i\theta t} \\ 0 & 1 \end{pmatrix}, \quad \widetilde{V}_{2}^{(5)} = \begin{pmatrix} 1 & 0 \\ \frac{r \, \delta^{-2} n^{2} e^{2i(g+\tilde{g})}}{1 + r\bar{r}} \, e^{-2i\theta t} \, 1 \end{pmatrix}, \\
\widetilde{V}_{3}^{(5)} = \begin{pmatrix} 1 & 0 \\ r \, \delta^{-2} n^{2} e^{2i(g+\tilde{g})} \, e^{-2i\theta t} \, 1 \end{pmatrix}, \widetilde{V}_{4}^{(5)} = \begin{pmatrix} 1 \, \bar{r} \, \delta^{2} n^{-2} e^{-2i(g+\tilde{g})} e^{2i\theta t} \\ 0 & 1 \end{pmatrix}, \\
\widetilde{V}_{p}^{(5)} = \begin{pmatrix} 1 & 0 \\ -\frac{n^{2}(p) \delta^{-2}(\xi, k) e^{2i[g(\xi, k) + \tilde{g}(k)]}}{c_{p} \, d(k) \, (k - p)} \, e^{-2i\theta(\xi, p)t} \, 1 \end{pmatrix}, \\
\widetilde{V}_{\bar{p}}^{(5)} = \begin{pmatrix} 1 & -\frac{n^{-2}(\bar{p}) \delta^{2}(\xi, k) e^{-2i[g(\xi, k) + \tilde{g}(k)]}}{c_{\bar{p}} \, d(k) \, (k - \bar{p})} \, e^{2i\theta(\xi, \bar{p})t} \\ 0 & 1 \end{pmatrix}, \quad (4.63)$$

the real quantity $g_{\infty}(\xi)$ is defined by (4.16), and the real constant \widetilde{g}_{∞} is the O(1) term of the expansions of $\widetilde{g}(k)$ as $k \to \infty$, i.e.

$$\widetilde{g}_{\infty} = \frac{1}{\pi} \int_{\zeta \in B} \frac{\ln\left(\frac{\zeta - \bar{p}}{\zeta - p}\right)}{\lambda(\zeta)} d\zeta. \tag{4.64}$$

At leading order, the jumps of problem (4.62) are the same with those of problem (4.14). Indeed, along B the jump of both problems is equal to V_B , while the remaining jumps in both cases tend to the identity as $t \to \infty$. Thus, at leading order, the only difference between the two problems is the presence of the constant phase \tilde{g}_{∞} in the normalization condition of problem (4.62). Therefore, noting that under transformations (4.56) and (4.59) the reconstruction formula (4.27) becomes

$$q(x,t) = -2i \lim_{k \to \infty} k \widetilde{N}_{12}^{(5)}(x,t,k) e^{i[g_{\infty}(\xi) + \widetilde{g}_{\infty}]}, \tag{4.65}$$

we conclude that the leading-order asymptotics in the range $v_s < \xi < v_o$ is equal to the plane wave (2.13) up to a *constant phase shift* of $2\tilde{g}_{\infty}$, i.e.

$$q(x,t) = e^{2i[g_{\infty}(\xi) + \widetilde{g}_{\infty}]} q_{-} + O\left(t^{-\frac{1}{2}}\right), \quad t \to \infty.$$

$$(4.66)$$

This result shows that the byproduct of the interaction of the plane wave emerging for $\xi < v_s$ with the soliton arising for $\xi = v_s$ is the constant phase shift $2\widetilde{g}_{\infty}$ for $v_s < \xi < v_o$. In fact, switching to the uniformization variable $z(k) = k + \lambda(k)$, we can compute the integral (4.64) via Cauchy's residue theorem and thereby obtain \widetilde{g}_{∞} in the explicit form

$$\widetilde{g}_{\infty} = 2\arg\left[p + \lambda(p)\right],$$
(4.67)

which corresponds to a phase shift of $4\arg [p + \lambda(p)]$ for the plane wave (4.66), in perfect agreement with the inverse scattering transform result of [BK]. In turn, the leading-order asymptotics (4.66) assume the form (2.17) of Theorem 2.1.

4.4. The range $v_o < \xi < 0$: modulated elliptic wave. In this range, the stationary points k_1 and k_2 of the phase function θ are complex [recall (3.17)]. This has a direct impact on the asymptotic analysis of Riemann–Hilbert problem (3.16), since the deformations used for $\xi < v_o$ (where k_1 and k_2 are real) are no longer effective.

First, second and third deformation The first deformation consists of switching from the solution $N^{(0)}$ of problem (3.16) to the function $N^{(1)}$ defined in terms of $N^{(0)}$ by Fig. 14. This step is very similar to the first stage of the first deformation in the plane wave region $\xi < v_s$ (recall Fig. 8) apart from the fact that the change of factorization of the jump along the real axis now takes place at the point k_o , which is yet to be determined, instead of the stationary point k_1 . The remaining three stages of the first deformation that were performed for $\xi < v_s$ (recall Figs. 9, 10 and 11) can also be carried out here, eventually allowing us to lift the jump contours L_j , j=1,2,3,4, away from the origin as well as from the branch points $\pm iq_o$. Importantly, the fact that $p \in D_1$ allows us to perform the first deformation without modifying the jumps along $\partial D_p^{\varepsilon}$ and $\partial D_{\bar{p}}^{\varepsilon}$, since the various transformations can be adjusted so that the disks $\overline{D_p^{\varepsilon}}$ and $\overline{D_p^{\varepsilon}}$ always lie in regions where $N^{(1)} = N^{(0)}$.

The second and the third deformation are identical to the corresponding ones in the plane wave region $\xi < v_s$, leading to the function $N^{(3)}(x, t, k)$, which is analytic in

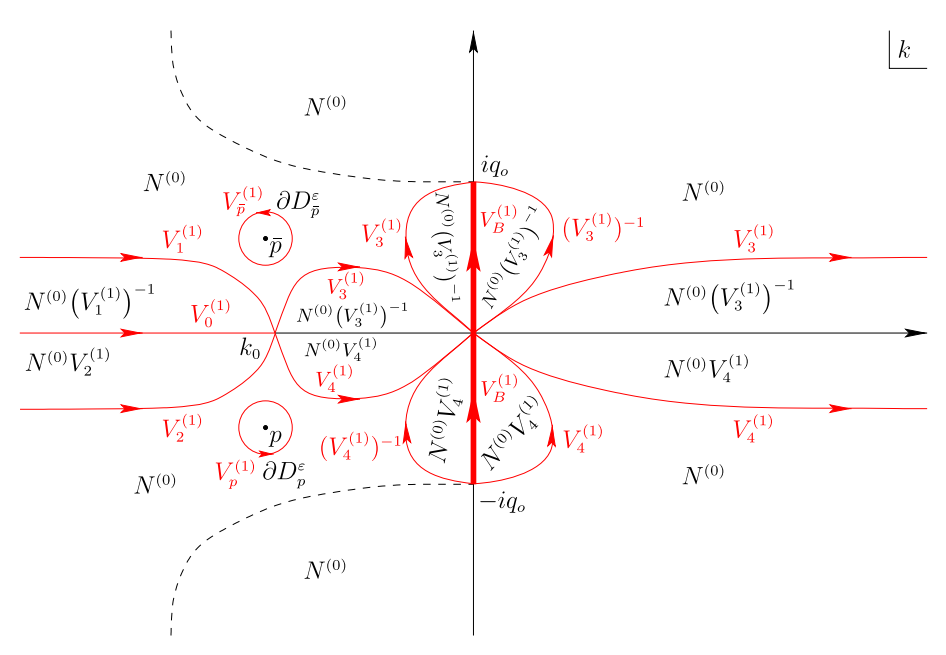


Fig. 14. Modulated elliptic wave region in the transmission regime: the first stage of the first deformation. Since $p \in D_1$, it is possible to choose the disks $\overline{D_p^{\varepsilon}}$ and $\overline{D_{\bar{p}}^{\varepsilon}}$ to always lie in regions where $N^{(1)} = N^{(0)}$

 $\mathbb{C}\setminus \left(\bigcup_{j=1}^4 L_j \cup B \cup \partial D_p^{\varepsilon} \cup \partial D_{\bar{p}}^{\varepsilon}\right)$ and satisfies the Riemann–Hilbert problem

$$N^{(3)+} = N^{(3)-}V_R^{(3)}, k \in B, (4.68a)$$

$$N^{(3)+} = N^{(3)-}V_j^{(3)}, k \in L_j, \ j = 1, 2, 3, 4, (4.68b)$$

$$N^{(3)+} = N^{(3)-}V_p^{(3)}, \qquad k \in \partial D_p^{\varepsilon},$$
 (4.68c)

$$N^{(3)+} = N^{(3)-}V_{\bar{p}}^{(3)}, \qquad k \in \partial D_{\bar{p}}^{\varepsilon},$$
 (4.68d)

$$N^{(3)} = I + O\left(\frac{1}{k}\right), \qquad k \to \infty, \tag{4.68e}$$

where the contours L_j are depicted in Fig. 15 and the relevant jumps are given by (4.8) and (4.9) but with the function $\delta(\xi, k)$ now modified to

$$\delta(\xi, k) = \exp\left\{\frac{1}{2i\pi} \int_{-\infty}^{k_o(\xi)} \frac{\ln\left[1 + r(\nu)\bar{r}(\nu)\right]}{\nu - k} d\nu\right\}, \quad k \notin (-\infty, k_o). \tag{4.69}$$

Importantly, we note that the jump $V_3^{(3)}$ grows exponentially as $t \to \infty$ along the portion of the contour L_3 colored in green in Fig. 15, i.e. along the portion of L_3 that connects k_o with the dashed curve $\operatorname{Re}(i\theta)=0$ lying in the second quadrant of the complex k-plane. The same is true for the jump $V_4^{(3)}$ and the green-colored portion of the contour L_4 that joins k_o with the dashed curve $\operatorname{Re}(i\theta)=0$ in the third quadrant of the complex k-plane. This growth, which was not present for $\xi < v_o$, can be removed with the help of appropriate factorizations and a *time-dependent* version of transformation (4.10), as shown in the course of the following two deformations.

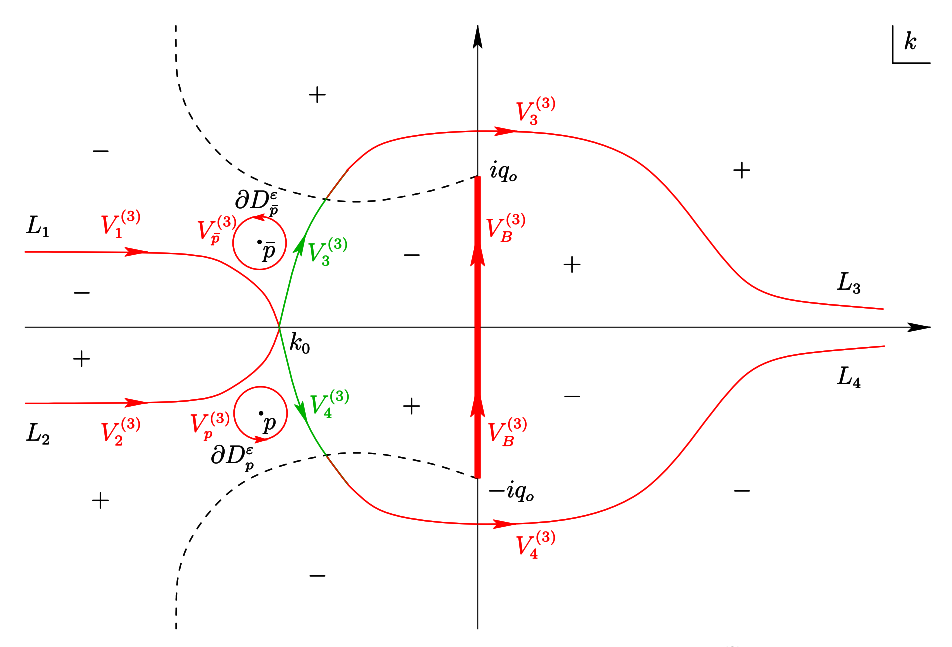


Fig. 15. Modulated elliptic wave region in the transmission regime: the jumps of $N^{(3)}$. As $t \to \infty$, the jumps $V_3^{(3)}$ and $V_4^{(3)}$ grow exponentially along the parts of the contours L_3 and L_4 connecting k_o with the curve $\text{Re}(i\theta) = 0$ (dashed). Moreover, like in the first deformation (see Fig. 14), the deformed contours do not interfere with the disks $\overline{D_p^E}$ and $\overline{D_p^E}$, leaving the corresponding jumps unaffected

Fourth deformation The jumps $V_3^{(3)}$ and $V_4^{(3)}$ can be factorized in the form

$$V_3^{(3)} = V_5^{(4)} V_7^{(4)} V_5^{(4)}, \quad V_4^{(3)} = V_6^{(4)} V_8^{(4)} V_6^{(4)},$$
 (4.70)

where

$$V_{5}^{(4)} = \begin{pmatrix} 1 & \frac{\delta^{2}}{r} e^{2i\theta t} \\ 0 & 1 \end{pmatrix}, \qquad V_{6}^{(4)} = \begin{pmatrix} 1 & 0 \\ \frac{1}{r\delta^{2}} e^{-2i\theta t} & 1 \end{pmatrix},$$

$$V_{7}^{(4)} = \begin{pmatrix} 0 & -\frac{\delta^{2}}{r} e^{2i\theta t} \\ \frac{r}{\delta^{2}} e^{-2i\theta t} & 0 \end{pmatrix}, \qquad V_{8}^{(4)} = \begin{pmatrix} 0 & \bar{r} \delta^{2} e^{2i\theta t} \\ -\frac{1}{r\delta^{2}} e^{-2i\theta t} & 0 \end{pmatrix}. \tag{4.71}$$

The advantage of the above factorization is that the matrices $V_5^{(4)}$ and $V_6^{(4)}$ each involve only one exponential and hence they have a definitive behavior as $t \to \infty$. In particular, in this limit $V_5^{(4)}$ and $V_6^{(4)}$ tend to the identity in regions of negative and positive sign of $\operatorname{Re}(i\theta)$ respectively. On the other hand, the matrices $V_7^{(4)}$ and $V_8^{(4)}$ still involve both of the exponentials $e^{\pm 2i\theta t}$ and so it is not possible to take their limit as $t \to \infty$. However, contrary to the original jumps $V_3^{(3)}$ and $V_4^{(3)}$, the matrices $V_7^{(4)}$ and $V_8^{(4)}$ are antidiagonal. This fact turns out to be crucial, as we will see in the fifth deformation below.

Using the factorization (4.70), we switch from $N^{(3)}$ to $N^{(4)}$ as shown in Fig. 16. By this definition, $N^{(4)}(x, t, k)$ is analytic in $\mathbb{C}\setminus \left(\bigcup_{j=1}^4 L_j \cup B \cup \partial D_p^\varepsilon \cup \partial D_{\bar{p}}^\varepsilon\right)$ and satisfies

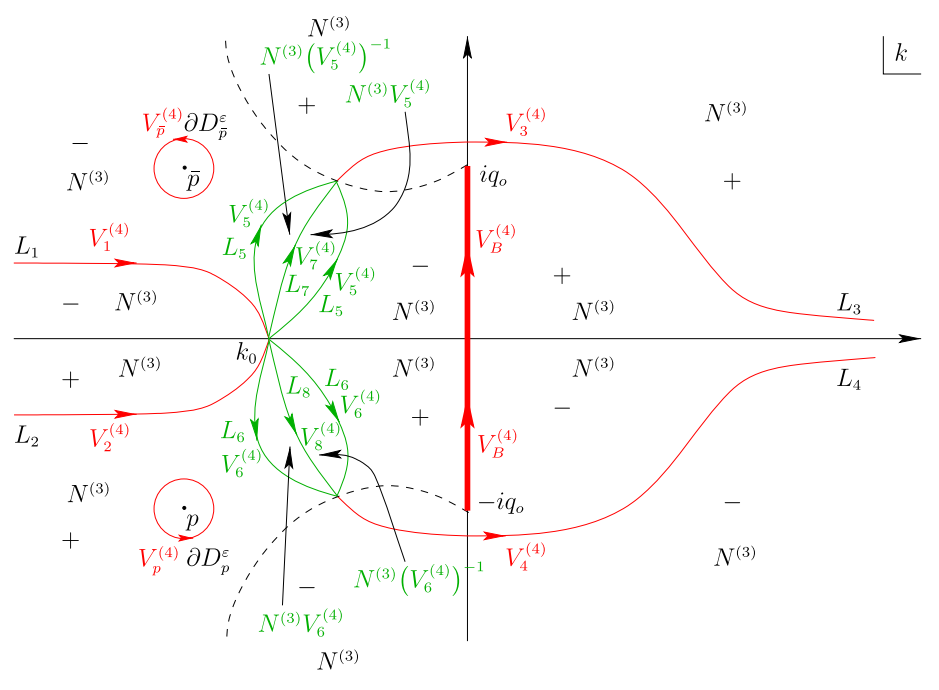


Fig. 16. Modulated elliptic wave region in the transmission regime: the fourth deformation. The various jump contours have been chosen so as not to interfere with the disks $\overline{D}^{arepsilon}_p$ and $\overline{D}^{arepsilon}_{ar{p}}$

the following Riemann-Hilbert problem:

$$N^{(4)+} = N^{(4)-}V_R^{(4)}, k \in B, (4.72a)$$

$$N^{(4)+} = N^{(4)-}V_B^{(4)}, k \in B, (4.72a)$$

$$N^{(4)+} = N^{(4)-}V_j^{(4)}, k \in L_j, j = 1, \dots, 8, (4.72b)$$

$$N^{(4)+} = N^{(4)-}V_j^{(4)}, k \in AD^{\varepsilon} (4.72c)$$

$$N^{(4)+} = N^{(4)-}V_p^{(4)}, \quad k \in \partial D_p^{\varepsilon},$$
 (4.72c)

$$N^{(4)+} = N^{(4)-}V_{\bar{p}}^{(4)}, \qquad k \in \partial D_{\bar{p}}^{\varepsilon},$$
 (4.72d)

$$N^{(4)} = I + O\left(\frac{1}{k}\right), \qquad k \to \infty, \tag{4.72e}$$

where the contours L_j are shown in Fig. 16, the jumps $V_5^{(4)}$, $V_6^{(4)}$, $V_7^{(4)}$, $V_8^{(4)}$ are given by (4.71), and the remaining jumps are as in problem (4.68).

The only growth surviving in problem (4.72) after the fourth deformation is located in the 21- and 12-elements of the jumps $V_7^{(4)}$ and $V_8^{(4)}$ respectively. The fact that these jumps are antidiagonal allows us to eliminate this growth by employing the following transformation, which is essentially the mechanism leading to a modulated elliptic wave (as opposed to a plane wave).

Fifth deformation Let the points $\alpha(\xi)$ and $\bar{\alpha}(\xi)$ be defined through the solution of the modulation equations (2.8), which was shown in [BM2] to be unique for $\xi \in (v_0, 0)$. In turn, let the point $k_o(\xi)$ be given by (2.7). Then, introduce the function $h(\xi, k)$ via the Abelian integral (2.5). Note that h involves the function $\gamma(\xi, k)$ defined by (2.9), which

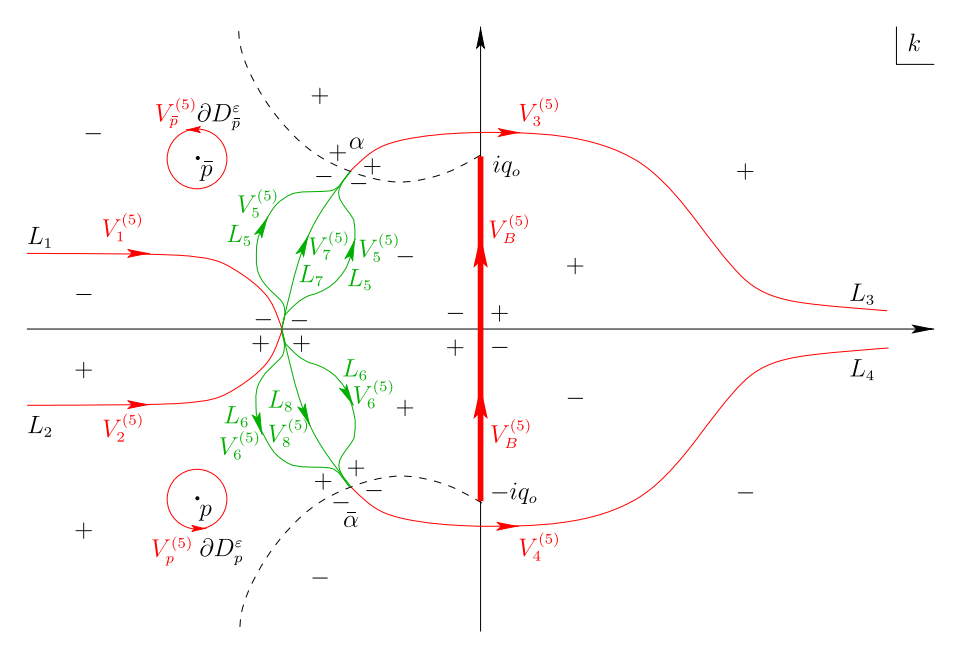


Fig. 17. Modulated elliptic wave region in the transmission regime: the fifth deformation

is made single-valued by taking branch cuts along B as well as along the curve

$$\widetilde{B} := L_7 \cup (-L_8) \tag{4.73}$$

with the contours L_7 and L_8 depicted in Fig. 17. We emphasize that \widetilde{B} must begin at $\overline{\alpha}$ and end at α by crossing the negative real axis at the point k_o but is otherwise arbitrary for the moment. The function γ is analytic for $k \in \mathbb{C} \setminus B \cup \widetilde{B}$ and changes sign as k crosses B and \widetilde{B} . Via (2.5), this induces analyticity of h in $\mathbb{C} \setminus B \cup \widetilde{B}$ as well as the following jump conditions along B and \widetilde{B} :

$$h^+ + h^- = 0, \qquad k \in B,$$
 (4.74a)

$$h^+ + h^- = \Omega, \quad k \in L_7 \cup L_8,$$
 (4.74b)

where the real quantity $\Omega(\xi)$, which is independent of k, is defined by

$$\Omega(\xi) = -4 \left(\int_{iq_o}^{\alpha} + \int_{-iq_o}^{\bar{\alpha}} \right) \frac{(z - k_o) (z - \alpha) (z - \bar{\alpha})}{\gamma(z)} dz. \tag{4.75}$$

Moreover, as shown in [BM2], Re(ih) has the same sign with Re($i\theta$) at infinity, near the origin, and near α and $\bar{\alpha}$.

The definition of h and, more specifically, the jump conditions (4.74) imply that the jumps of the function

$$N^{(5)}(x,t,k) = N^{(4)}(x,t,k)e^{-i[h(\xi,k)-\theta(\xi,k)]t\sigma_3}$$
(4.76)

along the contours L_7 and L_8 are bounded. Furthermore, those jumps that were bounded at the level of $N^{(4)}$ remain bounded at the level of $N^{(5)}$ [see discussion below (4.79)]. Specifically, Riemann–Hilbert problem (4.72) and transformation (4.76) imply that

 $N^{(5)}(x,t,k)$ is analytic for $k \in \mathbb{C} \setminus \left(\bigcup_{j=1}^{8} L_j \cup B \cup \partial D_p^{\varepsilon} \cup \partial D_{\bar{p}}^{\varepsilon}\right)$ and satisfies the jump conditions

$$N^{(5)+} = N^{(5)-}V_B^{(5)}, k \in B, (4.77a)$$

$$N^{(5)+} = N^{(5)-}V_j^{(5)}, k \in L_j, \ j = 1, \dots, 8, (4.77b)$$

$$N^{(5)+} = N^{(5)-}V_n^{(5)}, k \in \partial D_n^{\varepsilon}, (4.77c)$$

$$N^{(5)+} = N^{(5)-}V_{\bar{p}}^{(5)}, \qquad k \in \partial D_{\bar{p}}^{\varepsilon}, \tag{4.77d}$$

$$N^{(5)} = \left[I + O\left(\frac{1}{k}\right)\right] e^{-iG_{\infty}(\xi)t\sigma_3}, \qquad k \to \infty, \tag{4.77e}$$

where the contours L_i are shown in Fig. 17 and

$$V_{B}^{(5)} = \begin{pmatrix} 0 & \frac{q_{-}}{iq_{o}} \delta^{2} \\ \frac{\bar{q}_{-}}{iq_{o}} \delta^{-2} & 0 \end{pmatrix}, \quad V_{1}^{(5)} = \begin{pmatrix} 1 & \frac{\bar{r}\delta^{2}}{1+r\bar{r}} e^{2iht} \\ 0 & 1 \end{pmatrix}, \quad V_{2}^{(5)} = \begin{pmatrix} 1 & 0 \\ \frac{r\delta^{-2}}{1+r\bar{r}} e^{-2iht} & 1 \end{pmatrix},$$

$$V_{3}^{(5)} = \begin{pmatrix} 1 & 0 \\ r\delta^{-2}e^{-2iht} & 1 \end{pmatrix}, \quad V_{4}^{(5)} = \begin{pmatrix} 1 & \bar{r}\delta^{2}e^{2iht} \\ 0 & 1 \end{pmatrix}, \quad V_{5}^{(5)} = \begin{pmatrix} 1 & \frac{\delta^{2}}{r}e^{2iht} \\ 0 & 1 \end{pmatrix},$$

$$V_{6}^{(4)} = \begin{pmatrix} 1 & 0 \\ \frac{1}{r\delta^{2}}e^{-2iht} & 1 \end{pmatrix}, \quad V_{7}^{(5)} = \begin{pmatrix} 0 & -\frac{\delta^{2}}{r}e^{i\Omega t} \\ \frac{r}{\delta^{2}}e^{-i\Omega t} & 0 \end{pmatrix},$$

$$V_{8}^{(5)} = \begin{pmatrix} 0 & \bar{r}\delta^{2}e^{i\Omega t} \\ -\frac{1}{\bar{r}\delta^{2}}e^{-i\Omega t} & 0 \end{pmatrix},$$

$$V_{p}^{(5)} = \begin{pmatrix} 1 & -\frac{c_{p}\delta^{2}(\xi,k)d(k)}{k-p} e^{2i[h(\xi,k)+\theta(\xi,p)-\theta(\xi,k)]t} \\ 0 & 1 \end{pmatrix},$$

$$V_{p}^{(5)} = \begin{pmatrix} 1 & 0 \\ -\frac{c_{\bar{p}}\delta^{-2}(\xi,k)d(k)}{k-\bar{p}} e^{-2i[h(\xi,k)+\theta(\xi,\bar{p})-\theta(\xi,k)]t} \\ 1 \end{pmatrix},$$

$$(4.78)$$

with $\Omega(\xi)$ defined by (4.75) and the real quantity $G_{\infty}(\xi)$ given by

$$G_{\infty}(\xi) = -2\left(\int_{iq_o}^{\infty} + \int_{-iq_o}^{\infty}\right) \left[\frac{(z - k_o)(z - \alpha)(z - \bar{\alpha})}{\gamma(z)} - \left(z - \frac{\xi}{4}\right)\right] dz - q_o^2. \tag{4.79}$$

Remark 4.1. The fourth deformation, which affects only the jumps along the green contours of Fig. 15 by opening those contours into the lenses comprising the contours L_5 , L_6 , L_7 , L_8 of Fig. 16, could also be performed after the g-function deformation (4.76), leading again to Riemann–Hilbert problem (4.77). Nonetheless, the order we have followed here has the advantage of revealing the basic form of the jumps along the contours of growth (see (4.71)) before the introduction of the Abelian function h, thus allowing us to better motivate the desired properties that eventually lead to the definition of h. Of course, since for $v_0 < \xi < 0$ we switch the phase function from θ to h via deformation (4.76), it should be emphasized that the contours L_7 and L_8 of Fig. 17 are not those of Fig. 16, but rather the contours connecting α and $\bar{\alpha}$ with k_o .

The sign structure of Re(*ih*) at infinity and near the origin together with the fact that, by definition, *h* possesses precisely three critical points, namely k_0 , α , $\bar{\alpha}$, guarantee

the existence of a neighborhood around the point k_o where $\operatorname{Re}(ih) < 0$ in the second quadrant, $\operatorname{Re}(ih) > 0$ in the third quadrant, and $\operatorname{Re}(ih) = 0$ along $\mathbb R$ and the branch cut $\widetilde B$. Thus, thanks to the sign structure of $\operatorname{Re}(ih)$ near α , it is always possible to have a contour from k_o to α which lies to the right of the branch cut $\widetilde B$ and along which $\operatorname{Re}(ih) < 0.^2$ Similarly, thanks to the sign structure of $\operatorname{Re}(ih)$ at infinity and near k_o and α , as well as to the fact that h possesses precisely three critical points, we can always find a contour from k_o to α which lies to the left of the branch cut $\widetilde B$ and along which $\operatorname{Re}(ih) < 0$. Therefore, the contour L_5 of Fig. 17 can always be chosen to satisfy $\operatorname{Re}(ih) < 0$. In turn, by symmetry, the contour L_6 can always be chosen to satisfy $\operatorname{Re}(ih) > 0$. Hence, the jumps $V_5^{(5)}$ and $V_6^{(5)}$ are guaranteed to decay exponentially to the identity as $t \to \infty$. Analogous considerations ensure that $\operatorname{Re}(ih)$ has the same sign structure with $\operatorname{Re}(i\theta)$ along the contours L_1 , L_2 , L_3 and L_4 of Fig. 17. Thus, the jumps $V_1^{(5)}$, $V_2^{(5)}$, $V_3^{(5)}$ and $V_4^{(5)}$ inherit the behavior of their $N^{(4)}$ -counterparts, i.e. they decay exponentially to the identity as $t \to \infty$.

Furthermore, there exists at least one zero-contour (i.e. a contour along which $\operatorname{Re}(ih)=0$) connecting α and $\bar{\alpha}$ through k_o . This is because of the sign structure of $\operatorname{Re}(ih)$ near α and $\bar{\alpha}$ as well as due to the jump condition (4.74b) along \widetilde{B} , which implies that $\operatorname{Re}(ih^+)=-\operatorname{Re}(ih^-)$ since $\Omega\in\mathbb{R}$. Thus, either \widetilde{B} is itself a zero-contour, or there exists a region of positive sign adjacent to \widetilde{B} whose boundary will have to be a zero-contour due to the analyticity of h, the sign of $\operatorname{Re}(ih)$ at infinity and near the origin, and the existence of precisely three critical points of h. In the latter case, we can deform \widetilde{B} to this zero-contour so that $\operatorname{Re}(ih)=0$ throughout \widetilde{B} . In fact, any zero-contour connecting α and $\overline{\alpha}$ can only cross the negative real axis at k_o , since a zero-contour intersecting with the negative real axis at a point different than k_o would require this point to a critical point, leading to a contradiction. Therefore, taking into account once again the sign structure of $\operatorname{Re}(ih)$ near α and $\overline{\alpha}$, we conclude that for $\xi \in (v_o,0)$ there exists a unique zero-contour with endpoints α and $\overline{\alpha}$ and through the point k_o , namely the branch cut \widetilde{B} .

Furthermore, as ξ increases from v_o to 0 the branch cut \widetilde{B} remains within the finite region enclosed by the trace of $\overline{\alpha}$ and α (the dashed green curve in Fig. 1 and its reflection through the real axis) and the branch cut B. Hence, for $p \in D_1$, as ξ increases from v_o to 0 the branch cut \widetilde{B} remains to the right of the disks $\overline{D_p^\varepsilon}$ and $\overline{D_p^\varepsilon}$ without interfering with p and \overline{p} . The same is true for $p \in D_2^+$ since, as shown in Fig. 1, this region lies by definition below the trace of $\overline{\alpha}$ (while \widetilde{B} lies above that trace). On the other hand, if $p \in D_2^- \cup D_3$ then both p and \overline{p} are crossed by \widetilde{B} for some $\xi \in (v_o, 0)$, this being the mechanism that generates the soliton wake in the mixed regimes of Sect. 6.

Next, recall that the transition from θ to h in the jump matrices takes place at $\xi = v_o$, where $h(v_o, k) = \theta(v_o, k)$ and $\alpha(v_o) = \bar{\alpha}(v_o) = k_o(v_o) = v_o/8$. Hence, at $\xi = v_o$ the lower and upper dashed curves of Fig. 17 are, respectively, the solid blue curve of Fig. 1 and its reflection through the real k-axis. A numerical investigation then shows that, as ξ increases from v_o to 0, the upper dashed curve remains convex and moves

¹ Indeed, if such a neighborhood did not exist then there would have to be one or more saddle points other than k_0 along the negative real axis, leading to a contradiction.

² Indeed, the only way this could fail is if there were a strip of Re(ih) > 0 connecting the branch cut \widetilde{B} either with the real axis or with the branch cut B. The first scenario is not possible because if would create additional critical (saddle) points on the real axis. Moreover, the second scenario is also not realizable since, due to the continuity of Re(ih) away from the cuts and the jump condition $Re(ih^+) = -Re(ih^-)$, the boundary of the strip away from \widetilde{B} would have to be a zero-contour, i.e. a contour along which Re(ih) = 0. But then, deforming \widetilde{B} to this zero-contour we would get inconsistent jump conditions for h along the part of the zero-contour that overlaps with B, since $\Omega \neq 0$ independently of the branch cuts B and \widetilde{B} .

continuously upwards and to the right, eventually collapsing to the half-line $i[q_o,\infty)$. Analogously, the lower dashed curve remains concave and moves downwards and to the right, eventually collapsing to the half-line $i(-\infty,-q_o]$. Hence, no points inside the regions D_1 and D_3 of Fig. 1 are crossed by the lower dashed curve of Fig. 17 as ξ increases from v_o to 0. In particular, if $p \in D_1 \cup D_3$, then the circle $\partial D_p^{\varepsilon}$, which is between the negative real k-axis the solid blue curve of Fig. 1 at $\xi = v_o$, remains below the negative real k-axis and above the lower dashed curve of Fig. 17 throughout the range $(v_o, 0)$. On the other hand, if $p \in D_2^+ \cup D_2^-$, then it will be crossed at exactly one value of $\xi \in (v_o, 0)$ by the lower dashed curve of Fig. 17. An analogous statement can be made for \bar{p} by symmetry.

The dashed curves of Fig. 17 together with the branch cut \widetilde{B} and the negative real axis make up the contours along which $\operatorname{Re}(ih)=0$ on the left half of the complex k-plane. Hence, from the above-described behavior of these contours as ξ increases from v_o to 0, we conclude that

• If $p \in D_1$, then $\text{Re}(ih)(\xi, p) > 0$ for all $\xi \in (v_o, 0)$. Equivalently, the equation

$$\operatorname{Re}(ih)(\xi, p) = 0 \Leftrightarrow \operatorname{Re}(ih)(\xi, \bar{p}) = 0 \Leftrightarrow \int_{\bar{p}}^{p} dh(\xi, z) = 0 \tag{4.80}$$

has no solution for $\xi \in (v_0, 0)$. Hence, in the transmission regime $p \in D_1$ no soliton arises in the range $\xi \in (v_0, 0)$.

- If $p \in D_2^+$, then Eq. (4.80) has a *unique* solution $\widetilde{v}_s \in (v_o, 0)$, which gives rise to a soliton (see Sect. 5 for more details).
- If $p \in D_2^-$, then Eq. (4.80) has two solutions in the interval $(v_o, 0)$: one due to the crossing of p by the lower dashed curve of 17, denoted by \widetilde{v}_s , and another one due to the crossing of p by the branch cut \widetilde{B} , denoted by v_w . Moreover, $\widetilde{v}_s < v_w$ and the first solution corresponds to a soliton while the second one to a soliton wake (see Sect. 6 for more details).
- Finally, if $p \in D_3$, then Eq. (4.80) has a *unique* solution $v_w \in (v_o, 0)$, which arises from the crossing of p by the branch cut \widetilde{B} and corresponds to a soliton wake (see Sect. 6 for more details).

The integral Eq. (4.80) can be expressed in terms of the incomplete elliptic integrals of the first and second kind. Importantly, we note that when the poles coincide with the branch point $\pm iq_0$ equation (4.80) reduces to the modulation Eq. (2.8b). A numerical evaluation of the solutions of Eq. (4.80) for various choices of p that cover all four possible regions D_1 , D_2^+ , D_2^- and D_3 of the third quadrant is shown in Fig. 18.

The only jumps of Riemann–Hilbert problem (4.77) that are not bounded as $t \to \infty$ are the ones along $\partial D_p^{\varepsilon}$ and $\partial D_{\tilde{p}}^{\varepsilon}$, which grow exponentially since they are controlled by the sign of Re $(ih)(\xi,p)$.³ Thus, similarly to Sect. 4.3, we must employ the analogue of transformation (4.56) in order to convert this growth into decay. Before doing so, however, we apply the analogue of transformation (4.10) in order to remove the k-dependence from the jumps along B and \widetilde{B} .

The fact that $e^{2i[h(\xi,k)+\theta(\xi,p)-\theta(\xi,k)]t}$ is controlled by $\text{Re}(ih)(\xi,p)$ can be seen by recalling that the jump $V_p^{(5)}$ along the circle $\partial D_p^{\varepsilon}$ originates from the residue condition at p. Eventually, whenever the dominant problem contains the contribution from $\partial D_p^{\varepsilon}$, the jump $V_p^{(5)}$ will be converted back to a (modified) residue condition at p. Thus, eventually we will end up evaluating the quantity $h(\xi,k) + \theta(\xi,p) - \theta(\xi,k)$ at k=p.

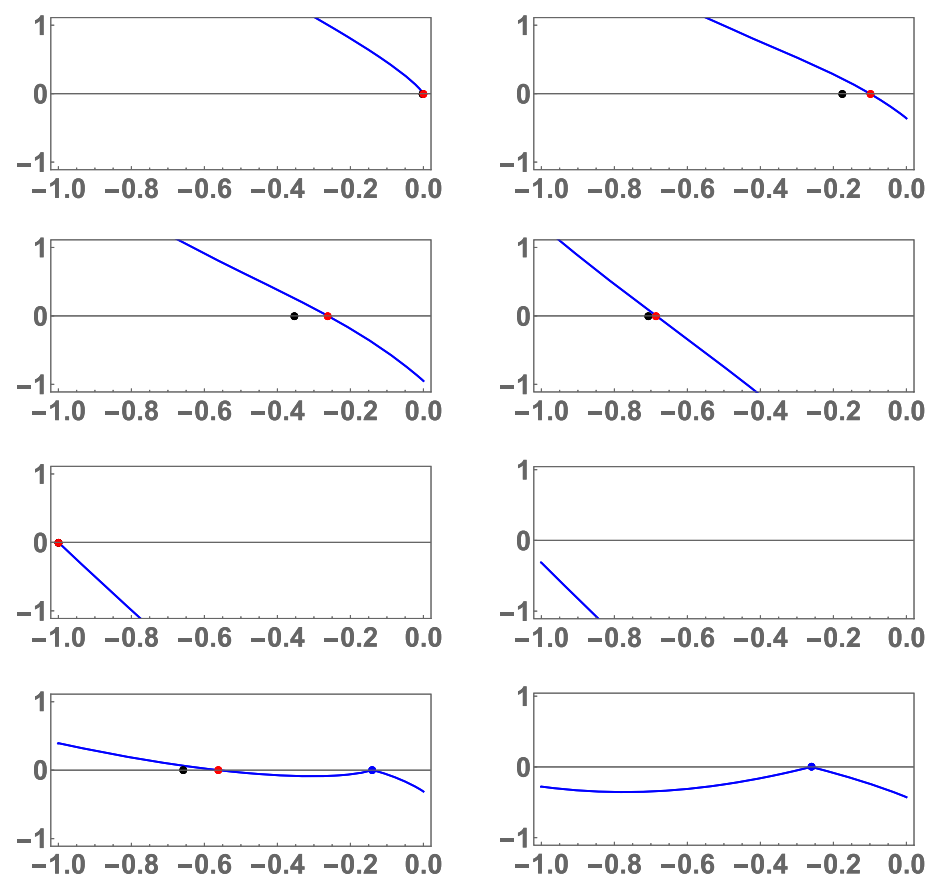


Fig. 18. Numerical evaluation of the solutions of Eq. (4.80) for $q_o=1$ and the different choices of p depicted by orange dots in Fig. 1. The horizontal axis corresponds to ξ , the vertical axis to Re(ih)(ξ , p), and the values on both axes are normalized by a factor of $|v_o|$ so that the range [-1,0] of ξ corresponds precisely to the modulated elliptic wave region $[v_o,0]$, where Eq. (4.80) is actually relevant. The black dots denote the unperturbed soliton velocity v_s given by (2.10), while the red and blue dots denote the solutions \tilde{v}_s and v_w of Eq. (4.80) corresponding to a soliton and a soliton wake respectively. First row: $p=-1.1i \in D_2^+$ and $p=-0.082-1.1i \in D_2^+$. Second row: $p=-0.216-1.1i \in D_2^+$ and $p=-0.69-1.1i \in D_2^+$. Third row: $p=-1.146-1.1i \in D_2^+$ and $p=-1.24-1.1i \in D_1$. Fourth row: $p=-0.082-0.95i \in D_2^-$ and $p=-0.214-0.5i \in D_3$. Note that in the left panel of the first and third rows v_s and \tilde{v}_s essentially coincide. In particular, the latter case, which concerns D_2^+ , is in complete agreement with the numerical simulation shown in the center panel of Fig. 4

Sixth deformation The jumps $V_B^{(5)}$, $V_7^{(5)}$ and $V_8^{(5)}$ can be made independent of k by means of the transformation

$$N^{(6)}(x,t,k) = N^{(5)}(x,t,k)e^{ig(\xi,k)\sigma_3},$$
(4.81)

where the function $g(\xi, k)$ is analytic in $\mathbb{C}\setminus (B \cup \widetilde{B})$ and satisfies the following jump conditions:

$$g^{+} + g^{-} = -i \ln \left(\delta^{2}\right), \qquad k \in B,$$
 (4.82a)

$$g^{+} + g^{-} = -i \ln \left(\frac{\delta^{2}}{r}\right) + \omega, \qquad k \in L_{7}, \tag{4.82b}$$

$$g^{+} + g^{-} = -i \ln \left(\delta^{2} \bar{r}\right) + \omega, \qquad k \in L_{8}, \tag{4.82c}$$

with $\delta(\xi, k)$ defined by (4.69) and with the real quantity $\omega(\xi)$ defined by

$$\omega(\xi) = i \frac{\int_{B} \frac{\ln \delta^{2}(\xi, \nu)}{\gamma(\xi, \nu)} d\nu + \int_{\widetilde{B}^{+}} \frac{\ln \left[\frac{\delta^{2}(\xi, \nu)}{r(\nu)}\right]}{\gamma(\xi, \nu)} d\nu + \int_{\widetilde{B}^{-}} \frac{\ln \left[\delta^{2}(\xi, \nu) \, \bar{r}(\nu)\right]}{\gamma(\xi, \nu)} d\nu}{\int_{\widetilde{B}} \frac{d\nu}{\gamma(\xi, \nu)}},$$

$$(4.83)$$

where we have introduced the notation

$$\widetilde{B}^{\pm} := \widetilde{B} \cap \mathbb{C}^{\pm}. \tag{4.84}$$

The solution of problem (4.82) is obtained via the Plemelj formulae as

$$g(\xi,k) = \frac{\gamma(\xi,k)}{2\pi} \left[\int_{B} \frac{\ln \delta^{2}(\xi,\nu)}{\gamma(\xi,\nu)(\nu-k)} d\nu + \int_{L_{7}} \frac{\ln \left[\frac{\delta^{2}(\xi,\nu)}{r(\nu)} \right] + i\omega(\xi)}{\gamma(\xi,\nu)(\nu-k)} d\nu - \int_{L_{8}} \frac{\ln \left[\delta^{2}(\xi,\nu)\,\bar{r}(\nu) \right] + i\omega(\xi)}{\gamma(\xi,\nu)(\nu-k)} d\nu \right]. \tag{4.85}$$

The presence of ω in the jump conditions (4.82) ensures that $g(\xi, k) = O(1)$ as $k \to \infty$. Indeed, expression (4.85) implies

$$g(\xi, k) = g_{\infty}(\xi) + O\left(\frac{1}{k}\right), \quad k \to \infty,$$
 (4.86)

where the real quantity $g_{\infty}(\xi)$ is defined by

$$g_{\infty}(\xi) = -\frac{1}{2\pi} \left[\int_{B} \frac{\ln \delta^{2}(\xi, \nu)}{\gamma(\xi, \nu)} \nu d\nu + \int_{\widetilde{B}^{+}} \frac{\ln \left[\frac{\delta^{2}(\xi, \nu)}{r(\nu)} \right] + i\omega(\xi)}{\gamma(\xi, \nu)} \nu d\nu + \int_{\widetilde{B}^{-}} \frac{\ln \left[\delta^{2}(\xi, \nu) \, \bar{r}(\nu) \right] + i\omega(\xi)}{\gamma(\xi, \nu)} \nu d\nu \right]. \tag{4.87}$$

In summary, the function $N^{(6)}$ defined by (4.81) is analytic in $\mathbb{C}\setminus \left(\bigcup_{j=1}^6 L_j \cup B \cup \widetilde{B} \cup \partial D_{\widetilde{p}}^\varepsilon \cup \partial D_{\widetilde{p}}^\varepsilon\right)$ and satisfies the Riemann–Hilbert problem

$$N^{(6)+} = N^{(6)-}V_B, k \in B, (4.88a)$$

$$N^{(6)+} = N^{(6)-}V_{\widetilde{R}}^{(6)}, \qquad k \in \widetilde{B}, \tag{4.88b}$$

$$N^{(6)+} = N^{(6)-}V_j^{(6)},$$
 $k \in L_j, \ j = 1, \dots, 6,$ (4.88c)

$$N^{(6)+} = N^{(6)-}V_p^{(6)}, k \in \partial D_p^{\varepsilon}, (4.88d)$$

$$N^{(6)+} = N^{(6)-}V_{\bar{p}}^{(6)}, \qquad k \in \partial D_{\bar{p}}^{\varepsilon}, \tag{4.88e}$$

$$N^{(6)} = \left[I + O\left(\frac{1}{k}\right)\right] e^{i\left[g_{\infty}(\xi) - G_{\infty}(\xi)t\right]\sigma_3}, \qquad k \to \infty, \tag{4.88f}$$

where the jump along B is given by (4.2), the jump along \widetilde{B} is equal to

$$V_{\widetilde{B}}^{(6)} = \begin{pmatrix} 0 & -e^{i(\Omega t - \omega)} \\ e^{-i(\Omega t - \omega)} & 0 \end{pmatrix}, \tag{4.89}$$

the jumps along $\partial D_p^{\varepsilon}$ and $\partial D_{\bar{p}}^{\varepsilon}$ are given by

$$V_p^{(6)} = \begin{pmatrix} 1 - \frac{c_p \, \delta^2(\xi, k) \, d(k) e^{-2ig(\xi, k)}}{k - p} \, e^{2i[h(\xi, k) + \theta(\xi, p) - \theta(\xi, k)]t} \\ 0 & 1 \end{pmatrix}, \tag{4.90a}$$

$$V_{\bar{p}}^{(6)} = \begin{pmatrix} 1 & 0 \\ -\frac{c_{\bar{p}} \delta^{-2}(\xi, k) d(k) e^{2ig(\xi, k)}}{k - \bar{p}} e^{-2i[h(\xi, k) + \theta(\xi, \bar{p}) - \theta(\xi, k)]t} & 1 \end{pmatrix}, \tag{4.90b}$$

the jumps along the contours L_i of Fig. 17 are equal to

$$V_{1}^{(6)} = \begin{pmatrix} 1 & \frac{\bar{r} \, \delta^{2} e^{-2ig}}{1 + r\bar{r}} \, e^{2iht} \\ 0 & 1 \end{pmatrix}, \qquad V_{2}^{(6)} = \begin{pmatrix} 1 & 0 \\ \frac{r\delta^{-2} e^{2ig}}{1 + r\bar{r}} \, e^{-2iht} \, 1 \end{pmatrix}, \qquad (4.91a)$$

$$V_{3}^{(6)} = \begin{pmatrix} 1 & 0 \\ r\delta^{-2} e^{2ig} e^{-2iht} \, 1 \end{pmatrix}, \qquad V_{4}^{(6)} = \begin{pmatrix} 1 & \bar{r} \, \delta^{2} e^{-2ig} e^{2iht} \\ 0 & 1 \end{pmatrix}, \qquad (4.91b)$$

$$V_3^{(6)} = \begin{pmatrix} 1 & 0 \\ r\delta^{-2}e^{2ig}e^{-2iht} & 1 \end{pmatrix}, \qquad V_4^{(6)} = \begin{pmatrix} 1 & \bar{r}\delta^2e^{-2ig}e^{2iht} \\ 0 & 1 \end{pmatrix}, \tag{4.91b}$$

$$V_5^{(6)} = \begin{pmatrix} 1 & \frac{\delta^2 e^{-2ig}}{r} e^{2iht} \\ 0 & 1 \end{pmatrix}, \qquad V_6^{(6)} = \begin{pmatrix} 1 & 0 \\ \frac{\delta^{-2} e^{2ig}}{\bar{r}} e^{-2iht} & 1 \end{pmatrix}, \tag{4.91c}$$

and the real quantities $G_{\infty}(\xi)$ and $g_{\infty}(\xi)$ are given by (4.79) and (4.87) respectively.

Converting growth into decay The growing exponentials in the jumps $V_p^{(6)}$ and $V_{\bar{p}}^{(6)}$ can be converted into decaying ones via the analogue of transformation (4.56), i.e. by letting

$$\widetilde{N}^{(6)} = \begin{cases} N^{(6)} n^{\sigma_3}, & k \in \mathbb{C} \setminus \left(\overline{D_p^{\varepsilon}} \cup \overline{D_{\bar{p}}^{\varepsilon}} \right), \\ N^{(6)} J_p n^{\sigma_3}, & k \in D_p^{\varepsilon}, \\ N^{(6)} J_{\bar{p}} n^{\sigma_3}, & k \in D_{\bar{p}}^{\varepsilon}, \end{cases}$$
(4.92a)

where

$$J_{p}(\xi,k) = \begin{pmatrix} \frac{1 - \frac{n^{2}(p)}{n^{2}(k)}}{k - p} & c_{p} d(k) \delta^{2}(\xi,k) e^{2i[(h(\xi,k) + \theta(\xi,p) - \theta(\xi,k))t - g]} \\ - \frac{n^{2}(p) e^{-2i[(h(\xi,k) + \theta(\xi,p) - \theta(\xi,k))t - g]}}{c_{p} d(k) \delta^{2}(\xi,k) (k - \bar{p})^{2}} & k - p \end{pmatrix},$$

$$(4.92b)$$

$$J_{\bar{p}}(\xi,k) = \begin{pmatrix} k - \bar{p} & -\frac{e^{2i[(h(\xi,k) + \theta(\xi,\bar{p}) - \theta(\xi,k))t - g]}}{n^2(\bar{p})c_{\bar{p}} d(k)\delta^{-2}(\xi,k)(k - p)^2} \\ c_{\bar{p}} d(k)\delta^{-2}(\xi,k)e^{-2i[(h(\xi,k) + \theta(\xi,\bar{p}) - \theta(\xi,k))t - g]} & \frac{1 - \frac{n^2(k)}{n^2(\bar{p})}}{k - \bar{p}} \end{pmatrix}.$$

$$(4.92c)$$

Then, $\widetilde{N}^{(6)}$ satisfies the Riemann–Hilbert problem

$$\widetilde{N}^{(6)+} = \widetilde{N}^{(6)-} \widetilde{V}_R^{(6)}, \qquad k \in B,$$
(4.93a)

$$\widetilde{N}^{(6)+} = \widetilde{N}^{(6)-} \widetilde{V}_{\widetilde{B}}^{(6)}, \qquad k \in \widetilde{B}, \tag{4.93b}$$

$$\widetilde{N}^{(6)+} = \widetilde{N}^{(6)-} \widetilde{V}_{j}^{(6)}, \qquad k \in L_{j}, \ j = 1, \dots, 6,$$
 (4.93c)

$$\widetilde{N}^{(6)+} = \widetilde{N}^{(6)} - \widetilde{V}_{p}^{(6)}, \qquad k \in \partial D_{p}^{\varepsilon}, \tag{4.93d}$$

$$\widetilde{N}^{(6)+} = \widetilde{N}^{(6)-} \widetilde{V}_{\bar{p}}^{(6)}, \qquad k \in \partial D_{\bar{p}}^{\varepsilon}, \tag{4.93e}$$

$$\widetilde{N}^{(6)} = \left[I + O\left(\frac{1}{k}\right)\right] e^{i\left[g_{\infty}(\xi) - G_{\infty}(\xi)t\right]\sigma_{3}}, \qquad k \to \infty, \tag{4.93f}$$

where the jumps along B and \widetilde{B} are given by

$$\widetilde{V}_{B}^{(6)} = \begin{pmatrix} 0 & \frac{q_{-}}{iq_{o}}n^{-2} \\ \frac{\widetilde{q}_{-}}{iq_{o}}n^{2} & 0 \end{pmatrix}, \quad \widetilde{V}_{\widetilde{B}}^{(6)} = \begin{pmatrix} 0 & -e^{i(\Omega t - \omega)}n^{-2} \\ e^{-i(\Omega t - \omega)}n^{2} & 0 \end{pmatrix}, \tag{4.94}$$

the jumps along $\partial D_p^{\varepsilon}$ and $\partial D_{\bar{p}}^{\varepsilon}$ are equal to

$$\widetilde{V}_{p}^{(6)} = \begin{pmatrix} 1 & 0 \\ -\frac{n^{2}(p)e^{2ig(\xi,k)}}{c_{p} \delta^{2}(\xi,k) d(k)(k-p)} e^{-2i[h(\xi,k)+\theta(\xi,p)-\theta(\xi,k)]t} & 1 \end{pmatrix}, \tag{4.95a}$$

$$\widetilde{V}_{\bar{p}}^{(6)} = \begin{pmatrix} 1 - \frac{n^{-2}(\bar{p}) \,\delta^{2}(\xi, k) e^{-2ig(\xi, k)}}{c_{\bar{p}} \,d(k)(k - \bar{p})} \,e^{2i[h(\xi, k) + \theta(\xi, \bar{p}) - \theta(\xi, k)]t} \\ 0 & 1 \end{pmatrix}, \tag{4.95b}$$

and the jumps along the contours L_i of Fig. 17 are given by

$$\widetilde{V}_{1}^{(6)} = \begin{pmatrix} 1 & \frac{\bar{r} \, \delta^{2} e^{-2ig}}{1 + r\bar{r}} e^{2iht} n^{-2} \\ 0 & 1 \end{pmatrix}, \qquad \widetilde{V}_{2}^{(6)} = \begin{pmatrix} 1 & 0 \\ \frac{r\delta^{-2} e^{2ig}}{1 + r\bar{r}} e^{-2iht} n^{2} & 1 \end{pmatrix}, \tag{4.96a}$$

$$\widetilde{V}_{3}^{(6)} = \begin{pmatrix} 1 & 0 \\ r\delta^{-2}e^{2ig}e^{-2iht}n^{2} & 1 \end{pmatrix}, \qquad \widetilde{V}_{4}^{(6)} = \begin{pmatrix} 1 & \bar{r}\delta^{2}e^{-2ig}e^{2iht}n^{-2} \\ 0 & 1 \end{pmatrix}, \quad (4.96b)$$

$$\widetilde{V}_{5}^{(6)} = \begin{pmatrix} 1 & \frac{\delta^{2}e^{-2ig}}{r} e^{2iht} n^{-2} \\ 0 & 1 \end{pmatrix}, \qquad \widetilde{V}_{6}^{(6)} = \begin{pmatrix} 1 & 0 \\ \frac{\delta^{-2}e^{2ig}}{\bar{r}} e^{-2iht} n^{2} & 1 \end{pmatrix}.$$
(4.96c)

Transformation (4.92) has re-introduced k in the jumps along B and \widetilde{B} , which had been made k-independent via the sixth deformation. Thus, motivated by the plane wave region, where having a constant jump along B allowed us to solve the dominant Riemann–Hilbert problem explicitly, we next perform a final, seventh deformation in order to remove the k-dependence from the jumps $\widetilde{V}_B^{(6)}$ and $\widetilde{V}_{\widetilde{R}}^{(6)}$.

Remark 4.2 (Order of deformations). In view of the above discussion, it becomes apparent that the sixth deformation should have been postponed until after transformation (4.92), since then the k-dependence from the jumps along B and \widetilde{B} would have to be removed only once instead of twice. However, the less efficient order of deformations that we have followed has the advantage of revealing precisely which part of the overall phase of the modulated elliptic wave (2.18) is generated by the soliton at $\xi = v_s$ (namely, the constant $4 \arg [p + \lambda(p)]$ via the seventh deformation as shown in (4.103)).

Seventh deformation Similarly to (4.81), we eliminate the dependence on k from the jumps $\widetilde{V}_{B}^{(6)}$ and $\widetilde{V}_{\widetilde{R}}^{(6)}$ by letting

$$\widetilde{N}^{(7)}(x,t,k) = \widetilde{N}^{(6)}(x,t,k)e^{i\widetilde{g}(\xi,k)\sigma_3},$$
(4.97)

where the function $\widetilde{g}(\xi, k)$ is analytic in $\mathbb{C}\setminus (B \cup \widetilde{B})$ and satisfies the jump conditions

$$\widetilde{g}^+ + \widetilde{g}^- = i \ln \left(n^2 \right), \qquad k \in B,$$
 (4.98a)

$$\widetilde{g}^+ + \widetilde{g}^- = i \ln \left(n^2 r \right) + \widetilde{\omega}, \qquad k \in L_7,$$
 (4.98b)

$$\widetilde{g}^+ + \widetilde{g}^- = i \ln \left(\frac{n^2}{\widetilde{r}} \right) + \widetilde{\omega}, \qquad k \in L_8,$$
 (4.98c)

with the real quantity $\widetilde{\omega}(\xi)$ given by

$$\widetilde{\omega}(\xi) = -i \frac{\int_{B} \frac{\ln n^{2}(\nu)}{\gamma(\xi, \nu)} d\nu + \int_{L_{7}} \frac{\ln \left[n^{2}(\nu)r(\nu)\right]}{\gamma(\xi, \nu)} d\nu + \int_{L_{8}} \frac{\ln \left[\frac{\bar{r}(\nu)}{n^{2}(\nu)}\right]}{\gamma(\xi, \nu)} d\nu}{\int_{\widetilde{B}} \frac{d\nu}{\gamma(\xi, \nu)}}.$$
 (4.99)

Similarly to (4.85), we have the explicit formula

$$\widetilde{g}(\xi,k) = -\frac{\gamma(\xi,k)}{2\pi} \left\{ \int_{B} \frac{\ln n^{2}(\nu)}{\gamma(\xi,\nu)(\nu-k)} d\nu + \int_{L_{7}} \frac{\ln \left[n^{2}(\nu)r(\nu)\right] - i\widetilde{\omega}(\xi)}{\gamma(\xi,\nu)(\nu-k)} d\nu + \int_{L_{8}} \frac{\ln \left[\frac{\tilde{r}(\nu)}{n^{2}(\nu)}\right] + i\widetilde{\omega}(\xi)}{\gamma(\xi,\nu)(\nu-k)} d\nu \right\},$$
(4.100)

which implies

$$\widetilde{g}(\xi, k) = \widetilde{g}_{\infty}(\xi) + O\left(\frac{1}{k}\right), \quad k \to \infty,$$
(4.101)

with the real quantity $\widetilde{g}_{\infty}(\xi)$ given by

$$\widetilde{g}_{\infty}(\xi) = \frac{1}{2\pi} \left\{ \int_{B} \frac{\ln n^{2}(v)}{\gamma(\xi, v)} v dv + \int_{L_{7}} \frac{\ln \left[n^{2}(v)r(v)\right] - i\widetilde{\omega}(\xi)}{\gamma(\xi, v)} v dv + \int_{L_{8}} \frac{\ln \left[\frac{\widetilde{r}(v)}{n^{2}(v)}\right] + i\widetilde{\omega}(\xi)}{\gamma(\xi, v)} v dv \right\}.$$

$$(4.102)$$

It turns out that \widetilde{g}_{∞} is actually independent of ξ and, more precisely,

$$\widetilde{g}_{\infty} = 2\arg\left[p + \lambda(p)\right]$$
 (4.103)

like in the plane wave region. Eventually (see Remark 4.5), this implies that the effect of the soliton at $\xi = v_o$ on the phase of the leading order asymptotics is the same both for $\xi \in (v_o, 0)$ and for $\xi \in (v_s, v_o)$.

The Riemann–Hilbert problem for $\widetilde{N}^{(6)}$ yields the following problem for $\widetilde{N}^{(7)}$:

$$\widetilde{N}^{(7)+} = \widetilde{N}^{(7)-} V_B, \qquad k \in B, \tag{4.104a}$$

$$\widetilde{N}^{(7)+} = \widetilde{N}^{(7)-} \widetilde{V}_{\widetilde{B}}^{(7)}, \qquad k \in \widetilde{B}, \tag{4.104b}$$

$$\widetilde{N}^{(7)+} = \widetilde{N}^{(7)-} \widetilde{V}_j^{(7)}, \qquad k \in L_j, \ j = 1, \dots, 6, \quad (4.104c)$$

$$\widetilde{N}^{(7)+} = \widetilde{N}^{(7)-} \widetilde{V}_n^{(7)}, \qquad k \in \partial D_n^{\varepsilon}, \tag{4.104d}$$

$$\widetilde{N}^{(7)+} = \widetilde{N}^{(7)-} \widetilde{V}_{\bar{p}}^{(7)}, \qquad k \in \partial D_{\bar{p}}^{\varepsilon}, \tag{4.104e}$$

$$N^{(f)+} = N^{(f)-}V_{\tilde{p}}^{(f)}, \qquad k \in \partial D_{\tilde{p}}^{\varepsilon}, \qquad (4.104e)$$

$$\tilde{N}^{(7)} = \left[I + O\left(\frac{1}{k}\right)\right] e^{i\left[g_{\infty}(\xi) + \tilde{g}_{\infty} - G_{\infty}(\xi)t\right]\sigma_{3}}, \qquad k \to \infty, \qquad (4.104f)$$

where the jump along B is given by (4.2), the jump along \widetilde{B} is equal to

$$\widetilde{V}_{\widetilde{B}}^{(7)} = \begin{pmatrix} 0 & -e^{i(\Omega t - \omega - \widetilde{\omega})} \\ e^{-i(\Omega t - \omega - \widetilde{\omega})} & 0 \end{pmatrix}$$
(4.105)

with the real quantities Ω , ω and $\widetilde{\omega}$ given by (4.75), (4.83) and (4.99) respectively, the jumps along $\partial D_p^{\varepsilon}$ and $\partial D_{\bar{p}}^{\varepsilon}$ are given by

$$\widetilde{V}_{p}^{(7)} = \begin{pmatrix} 1 & 0 \\ -\frac{n^{2}(p)e^{2i[g(\xi,k)+\widetilde{g}(\xi,k)]}}{c_{p}\delta^{2}(\xi,k)d(k)(k-p)} e^{-2i[h(\xi,k)+\theta(\xi,p)-\theta(\xi,k)]t} & 1 \end{pmatrix}, \tag{4.106a}$$

$$\begin{pmatrix}
c_{p} \delta^{2}(\xi, k) d(k)(k - p) \\
\tilde{V}_{\bar{p}}^{(7)} = \begin{pmatrix}
1 - \frac{n^{-2}(\bar{p}) \delta^{2}(\xi, k) e^{-2i[g(\xi, k) + \tilde{g}(\xi, k)]}}{c_{\bar{p}} d(k)(k - \bar{p})} e^{2i[h(\xi, k) + \theta(\xi, \bar{p}) - \theta(\xi, k)]t} \\
0
\end{pmatrix} (4.106b)$$

with the functions d, n, δ , g and \widetilde{g} defined by (3.4), (4.56), (4.69), (4.85) and (4.100) respectively, the jumps along the contours L_i of Fig. 17 are given by

$$\begin{split} \widetilde{V}_{1}^{(7)} &= \begin{pmatrix} 1 & \frac{\bar{r} \, \delta^{2} e^{-2i(g+\bar{g})}}{1 + r\bar{r}} \, e^{2iht} n^{-2} \\ 0 & 1 \end{pmatrix}, \qquad \widetilde{V}_{2}^{(7)} &= \begin{pmatrix} 1 & 0 \\ \frac{r\delta^{-2} e^{2i(g+\bar{g})}}{1 + r\bar{r}} \, e^{-2iht} n^{2} \, 1 \end{pmatrix}, \quad (4.107a) \\ \widetilde{V}_{3}^{(7)} &= \begin{pmatrix} 1 & 0 \\ r\delta^{-2} e^{2i(g+\bar{g})} e^{-2iht} n^{2} \, 1 \end{pmatrix}, \qquad \widetilde{V}_{4}^{(7)} &= \begin{pmatrix} 1 & \bar{r} \, \delta^{2} e^{-2i(g+\bar{g})} e^{2iht} n^{-2} \\ 0 & 1 \end{pmatrix}, \quad (4.107b) \end{split}$$

$$\widetilde{V}_{5}^{(7)} = \begin{pmatrix} 1 & \frac{\delta^{2}e^{-2i(g+\widetilde{g})}}{r} e^{2iht} n^{-2} \\ 0 & 1 \end{pmatrix}, \qquad \widetilde{V}_{6}^{(7)} = \begin{pmatrix} 1 & 0 \\ \frac{\delta^{-2}e^{2i(g+\widetilde{g})}}{r} e^{-2iht} n^{2} & 1 \end{pmatrix}, \quad (4.107c)$$

the real quantities G_{∞} and g_{∞} are defined by (4.79) and (4.87), and the real constant \widetilde{g}_{∞} is given by (4.103).

Decomposition into dominant and error problems The jumps $\widetilde{V}_{i}^{(7)}$, $j=1,\ldots,6$, do not contribute to the leading-order long-time asymptotics since they decay to the identity as $t \to \infty$ due to the sign structure of Re(ih) (see Fig. 17). The same is true for the jumps $\widetilde{V}_p^{(7)}$ and $\widetilde{V}_{\bar{p}}^{(7)}$ since the exponentials involved in these jumps are controlled by the sign of $Re(ih)(\xi, p)$. Therefore, the dominant component of Riemann–Hilbert problem (4.104) must come from the jumps V_B and $\widetilde{V}_{\widetilde{R}}^{(7)}$. With these in mind, we decompose problem (4.104) as follows.

Let $D_{k_o}^{\epsilon}$, D_{α}^{ϵ} and $D_{\bar{\alpha}}^{\epsilon}$ be disks of radius ϵ centered at k_o , α and $\bar{\alpha}$ respectively, where ϵ is sufficiently small so that these disks do not intersect with each other or with $B \cup \overline{D_n^{\varepsilon}} \cup \overline{D_n^{\varepsilon}}$. Then, write

$$\widetilde{N}^{(7)} = \widetilde{N}^{\text{err}} \widetilde{N}^{\text{asymp}} \tag{4.108}$$

where

$$\widetilde{N}^{\text{asymp}} = \begin{cases} \widetilde{N}^{\text{dom}}, & k \in \mathbb{C} \setminus (D_{k_o}^{\epsilon} \cup D_{\alpha}^{\epsilon} \cup D_{\bar{\alpha}}^{\epsilon}), \\ \widetilde{N}^{D}, & k \in D_{k_o}^{\epsilon} \cup D_{\alpha}^{\epsilon} \cup D_{\bar{\alpha}}^{\epsilon}, \end{cases}$$
(4.109)

and the functions $\widetilde{N}^{\text{dom}}$, \widetilde{N}^{D} and $\widetilde{N}^{\text{err}}$ are defined as follows:

• $\widetilde{N}^{\mathrm{dom}}(x,t,k)$ is analytic in $\mathbb{C}\setminus (B\cup\widetilde{B})$ and satisfies the Riemann–Hilbert problem

$$\widetilde{N}^{\text{dom+}} = \widetilde{N}^{\text{dom-}} V_B, \qquad k \in B, \qquad (4.110a)$$

$$\widetilde{N}^{\text{dom+}} = \widetilde{N}^{\text{dom}} \widetilde{V}_{\widetilde{B}}^{(7)}, \qquad k \in \widetilde{B}, \qquad (4.110b)$$

$$\widetilde{N}^{\text{dom}} = \left[I + O\left(\frac{1}{k}\right)\right] e^{i[g_{\infty}(\xi) + \widetilde{g}_{\infty} - G_{\infty}(\xi)t]\sigma_{3}}, \qquad k \to \infty. \qquad (4.110c)$$

$$\widetilde{N}^{\text{dom}} = \left[I + O\left(\frac{1}{k}\right)\right] e^{i\left[g_{\infty}(\xi) + \widetilde{g}_{\infty} - G_{\infty}(\xi)t\right]\sigma_{3}}, \qquad k \to \infty. \tag{4.110c}$$

• $\widetilde{N}^D(x, t, k)$ is analytic in $D_{k_0}^{\epsilon} \cup D_{\alpha}^{\epsilon} \cup D_{\alpha}^{\epsilon} \setminus \bigcup_{i=1}^{8} L_j$ with jumps

$$\widetilde{N}^{D+} = \widetilde{N}^{D-} \widetilde{V}_j^{(6)}, \quad k \in \widehat{L}_j := L_j \cap \left(D_{k_o}^{\epsilon} \cup D_{\alpha}^{\epsilon} \cup D_{\bar{\alpha}}^{\epsilon} \right), \quad j = 1, \dots, 8, \quad (4.111)$$

as shown in Fig. 19.

• $\widetilde{N}^{\text{err}}(x,t,k)$ is analytic in $\mathbb{C}\setminus(\bigcup_{i=1}^{6} \widecheck{L}_{i} \cup \partial D_{k}^{\epsilon} \cup \partial D_{\alpha}^{\epsilon} \cup \partial D_{\alpha}^{\epsilon} \cup \partial D_{p}^{\epsilon} \cup \partial D_{p}^{\epsilon})$ with $\widecheck{L}_i := L_i \setminus (\overline{D_{k_{\alpha}}^{\epsilon}} \cup \overline{D_{\alpha}^{\epsilon}}) \cup \overline{D_{\alpha}^{\epsilon}})$ and satisfies the Riemann–Hilbert problem (see Fig. 20)

$$\widetilde{N}^{\text{err+}} = \widetilde{N}^{\text{err}} \widetilde{V}^{\text{err}}, \qquad k \in \bigcup_{j=1}^{6} \widecheck{\mathbf{L}}_{j} \cup \partial D_{k_{o}}^{\epsilon} \cup \partial D_{\alpha}^{\epsilon} \cup \partial D_{\bar{\alpha}}^{\epsilon} \cup \partial D_{p}^{\epsilon} \cup \partial D_{\bar{p}}^{\epsilon}, \tag{4.112a}$$

$$\widetilde{N}^{\text{err}} = I + O\left(\frac{1}{k}\right), \qquad k \to \infty,$$
(4.112b)

where

$$\widetilde{V}^{\text{err}} = \begin{cases} \widetilde{N}^{\text{dom}} \widetilde{V}_{j}^{(7)} (\widetilde{N}^{\text{dom}})^{-1}, & k \in \widecheck{L}_{j}, \\ \widetilde{N}^{\text{dom}} \widetilde{V}_{p}^{(7)} (\widetilde{N}^{\text{dom}})^{-1}, & k \in \partial D_{p}^{\varepsilon}, \\ \widetilde{N}^{\text{dom}} \widetilde{V}_{\bar{p}}^{(7)} (\widetilde{N}^{\text{dom}})^{-1}, & k \in \partial D_{\bar{p}}^{\varepsilon}, \\ \widetilde{N}^{\text{asymp}} (\widetilde{V}_{D}^{\text{asymp}})^{-1} (\widetilde{N}^{\text{asymp}})^{-1}, & k \in \partial D_{k_{o}}^{\epsilon} \cup \partial D_{\alpha}^{\epsilon} \cup \partial D_{\alpha}^{\epsilon}, \end{cases}$$
(4.113)

and

$$\widetilde{V}_{D}^{\text{asymp}} = \begin{cases} \widetilde{V}_{D_{\alpha}}^{\text{asymp}}, & k \in \partial D_{\alpha}^{\epsilon}, \\ \widetilde{V}_{D_{\alpha}}^{\text{asymp}}, & k \in \partial D_{\bar{\alpha}}^{\epsilon}, \\ \widetilde{V}_{D_{k}}^{\text{asymp}}, & k \in \partial D_{k}^{\epsilon}. \end{cases}$$

$$(4.114)$$

Importantly, despite the fact that the jump $\widetilde{V}_D^{\rm asymp}$ is unknown, in [BM2] it was estimated to be equal to the identity up to $O(t^{-1/2})$ and hence it does not affect the leading-order asymptotics.

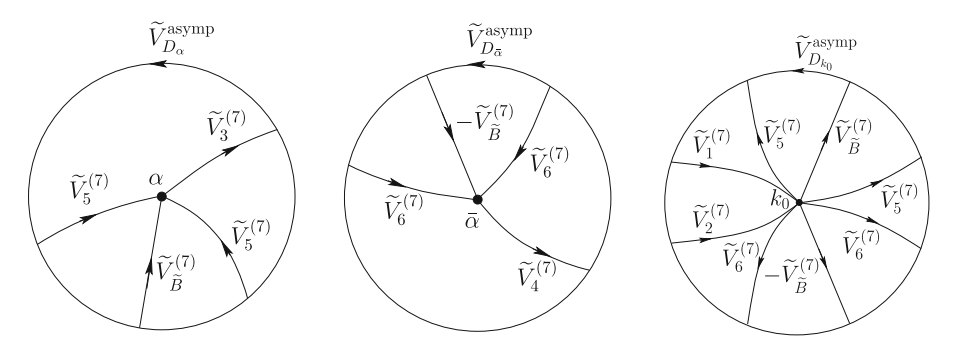


Fig. 19. Modulated elliptic wave in the transmission regime: The jumps of \widetilde{N}^D in the interior of and along the boundary of the disks $\overline{D_{\alpha}^{\epsilon}}$, $\overline{D_{\alpha}^{\epsilon}}$ and $\overline{D_{k_o}^{\epsilon}}$. Note that, although the jumps $\widetilde{V}_{D_{\alpha}}^{\text{asymp}}$, $\widetilde{V}_{D_{\alpha}}^{\text{asymp}}$, $\widetilde{V}_{D_{k_o}}^{\text{asymp}}$ are unknown, they are equal to the identity up to $O(t^{-1/2})$ and hence do not affect the dominant problem

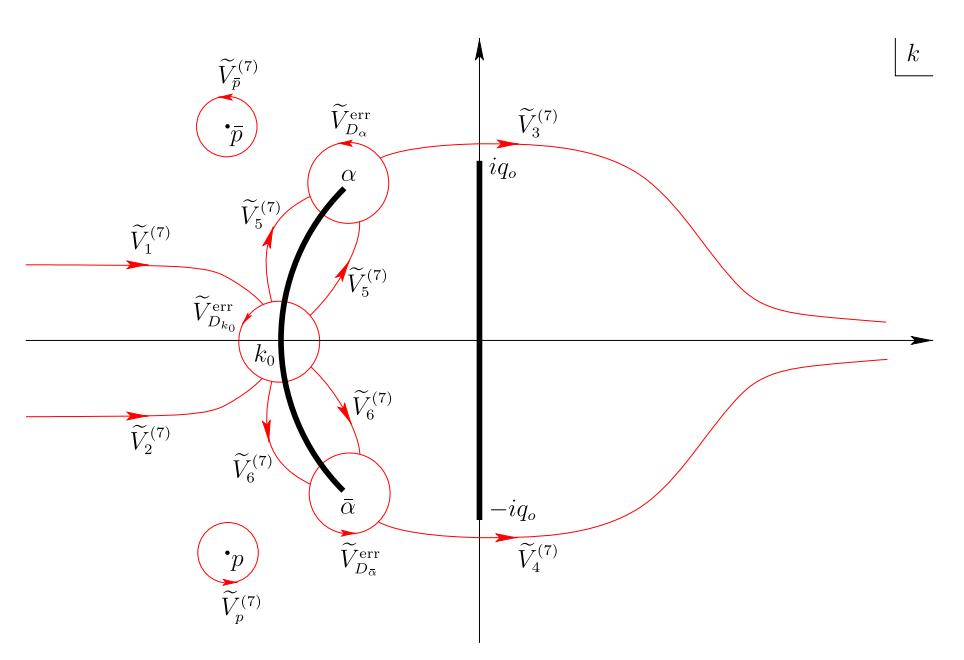


Fig. 20. Modulated elliptic wave in the transmission regime: The jumps of $\widetilde{N}^{\rm err}$

Solution of the dominant problem We begin by noting that, at the level of the dominant problem (4.110), since the jump $\widetilde{V}_{\widetilde{B}}^{(7)}$ is independent of k, the jump contour \widetilde{B} can be deformed to the straight line segment B' from $\bar{\alpha}$ to α so that the jump contours of problem (4.110) are as shown in Fig. 21. Problem (4.110) was solved in [BM2] in the case of $\widetilde{\omega} = \widetilde{g}_{\infty} = 0$. Adapting that analysis to account for the presence of $\widetilde{\omega}$ and \widetilde{g}_{∞} , we obtain

$$\widetilde{N}^{\text{dom}}(x,t,k) = e^{i[g_{\infty}(\xi) + \widetilde{g}_{\infty} - G_{\infty}(\xi)t]\sigma_{3}} \widetilde{\mathcal{N}}^{-1}(\xi,\infty,c) \widetilde{\mathcal{N}}(\xi,k,c)$$
(4.115)

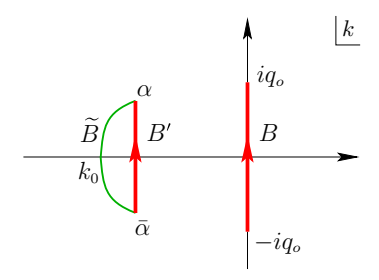


Fig. 21. Modulated elliptic wave in the transmission regime: The jump contours of $\widetilde{N}^{\text{dom}}$. The fact that the jump $\widetilde{V}_{\widetilde{B}}^{(7)}$ is independent of k has allowed us to deform \widetilde{B} to the straight line segment B' from $\bar{\alpha}$ to α . Note that the original and deformed versions of $\widetilde{N}^{\text{dom}}$ agree outside the finite region \mathcal{D} enclosed by \widetilde{B} and B'

with

$$\widetilde{\mathcal{N}}(\xi,k,c) = \frac{1}{2} \begin{pmatrix} \left[\eta(\xi,k) + \eta^{-1}(\xi,k) \right] \widetilde{N}_1(\xi,k,c) & i \left[\eta(\xi,k) - \eta^{-1}(\xi,k) \right] \widetilde{N}_2(\xi,k,c) \\ -i \left[\eta(\xi,k) - \eta^{-1}(\xi,k) \right] \widetilde{N}_1(\xi,k,-c) & \left[\eta(\xi,k) + \eta^{-1}(\xi,k) \right] \widetilde{N}_2(\xi,k,-c) \end{pmatrix} \tag{4.116}$$

and

$$\widetilde{\mathcal{N}}(\xi, \infty, c) := \lim_{k \to \infty} \widetilde{\mathcal{N}}(\xi, k, c), \tag{4.117}$$

where the function η with branch cuts along B and B' (see Fig. 21) is defined by

$$\eta(\xi, k) := \left[\frac{(k - iq_0)(k - \alpha)}{(k + iq_0)(k - \bar{\alpha})} \right]^{\frac{1}{4}}$$
(4.118)

and where \widetilde{N}_1 and \widetilde{N}_2 denote the first and second component of the vector-valued function

$$\widetilde{N}(\xi,k,c) := \left(\frac{\Theta\left(-\frac{\Omega t}{2\pi} + \frac{\omega + \widetilde{\omega}}{2\pi} + \frac{i \ln\left(\frac{\widetilde{q}_{-}}{iq_{0}}\right)}{2\pi} + \nu(k) + c\right)}{\sqrt{\frac{iq_{o}}{\widetilde{q}_{-}}} \Theta\left(\nu(k) + c\right)}, \frac{\Theta\left(-\frac{\Omega t}{2\pi} + \frac{\omega + \widetilde{\omega}}{2\pi} + \frac{i \ln\left(\frac{\widetilde{q}_{-}}{iq_{0}}\right)}{2\pi} - \nu(k) + c\right)}{\sqrt{\frac{\widetilde{q}_{-}}{iq_{0}}} \Theta\left(-\nu(k) + c\right)} \right). \tag{4.119}$$

In the above definition, the dependence of Ω , ω , $\widetilde{\omega}$, ν and c on ξ has been suppressed for convenience. Moreover, $\Theta(k) = \Theta(\xi, k)$ is the following variant of the third Jacobi theta function:

$$\Theta(\xi, k) = \theta_3(\pi k, e^{i\pi\tau(\xi)}), \quad \theta_3(z, \varrho) := \sum_{\ell \in \mathbb{Z}} e^{2i\ell z} \varrho^{\ell^2}, \tag{4.120}$$

with Riemann period

$$\tau(\xi) := \left(\oint_{\beta} \frac{dk}{\Gamma(\xi, k)} \right)^{-1} \oint_{\alpha} \frac{dk}{\Gamma(\xi, k)} = \frac{i K\left(\sqrt{1 - m^2}\right)}{K(m)}, \tag{4.121}$$

where the function Γ is defined in terms of the function γ of (2.9) by

$$\Gamma(\xi, k) = \begin{cases} \gamma(\xi, k), & k \in \mathbb{C} \backslash \overline{\mathcal{D}}, \\ -\gamma(\xi, k), & k \in \mathcal{D}, \end{cases}$$
(4.122)

where \mathcal{D} denotes the finite region enclosed by \widetilde{B} and B' (see Fig. 21). This definition implies that Γ has branch cuts along B and B', i.e. the branch cut \widetilde{B} of γ has been

deformed to B' in the case of Γ . The cycles $\{\alpha, \beta\}$ of the genus-1 Riemann surface associated with Γ are depicted in Fig. 22. Furthermore, the Abelian map ν in the arguments of the Θ -functions in (4.119) is defined by

$$v(k) = v(\xi, k) = \left(\oint_{\beta} \frac{dv}{\Gamma(\xi, v)}\right)^{-1} \int_{ia_0}^{k} \frac{dv}{\Gamma(\xi, v)},\tag{4.123}$$

and, finally,

$$c = c(\xi) := v \left(\frac{q_o \alpha_{\text{re}}}{q_o + \alpha_{\text{im}}} \right) + \frac{1}{2} (1 + \tau).$$
 (4.124)

Remark 4.3 (Analyticity of $\widetilde{\mathcal{N}}(\xi,k,c)$). The definition (4.124) of c ensures that the only possible singularity of $\widetilde{\mathcal{N}}(\xi,k,c)$ on the first sheet of the Riemann surface may occur at $k=\frac{q_o\alpha_{\rm re}}{q_o+\alpha_{\rm im}}$. This is because $\Theta(-\nu(k)+c)$ vanishes whenever $-\nu(k)+c=\frac{1}{2}(1+\tau)+\mathbb{Z}+\tau\mathbb{Z}$ and $\nu(k)$ is injective on each sheet of the Riemann surface as an Abelian map. Furthermore, this singularity is actually removable since it is the unique (finite) zero of $\eta-\eta^{-1}$ on the first sheet of the Riemann surface. Hence, all four entries of $\widetilde{\mathcal{N}}(\xi,k,c)$ are analytic away from the branch cuts B and B'.

Remark 4.4 (Invertibility of $\widetilde{\mathcal{N}}(\xi, \infty, c)$). Since $\lim_{k\to\infty} \eta(\xi, k) = 1$ and $\Theta(k) = \Theta(-k)$, letting

$$\nu_{\infty} = \nu_{\infty}(\xi) := \lim_{k \to \infty} \nu(\xi, k) \tag{4.125}$$

we have

$$\det \widetilde{\mathcal{N}}(\xi, \infty, c) = \frac{\Theta\left(-\frac{\Omega t}{2\pi} + \frac{\omega + \widetilde{\omega}}{2\pi} + \frac{i \ln\left(\frac{\widetilde{q}_{-}}{iq_{o}}\right)}{2\pi} + \nu_{\infty} + c\right)\Theta\left(-\frac{\Omega t}{2\pi} + \frac{\omega + \widetilde{\omega}}{2\pi} + \frac{i \ln\left(\frac{\widetilde{q}_{-}}{iq_{o}}\right)}{2\pi} - \nu_{\infty} - c\right)}{\Theta^{2}(\nu_{\infty} + c)}.$$

The denominator of this expression is always nonzero thanks to the choice of c (see Remark 4.3). Moreover, noting that $\Delta:=\left\{-\Omega t + \omega + \widetilde{\omega} + i \ln \left[\bar{q}_-/(iq_o)\right]\right\}/2\pi \in \mathbb{R}$ we observe that subtracting or adding Δ to $\nu_\infty + c$ does not affect the imaginary part of the argument of the Θ -functions in the numerator of $\det \widetilde{\mathcal{N}}(\xi,\infty,c)$. Thus, recalling that the zeros of $\Theta(k)$ are located at $k=\frac{1}{2}(1+\tau)+\mathbb{Z}+\tau\mathbb{Z}$ and noting that τ is purely imaginary, we deduce that $\det \widetilde{\mathcal{N}}(\xi,\infty,c)$ is nonzero and hence $\widetilde{\mathcal{N}}(\xi,\infty,c)$ is invertible, as required by (4.115).

Starting from the reconstruction formula (3.13) and applying the successive deformations that lead from $N=N^{(0)}$ to $\widetilde{N}^{(7)}$ while keeping in mind that $n,d,\delta \to 1$ as $k \to \infty$, we obtain

$$q(x,t) = -2i \lim_{k \to \infty} k \widetilde{N}_{12}^{(7)}(x,t,k) e^{i[g_{\infty}(\xi) + \widetilde{g}_{\infty} - G_{\infty}(\xi)t]}.$$
 (4.126)

Furthermore, according to the decomposition (4.108), for large k we have

$$\widetilde{N}_{12}^{(7)} = \widetilde{N}_{11}^{\text{err}} \widetilde{N}_{12}^{\text{dom}} + \widetilde{N}_{12}^{\text{err}} \widetilde{N}_{22}^{\text{dom}}.$$
 (4.127)

Hence, using also the asymptotic conditions (4.110c) and (4.112b), we find

$$q(x,t) = -2i \lim_{k \to \infty} k \widetilde{N}_{12}^{\text{dom}}(x,t,k) e^{i[g_{\infty}(\xi) + \widetilde{g}_{\infty} - G_{\infty}(\xi)t]} - 2i \lim_{k \to \infty} k \widetilde{N}_{12}^{\text{err}}(x,t,k).$$

$$(4.128)$$

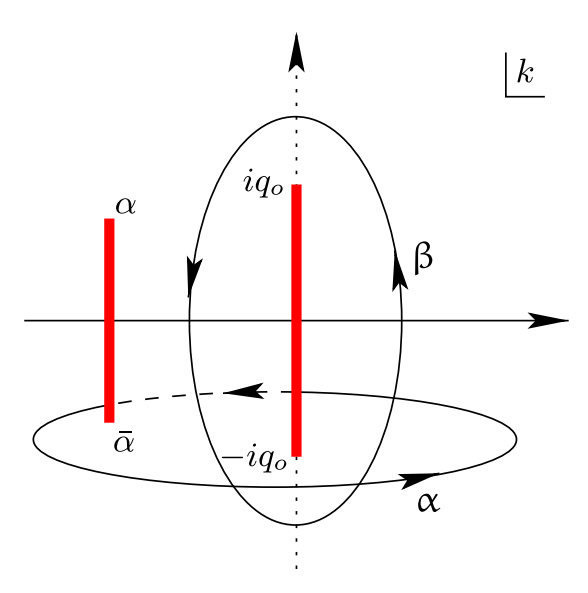


Fig. 22. Modulated elliptic wave in the transmission regime: The basis $\{\alpha, \beta\}$ of cycles for the genus-1 Riemann surface associated with the function $\Gamma(\xi, k)$. The cycle β is a closed, anti-clockwise contour that encircles the branch cut B while lying on the first sheet of the Riemann surface. The cycle α consists of an anti-clockwise contour that begins from the left of the branch cut B' and approaches the branch cut B from the right while lying on the first sheet, and then returns to B' via the second sheet (dashed portion)

All of the jumps of $\widetilde{N}^{\text{err}}$, including those along $\partial D_p^{\varepsilon}$ and $\partial D_{\overline{p}}^{\varepsilon}$, tend to the identity exponentially fast as $t \to \infty$. Hence, the second term in (4.128) is of lower order. In fact, similarly to [BM2] (see also [BV]) we have

$$\lim_{k \to \infty} k \widetilde{N}_{12}^{\text{err}}(x, t, k) = O\left(t^{-\frac{1}{2}}\right), \quad t \to \infty.$$
(4.129)

Moreover, since the original and deformed versions of $\widetilde{N}^{\text{dom}}$ agree outside the finite region \mathcal{D} enclosed by \widetilde{B} and B' (see Fig. 21) and hence in the limit $k \to \infty$, formula (4.115) together with the expansion

$$\eta(\xi, k) = 1 - \frac{i(q_o + \alpha_{\rm im})}{2k} + O\left(\frac{1}{k^2}\right), \quad k \to \infty,$$
(4.130)

imply

$$\lim_{k \to \infty} k \widetilde{N}_{12}^{\text{dom}}(x, t, k) = \frac{1}{2} \left(q_o + \alpha_{\text{im}} \right) \frac{\widetilde{N}_2(\xi, \infty, c)}{\widetilde{N}_1(\xi, \infty, c)} e^{i \left[g_{\infty}(\xi) + \widetilde{g}_{\infty} - G_{\infty}(\xi) t \right]}. \tag{4.131}$$

Therefore, at leading order the reconstruction formula (4.128) yields the modulated elliptic wave

$$q(x,t) = \frac{q_o(q_o + \alpha_{\text{im}})}{\bar{q}_-} \frac{\Theta\left(-\frac{\Omega t}{2\pi} + \frac{\omega + \tilde{\omega}}{2\pi} + \frac{i\ln\left(\frac{\bar{q}_-}{iq_o}\right)}{2\pi} - \nu_\infty + c\right)\Theta\left(\nu_\infty + c\right)}{\Theta\left(-\frac{\Omega t}{2\pi} + \frac{\omega + \tilde{\omega}}{2\pi} + \frac{i\ln\left(\frac{\bar{q}_-}{iq_o}\right)}{2\pi} + \nu_\infty + c\right)\Theta\left(-\nu_\infty + c\right)}$$

$$e^{2i[g_\infty(\xi) + \tilde{g}_\infty - G_\infty(\xi)t]}$$

$$+ O\left(t^{-\frac{1}{2}}\right), \quad t \to \infty,$$

$$(4.132)$$

where the real quantities $\alpha_{\rm im}$, Ω , ω , $\widetilde{\omega}$, G_{∞} , g_{∞} , depend only on ξ and are given respectively by (2.8), (4.75), (4.83), (4.99), (4.79), (4.87), the real constant \widetilde{g}_{∞} is given by (4.103), and the quantities $c(\xi)$ and $v_{\infty}(\xi)$ are defined by (4.124) and (4.125) respectively. In fact, as shown in [BM2], Ω can be expressed as

$$\Omega(\xi) = \frac{\pi |\alpha + iq_o|}{K(m)} (\xi - 2\alpha_{re})$$
(4.133)

with K(m) being the complete elliptic integral of the first kind with elliptic modulus m obtained via the modulation equations (2.8). Then, performing some straightforward manipulations of the relevant theta functions, we can write (4.132) in the more explicit form (2.18)–(2.19) with

$$X_o = X_o(\xi) := \frac{1}{2\pi} \left[\omega(\xi) - i \ln\left(\frac{q_-}{q_o}\right) \right] + \frac{1}{4}.$$
 (4.134)

The proof of Theorem 2.1 for the leading-order asymptotics in the transmission regime $p \in D_1$ is complete.

Remark 4.5 (Phase and position shifts). Setting $\widetilde{\omega} = \widetilde{g}_{\infty} = 0$ in (2.18)–(2.19) gives (2.21), which is precisely the modulated elliptic wave of [BM2]. That is, the effect of the soliton arising at $\xi = v_s$ on the leading-order asymptotics for $\xi \in (v_o, 0)$ is the constant phase shift $2\widetilde{g}_{\infty} = 4\arg [p + \lambda(p)]$ as well as a position shift related to the presence of the quantity $\widetilde{\omega}$.

5. The Trap Regime: Proof of Theorem 2.2

This regime arises for p inside the region D_2^+ of Fig. 1. In that case, we have $v_s > v_o$ i.e. $\text{Re}(i\theta)(\xi,p) < 0$ throughout the interval $(-\infty,v_o)$ and hence no soliton arises there. Furthermore, as already noted in the context of the fifth deformation of Sect. 4.4, for $p \in D_2^+$ the equation $\text{Re}(ih)(\xi,p) = 0$ has a *unique* solution \widetilde{v}_s in the interval $(v_o,0)$ (in fact, it turns out that $\widetilde{v}_s > v_s$). Thus, we split the range $(-\infty,0)$ into the subintervals $\xi < v_o$; $v_o < \xi < \widetilde{v}_s$; $\xi = \widetilde{v}_s$; and $\widetilde{v}_s < \xi < 0$.

- 5.1. The range $\xi < v_o$: plane wave. No soliton arises in this range since the asymptotics is dictated by the phase function θ and the fact that $v_o < v_s$ means that $\text{Re}(i\theta)(\xi, p) < 0$ throughout $(-\infty, v_o)$. Therefore, the analysis required is the same with the one carried out for $\xi < v_s$ in the transmission regime (see Sect. 4.1) and the leading-order asymptotics is given by the plane wave (2.13).
- 5.2. The range $v_o < \xi < \widetilde{v}_s$: modulated elliptic wave. This range is very similar to the range $(v_o, 0)$ of the transmission regime. In particular, applying the first six deformations of Sect. 4.4 we arrive again at Riemann–Hilbert problem (4.88) for the function $N^{(6)}$. For $p \in D_2^+$, however, $\text{Re}(ih)(\xi, p) < 0$ as opposed to $\text{Re}(ih)(\xi, p) > 0$ (see Fig. 23 and the relevant discussion in Sect. 4.4). Therefore, the jumps along ∂D_p^ε and ∂D_p^ε now tend to the identity exponentially fast as $t \to \infty$, allowing us to proceed to the decomposition of problem (4.88) into dominant and error components directly, without the need for transformations (4.92) and (4.97).

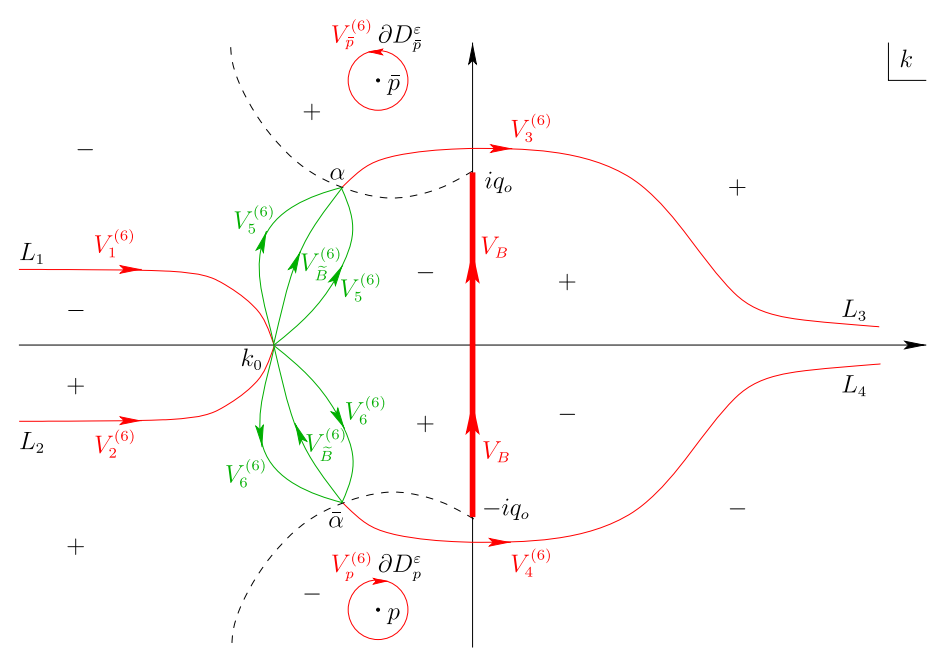


Fig. 23. Modulated elliptic wave in the trap regime: the jumps of Riemann-Hilbert problem (4.88). Contrary to the corresponding region in the transmission regime, the jumps along $\partial D_p^{\varepsilon}$ and $\partial D_{\bar{n}}^{\varepsilon}$ tend to the identity as $t \to \infty$

Indeed, performing the analogue of decomposition (4.108) and proceeding as in Sect. 4.4, we find

$$q(x,t) = -2i \lim_{k \to \infty} k N_{12}^{\text{dom}}(x,t,k) e^{i[g_{\infty}(\xi) - G_{\infty}(\xi)t]} + O(t^{-\frac{1}{2}}),$$
 (5.1)

where N^{dom} denotes the solution of the dominant component of Riemann–Hilbert problem (4.88) in the case $p \in D_2^+$. Specifically, as expected from the discussion above, N^{dom} satisfies problem (4.110) with $\widetilde{\omega} = \widetilde{g}_{\infty} = 0$, i.e. N^{dom} is analytic in $\mathbb{C} \setminus (B \cup \widetilde{B})$ with

$$N^{\text{dom+}} = N^{\text{dom-}} V_B, \qquad k \in B, \tag{5.2a}$$

$$N^{\text{dom+}} = N^{\text{dom-}} V_B, \qquad k \in B,$$
 (5.2a)
 $N^{\text{dom+}} = N^{\text{dom-}} V_{\widetilde{B}}^{(6)}, \qquad k \in \widetilde{B},$ (5.2b)

$$N^{\text{dom}} = \left[I + O\left(\frac{1}{k}\right)\right] e^{i[g_{\infty}(\xi) - G_{\infty}(\xi)t]\sigma_3}, \quad k \to \infty.$$
 (5.2c)

Problem (5.2) arises in the case of empty discrete spectrum analyzed in [BM2]. Actually, thanks to the fact that the jump $V_{\widetilde{R}}^{(6)}$ is independent of k, the jump contour \widetilde{B} in problem (5.2) can be deformed to the straight line segment B' from $\bar{\alpha}$ to α (see Fig. 21). Then, following [BM2], we obtain the solution of this deformed problem as

$$N^{\text{dom}}(x,t,k) = e^{i[g_{\infty}(\xi) - G_{\infty}(\xi)t]\sigma_3} \mathcal{N}^{-1}(\xi,\infty,c) \,\mathcal{N}(\xi,k,c),\tag{5.3}$$

where

$$\mathcal{N}(\xi, k, c) = \frac{1}{2} \begin{pmatrix} \left[\eta(\xi, k) + \eta^{-1}(\xi, k) \right] N_1(\xi, k, c) & i \left[\eta(\xi, k) - \eta^{-1}(\xi, k) \right] N_2(\xi, k, c) \\ -i \left[\eta(\xi, k) - \eta^{-1}(\xi, k) \right] N_1(\xi, k, -c) & \left[\eta(\xi, k) + \eta^{-1}(\xi, k) \right] N_2(\xi, k, -c) \end{pmatrix}$$
(5.4)

and

$$\mathcal{N}(\xi, \infty, c) := \lim_{k \to \infty} \mathcal{N}(\xi, k, c)$$
 (5.5)

with the function η defined by (4.118) and with N_1 and N_2 denoting the first and second column of the vector-valued function

$$N(\xi, k, c) = \left(\frac{\Theta\left(-\frac{\Omega t}{2\pi} + \frac{\omega}{2\pi} + \frac{i\ln\left(\frac{\tilde{q}}{iq_o}\right)}{2\pi} + \nu(k) + c\right)}{\sqrt{\frac{iq_o}{\tilde{q}_-}}\Theta\left(\nu(k) + c\right)}, \frac{\Theta\left(-\frac{\Omega t}{2\pi} + \frac{\omega}{2\pi} + \frac{i\ln\left(\frac{\tilde{q}_-}{iq_o}\right)}{2\pi} - \nu(k) + c\right)}{\sqrt{\frac{\tilde{q}_-}{iq_o}}\Theta\left(-\nu(k) + c\right)}\right),$$

$$(5.6)$$

where Ω , ω , ν and c are given by (4.133), (4.83), (4.123) and (4.124) respectively. We note that formula (5.3) is consistent with formula (4.115) after setting $\widetilde{\omega} = \widetilde{g}_{\infty} = 0$.

Recall that the original and deformed versions of N^{dom} agree outside the finite region \mathcal{D} enclosed by \widetilde{B} and B' (see Fig. 21) and hence in the limit $k \to \infty$. Thus, inserting the solution (5.3) in the reconstruction formula (5.1) and utilizing the explicit form (4.133) of Ω together with the theta functions manipulations performed in [BM2], we obtain the leading-order asymptotics (2.20)–(2.21).

5.3. The case $\xi = \widetilde{v}_s$: soliton on top of a modulated elliptic wave. Recall that in the trap regime currently under consideration the value \widetilde{v}_s is the unique solution of Eq. (2.12) in the interval $(v_o,0)$. That is, for $p \in D_2^+$ the quantities $\operatorname{Re}(ih)(\xi,p)$ and $\operatorname{Re}(ih)(\xi,\bar{p})$ vanish inside $(v_o,0)$ only at $\xi = \widetilde{v}_s$. In turn, the jumps $V_p^{(6)}$ and $V_{\bar{p}}^{(6)}$ given by (4.90) become part of the dominant component of Riemann–Hilbert problem (4.88) only for $\xi = \widetilde{v}_s$. Indeed, as noted earlier³ and will be confirmed below, whenever these jumps are part of the dominant problem they are eventually converted to residue conditions at p and \bar{p} . Thus, the relevant exponentials reduce to $e^{\pm 2ih(\xi,p)t}$, which for $p \in D_2^+$ are purely oscillatory (as opposed to growing or decaying) only for $\xi = \widetilde{v}_s$. On the other hand, thanks to the global sign structure of $\operatorname{Re}(ih)$ (see Fig. 23) the jumps $V_j^{(6)}$ tend to the identity exponentially fast as $t \to \infty$, like in the range (v_o, \widetilde{v}_s) .

Following the above remarks, for $\xi = \tilde{v}_s$ we write the solution of problem (4.88) as

$$N^{(6)} = N^{\text{err}} N^{\text{asymp}}, \tag{5.7}$$

where for disks $D_{k_o}^{\epsilon}$, D_{α}^{ϵ} , $D_{\bar{\alpha}}^{\epsilon}$ of radius ϵ centered at k_o , α , $\bar{\alpha}$ and such that they do not intersect with each other or with $B \cup \overline{D_p^{\epsilon}} \cup \overline{D_p^{\epsilon}}$, we let

$$N^{\text{asymp}} = \begin{cases} N^{\text{dom}}, & k \in \mathbb{C} \setminus (D_{k_o}^{\epsilon} \cup D_{\alpha}^{\epsilon} \cup D_{\tilde{\alpha}}^{\epsilon}), \\ N^{D}, & k \in D_{k_o}^{\epsilon} \cup D_{\alpha}^{\epsilon} \cup D_{\tilde{\alpha}}^{\epsilon}, \end{cases}$$
(5.8)

and define the functions N^{dom} , N^D and N^{err} as follows:

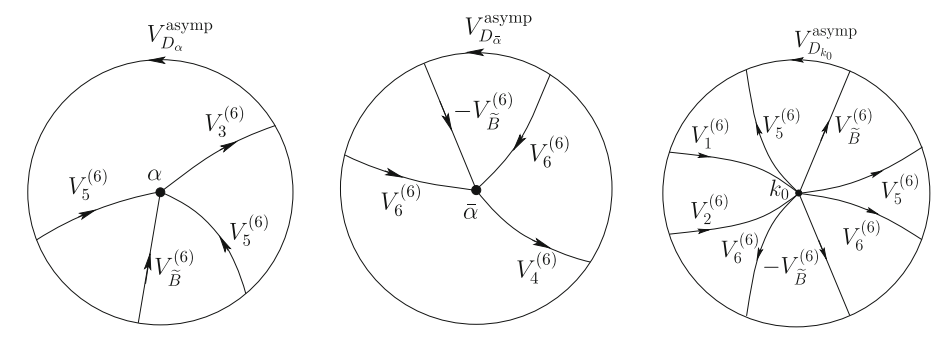


Fig. 24. Modulated elliptic wave in the trap regime: The jumps of N^D in the interior of and along the boundary of the disks $\overline{D_{\alpha}^{\epsilon}}$, $\overline{D_{\alpha}^{\epsilon}}$ and $\overline{D_{k_o}^{\epsilon}}$. Although the jumps $V_{D_{\alpha}}^{\text{asymp}}$, $V_{D_{\alpha}}^{\text{asymp}}$, $V_{D_{k_o}}^{\text{asymp}}$ are unknown, they are equal to the identity up to $O(t^{-1/2})$ and hence do not affect the dominant problem

• $N^{\mathrm{dom}}(\widetilde{v}_s t, t, k)$ is analytic in $\mathbb{C}\setminus (B\cup \widetilde{B}\cup \partial D_p^{\varepsilon}\cup \partial D_{\widetilde{p}}^{\varepsilon})$ and satisfies the Riemann–Hilbert problem

$$N^{\text{dom+}} = N^{\text{dom-}} V_B, \qquad k \in B, \qquad (5.9a)$$

$$N^{\text{dom+}} = N^{\text{dom-}} V_{\widetilde{B}}^{(6)}, \qquad k \in \widetilde{B}, \qquad (5.9b)$$

$$N^{\text{dom+}} = N^{\text{dom-}} V_p^{(6)}, \qquad k \in \partial D_p^{\varepsilon}, \qquad (5.9c)$$

$$N^{\text{dom+}} = N^{\text{dom-}} V_{\bar{p}}^{(6)}, \qquad k \in \partial D_{\bar{p}}^{\varepsilon}, \qquad (5.9d)$$

$$N^{\text{dom}} = \left[I + O\left(\frac{1}{k}\right)\right] e^{i\left[g_{\infty}(\widetilde{v}_s) - G_{\infty}(\widetilde{v}_s)t\right]\sigma_3}, \qquad k \to \infty.$$
 (5.9e)

• $N^D(\widetilde{v}_s t, t, k)$ is analytic in $D_{k_o}^{\epsilon} \cup D_{\alpha}^{\epsilon} \cup D_{\bar{\alpha}}^{\epsilon} \setminus \bigcup_{j=1}^{8} L_j$ with jumps

$$N^{D+} = N^{D-} V_j^{(6)}, \quad k \in \widehat{L}_j := L_j \cap \left(D_{k_o}^{\epsilon} \cup D_{\alpha}^{\epsilon} \cup D_{\tilde{\alpha}}^{\epsilon} \right), \quad j = 1, \dots, 8, \quad (5.10)$$

as shown in Fig. 24.

• $N^{\text{err}}(\widetilde{v}_s t, t, k)$ is analytic in $\mathbb{C}\setminus \left(\bigcup_{j=1}^6 \widecheck{L}_j \cup \partial D_{k_o}^\epsilon \cup \partial D_{\alpha}^\epsilon \cup \partial D_{\alpha}^\epsilon\right)$ with $\widecheck{L}_j := L_j\setminus (\overline{D_{k_o}^\epsilon} \cup \overline{D_{\alpha}^\epsilon} \cup \overline{D_{\alpha}^\epsilon})$ and satisfies the Riemann–Hilbert problem

$$N^{\text{err+}} = N^{\text{err-}} V^{\text{err}}, \qquad k \in \bigcup_{j=1}^{6} \widecheck{L}_{j} \cup \partial D_{k_{o}}^{\epsilon} \cup \partial D_{\alpha}^{\epsilon} \cup \partial D_{\bar{\alpha}}^{\epsilon},$$
 (5.11a)

$$N^{\text{err}} = I + O\left(\frac{1}{k}\right), \qquad k \to \infty,$$
 (5.11b)

with

$$V^{\text{err}} = \begin{cases} N^{\text{dom}} V_j^{(6)} (N^{\text{dom}})^{-1}, & k \in \widecheck{\mathbf{L}}_j, \\ N^{\text{asymp}-} (V_D^{\text{asymp}})^{-1} (N^{\text{asymp}-})^{-1}, & k \in \partial D_{k_o}^{\epsilon} \cup \partial D_{\alpha}^{\epsilon} \cup \partial D_{\alpha}^{\epsilon}, \end{cases}$$
(5.12)

and

$$V_{D}^{\text{asymp}} = \begin{cases} V_{D_{\alpha}}^{\text{asymp}}, & k \in \partial D_{\alpha}^{\epsilon}, \\ V_{D_{\alpha}}^{\text{asymp}}, & k \in \partial D_{\bar{\alpha}}^{\epsilon}, \\ V_{D_{k_{\alpha}}}^{\text{asymp}}, & k \in \partial D_{k_{\alpha}}^{\epsilon}. \end{cases}$$

$$(5.13)$$

Although $V_D^{\rm asymp}$ is unknown, in [BM2] it was shown that the contribution of the error problem (5.11) to the leading-order asymptotics is of $O(t^{-1/2})$. Therefore, starting from the reconstruction formula (3.13) and applying the six deformations that lead to $N^{(6)}$, we find

$$q(x,t) = -2i \lim_{k \to \infty} k N_{12}^{\text{dom}}(\widetilde{v}_s t, t, k) e^{i[g_{\infty}(\widetilde{v}_s) - G_{\infty}(\widetilde{v}_s)t]} + O\left(t^{-\frac{1}{2}}\right), \quad t \to \infty. \quad (5.14)$$

It remains to determine N^{dom} .

Solution of the dominant problem We now determine the solution N^{dom} of problem (5.9) via the same series of steps followed in Sect. 4.2. First, we convert the jumps $V_p^{(6)}$ and $V_{\bar{p}}^{(6)}$ along the circles $\partial D_p^{\varepsilon}$ and $\partial D_{\bar{p}}^{\varepsilon}$ to residue conditions at p and \bar{p} via the transformation

$$M^{\text{dom}} = \begin{cases} N^{\text{dom}}(V_p^{(6)})^{-1}, & k \in D_p^{\varepsilon}, \\ N^{\text{dom}}, & k \in \mathbb{C}^- \setminus (B^- \cup \widetilde{B}^- \cup \overline{D_p^{\varepsilon}}), \\ N^{\text{dom}}(V_{\overline{p}}^{(6)})^{-1}, & k \in D_{\overline{p}}^{\varepsilon}, \\ N^{\text{dom}}, & k \in \mathbb{C}^+ \setminus (B^+ \cup \widetilde{B}^+ \cup \overline{D_{\overline{p}}^{\varepsilon}}). \end{cases}$$
(5.15)

Indeed, the function M^{dom} maintains the jumps of N^{dom} along B and \widetilde{B} but has simple poles at p and \bar{p} instead of jumps along $\partial D_p^{\varepsilon}$ and $\partial D_{\bar{p}}^{\varepsilon}$. Specifically, M^{dom} satisfies the Riemann–Hilbert problem

$$M^{\text{dom+}} = M^{\text{dom-}} V_B, \qquad k \in B, \qquad (5.16a)$$

$$M^{\text{dom}+} = M^{\text{dom}-} V_{\widetilde{B}}^{(6)}, \qquad k \in \widetilde{B}, \qquad (5.16b)$$

$$M^{\text{dom}} = \left[I + O\left(\frac{1}{k}\right)\right] e^{i[g_{\infty}(\widetilde{v_s}) - G_{\infty}(\widetilde{v_s})t]\sigma_3}, \qquad k \to \infty, \tag{5.16c}$$

$$\operatorname{Res}_{k=p} M^{\operatorname{dom}} = \left(0, \rho_p \, M_1^{\operatorname{dom}}(p)\right),\tag{5.16d}$$

$$\operatorname{Res}_{k=\bar{p}} M^{\operatorname{dom}} = \left(\rho_{\bar{p}} M_2^{\operatorname{dom}}(\bar{p}), 0 \right), \tag{5.16e}$$

where M_1^{dom} , M_2^{dom} denote the first and second column of the matrix M^{dom} and

$$\rho_p = c_p \delta^2(\widetilde{v}_s, p) d(p) e^{2i[h(\widetilde{v}_s, p)t - g(\widetilde{v}_s, p)]}, \tag{5.17a}$$

$$\rho_{\bar{p}} = c_{\bar{p}} \delta^{-2}(\widetilde{v}_s, \bar{p}) d(\bar{p}) e^{-2i[h(\widetilde{v}_s, \bar{p})t - g(\widetilde{v}_s, \bar{p})]}.$$
 (5.17b)

In fact, similarly to Sect. 4.2, we can use the definitions (3.11a) and (3.11b) of c_p and $c_{\bar{p}}$ together with the symmetries $C_{\bar{p}} = -\overline{C_p}$, $d(\bar{k}) = \overline{d(k)}$, $\bar{d}'(\bar{k}) = \overline{a'(k)}$, $\delta(\xi, \bar{k}) = \overline{\delta^{-1}(\xi, k)}$, $g(\xi, \bar{k}) = \overline{g(\xi, k)}$, $h(\xi, \bar{k}) = \overline{h(\xi, k)}$ and the fact that $h(\tilde{v}_s, \bar{p}) \in \mathbb{R}$ to write expressions (5.17) as

$$\rho_p = R_p e^{2ih(\widetilde{v}_s, p)t}, \quad \rho_{\bar{p}} = -\overline{R_p} e^{-2ih(\widetilde{v}_s, p)t}, \quad R_p := C_p \frac{\delta^2(\widetilde{v}_s, p)e^{-2ig(\widetilde{v}_s, p)}}{a'(p)}.$$
(5.18)

Note that the writing (5.18) reveals that $\rho_{\bar{p}} = -\overline{\rho_p}$.

In order to solve problem (5.16), it is convenient to let

$$M^{\text{dom}} = \mathcal{M}^{\text{dom}} W \tag{5.19}$$

with W being the solution of the continuous spectrum component problem

$$W^{+} = W^{-}V_{B}, k \in B, (5.20a)$$

$$W^{+} = W^{-}V_{\widetilde{R}}^{(6)}, \qquad k \in \widetilde{B},$$
 (5.20b)

$$W = \left[I + O\left(\frac{1}{k}\right)\right] e^{i[g_{\infty}(\widetilde{v}_s) - G_{\infty}(\widetilde{v}_s)t]\sigma_3}, \qquad k \to \infty.$$
 (5.20c)

Observe that problem (5.20) is simply problem (5.2) evaluated at $\xi = \tilde{v}_s$. Therefore, as for problem (5.2), its jump contour \tilde{B} in problem (5.20) can be deformed to the straight line segment B' connecting $\bar{\alpha}$ with α (see Fig. 21), and the solution of this deformed problem is given by formula (5.3) as

$$W = e^{i[g_{\infty}(\widetilde{v}_s) - G_{\infty}(\widetilde{v}_s)t]\sigma_3} \mathcal{N}^{-1}(\widetilde{v}_s, \infty, c) \mathcal{N}(\widetilde{v}_s, k, c)$$
(5.21)

with \mathcal{N} defined by (5.4). Note further that det W inherits the analyticity of W away from B and \widetilde{B} , while (5.20) implies that

$$\det W^+ = \det W^- \det V_B, \qquad k \in B,$$

$$\det W^+ = \det W^- \det V_{\widetilde{s}}^{(6)}, \qquad k \in \widetilde{B}.$$

Therefore, since det $V_B \equiv \det V_{\widetilde{B}}^{(6)} \equiv 1$, we deduce that det W does not have jumps along

B and \widetilde{B} , i.e. det W is entire in k. Moreover, the asymptotic condition (5.20c) implies that $\lim_{k\to\infty} \det W = 1$. Thus, we conclude via Liouville's theorem that $\det W = 1$ for all $k \in \mathbb{C}$.

Combining (5.19) and (5.20), we find that the discrete component \mathcal{M}^{dom} of M^{dom} is analytic in $\mathbb{C}\setminus\{p,\bar{p}\}$ and has simple poles at p and \bar{p} with the following residues:

$$\operatorname{Res}_{k=p} \mathcal{M}_{1}^{\text{dom}} = -W_{21}(p)\rho_{p} M_{1}^{\text{dom}}(p), \tag{5.22a}$$

$$\operatorname{Res}_{k=p} \mathcal{M}_{2}^{\text{dom}} = W_{11}(p)\rho_{p} M_{1}^{\text{dom}}(p), \tag{5.22b}$$

$$\operatorname{Res}_{k=\bar{p}} \mathcal{M}_{1}^{\text{dom}} = W_{22}(\bar{p})\rho_{\bar{p}} M_{2}^{\text{dom}}(\bar{p}), \tag{5.22c}$$

$$\operatorname{Res}_{k=\bar{p}} \mathcal{M}_{2}^{\text{dom}} = -W_{12}(\bar{p})\rho_{\bar{p}} M_{2}^{\text{dom}}(\bar{p}). \tag{5.22d}$$

Moreover, \mathcal{M}^{dom} satisfies the asymptotic condition

$$\mathcal{M}^{\text{dom}} = I + O\left(\frac{1}{k}\right), \quad k \to \infty.$$
 (5.23)

Then, arguing as in Sect. 4.2, we deduce that

$$\mathcal{M}^{\text{dom}} = I + \frac{\underset{k=p}{\text{Res } \mathcal{M}^{\text{dom}}}}{k-p} + \frac{\underset{k=\bar{p}}{\text{Res } \mathcal{M}^{\text{dom}}}}{k-\bar{p}}.$$
 (5.24)

Thus, in order to determine \mathcal{M}^{dom} it suffices to determine its two residues at p and \bar{p} .

From (5.19) we have

$$M_{1}^{\text{dom}} = W_{1} + W_{11} \left[-\frac{W_{21}(p) \rho_{p} M_{1}^{\text{dom}}(p)}{k - p} + \frac{W_{22}(\bar{p}) \rho_{\bar{p}} M_{2}^{\text{dom}}(\bar{p})}{k - \bar{p}} \right] + W_{21} \left[\frac{W_{11}(p) \rho_{p} M_{1}^{\text{dom}}(p)}{k - p} - \frac{W_{12}(\bar{p}) \rho_{\bar{p}} M_{2}^{\text{dom}}(\bar{p})}{k - \bar{p}} \right]$$
(5.25a)

and

$$M_{2}^{\text{dom}} = W_{2} + W_{12} \left[-\frac{W_{21}(p) \rho_{p} M_{1}^{\text{dom}}(p)}{k - p} + \frac{W_{22}(\bar{p}) \rho_{\bar{p}} M_{2}^{\text{dom}}(\bar{p})}{k - \bar{p}} \right]$$

$$+ W_{22} \left[\frac{W_{11}(p) \rho_{p} M_{1}^{\text{dom}}(p)}{k - p} - \frac{W_{12}(\bar{p}) \rho_{\bar{p}} M_{2}^{\text{dom}}(\bar{p})}{k - \bar{p}} \right].$$
 (5.25b)

Evaluating the first of the above equations at k=p and the second one at $k=\bar{p}$ (recall that $M_1^{\rm dom}$ and $M_2^{\rm dom}$ are analytic at p and \bar{p} respectively), we obtain the system

$$\begin{split} M_{1}^{\text{dom}}(p) &= W_{1}(p) + \rho_{\bar{p}} \, \frac{W_{11}(p)W_{22}(\bar{p}) - W_{21}(p)W_{12}(\bar{p})}{p - \bar{p}} \, M_{2}^{\text{dom}}(\bar{p}) \\ &+ \rho_{p} \left[W_{21}'(p)W_{11}(p) - W_{11}'(p)W_{21}(p) \right] M_{1}^{\text{dom}}(p), \\ M_{2}^{\text{dom}}(\bar{p}) &= W_{2}(\bar{p}) + \rho_{p} \, \frac{W_{12}(\bar{p})W_{21}(p) - W_{22}(\bar{p})W_{11}(p)}{p - \bar{p}} \, M_{1}^{\text{dom}}(p) \\ &+ \rho_{\bar{p}} \left[W_{12}'(\bar{p})W_{22}(\bar{p}) - W_{22}'(\bar{p})W_{12}(\bar{p}) \right] M_{2}^{\text{dom}}(\bar{p}), \end{split} \tag{5.26b}$$

which can be solved to yield

$$M_1^{\text{dom}}(p) = \frac{-\mathcal{B}\rho_{\bar{p}}W_2(\bar{p}) + \left(1 + \mathcal{C}\rho_{\bar{p}}\right)W_1(p)}{\mathcal{B}^2\rho_p\rho_{\bar{p}} + \left(1 + \mathcal{C}\rho_{\bar{p}}\right)\left(1 + \mathcal{A}\rho_p\right)},\tag{5.27a}$$

$$M_2^{\text{dom}}(\bar{p}) = \frac{\mathcal{B}\rho_p W_1(p) + \left(1 + \mathcal{A}\rho_p\right) W_2(\bar{p})}{\mathcal{B}^2 \rho_p \rho_{\bar{p}} + \left(1 + \mathcal{C}\rho_{\bar{p}}\right) \left(1 + \mathcal{A}\rho_p\right)},\tag{5.27b}$$

where

$$A = W'_{11}(p)W_{21}(p) - W_{11}(p)W'_{21}(p), \tag{5.28a}$$

$$\mathcal{B} = \frac{W_{21}(p)W_{12}(\bar{p}) - W_{11}(p)W_{22}(\bar{p})}{p - \bar{p}},\tag{5.28b}$$

$$C = W'_{22}(\bar{p})W_{12}(\bar{p}) - W'_{12}(\bar{p})W_{22}(\bar{p}).$$
(5.28c)

Expressions (5.27) determine \mathcal{M}^{dom} through (5.24) and the residue relations (5.22). Having computed \mathcal{M}^{dom} , we return to the reconstruction formula (5.14) which upon (5.15) and (5.19) reads

$$q(x,t) = -2i \lim_{k \to \infty} k \left(\mathcal{M}^{\text{dom}} W \right)_{12} e^{i[g_{\infty}(\widetilde{v}_s) - G_{\infty}(\widetilde{v}_s)t]} + O\left(t^{-\frac{1}{2}}\right), \quad t \to \infty.$$
 (5.29)

Now, the asymptotic conditions (5.20c) and (5.23) imply

$$W = e^{i[g_{\infty}(\widetilde{v}_s) - G_{\infty}(\widetilde{v}_s)t]\sigma_3} + \frac{w}{k} + O\left(\frac{1}{k^2}\right), \quad \mathcal{M}^{\text{dom}} = I + \frac{\mu}{k} + O\left(\frac{1}{k^2}\right), \quad k \to \infty,$$

where the matrix-valued functions w and μ may depend on x and t but not on k. Therefore,

$$\left(\mathcal{M}^{\mathrm{dom}}W\right)_{12} = \frac{w_{12} + \mu_{12} \, e^{-i\left[g_{\infty}(\widetilde{v}_s) - G_{\infty}(\widetilde{v}_s)t\right]}}{k} + O\left(\frac{1}{k^2}\right), \quad k \to \infty.$$

Substituting for w_{12} via (5.21) (note that the original and deformed versions of W agree outside the finite region \mathcal{D} enclosed by \widetilde{B} and B' in Fig. 21 and hence as $k \to \infty$) and for μ_{12} via (5.22) and (5.24) yields the leading-order asymptotics (2.22)–(2.23) via the reconstruction formula (5.29).

Remark 5.1 (Dependence on g_{∞} and G_{∞}). Formula (5.21) implies that W_{11} and W_{12} depend on g_{∞} and G_{∞} through the exponential $e^{i[g_{\infty}(\widetilde{v}_s)-G_{\infty}(\widetilde{v}_s)t]}$ while W_{21} and W_{22} instead contain the exponential $e^{-i[g_{\infty}(\widetilde{v}_s)-G_{\infty}(\widetilde{v}_s)t]}$. Hence, the quantities \mathcal{A} , \mathcal{B} , \mathcal{C} defined by (5.28) are independent of g_{∞} and G_{∞} , and the overall dependence of the leading-order asymptotics (2.22) on g_{∞} and G_{∞} comes through a factor of $e^{2i[g_{\infty}(\widetilde{v}_s)-G_{\infty}(\widetilde{v}_s)t]}$.

5.4. The range $\tilde{v}_s < \xi < 0$: modulated elliptic wave with a phase shift. This range can be handled identically to the range $v_o < \xi < 0$ of the transmission regime that was analyzed in Sect. 4.4. Consequently, the leading-order asymptotics is characterized once again by (4.132) as the modulated elliptic wave (2.19) with a phase shift of $4\arg[p+\lambda(p)]$.

The proof of Theorem 2.2 for the leading-order asymptotics in the trap regime $p \in D_2^+$ is complete.

6. The Mixed Regimes: Proof of Theorems 2.3 and 2.4

In Sects. 4 and 5, we showed that the scenarios $p \in D_1$ and $p \in D_2^+$ give rise to *pure* asymptotic regimes, namely a transmission regime (Theorem 2.1) and a trap regime (Theorem 2.2) respectively. We now proceed to the analysis of the remaining two regions of Fig. 1, namely D_2^- and D_3 . We shall show that these regions correspond to *mixed* asymptotic regimes, specifically a trap/wake regime (Theorem 2.3) and a transmission/wake regime (Theorem 2.4) respectively.

6.1. The trap/wake regime. Recall that for $p \in D_2^-$ we have $v_o < v_s < 0$. Furthermore, as noted in Sect. 4.4, the integral Eq. (4.80) possesses exactly two solutions in the interval $(v_o, 0)$: \widetilde{v}_s , which corresponds to the crossing of the pole p by the dashed black curve in the third quadrant of Fig. 25 (for $\xi < \widetilde{v}_s$, the pole lies below this curve), and $v_w > \widetilde{v}_s$, which corresponds to the crossing of p by the branch cut \widetilde{B} (green contour connecting α and α in Fig. 25). Note that the latter crossing can happen only if p lies on the right (as opposed to the left) of \widetilde{B} immediately after $\xi = \widetilde{v}_s$, and this is the way one distinguishes the trap/wake regime $p \in D_2^-$ from the trap regime $p \in D_2^+$.

For $\xi < v_o$, the deformations performed in the trap regime can be repeated to lead once again to Riemann–Hilbert problem (4.14). Furthermore, like in the trap regime,

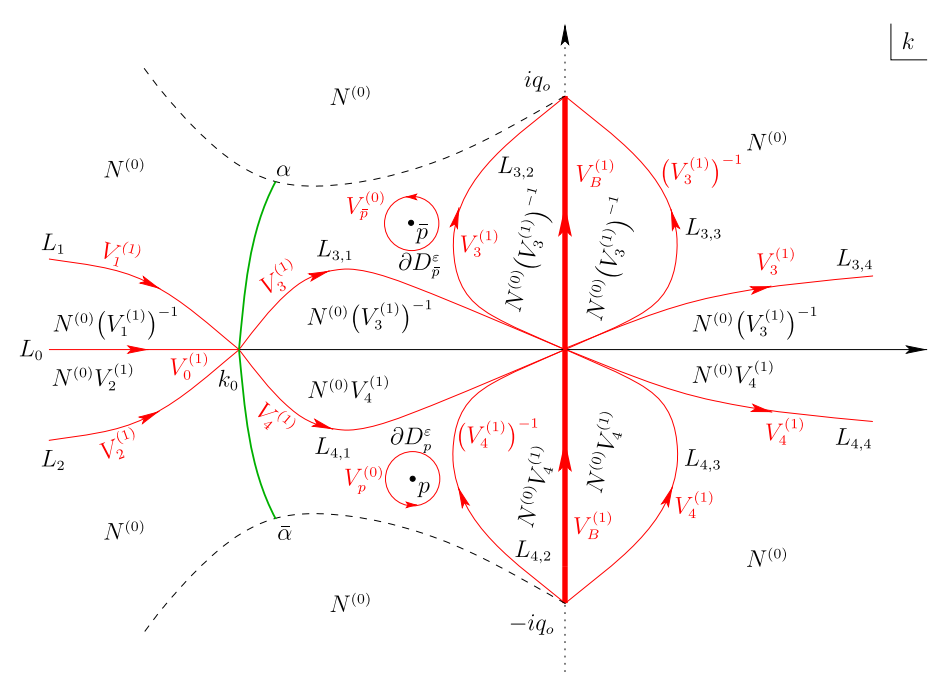


Fig. 25. Modulated elliptic wave in the trap/wake $(p \in D_2^-)$ and transmission/wake $(p \in D_3)$ regimes in the ranges $\widetilde{v}_s < \xi < v_w$ (for $p \in D_2^-$) and $v_o < \xi < v_w$ (for $p \in D_3$): the initial stage of the first deformation. The jumps along $\partial D_p^{\varepsilon}$ are not affected

for $\xi < v_o$ the dominant component of this problem only involves the jump along the branch cut B since the jumps along $\partial D_{\bar{p}}^{\varepsilon}$ and $\partial D_{\bar{p}}^{\varepsilon}$ tend to the identity exponentially fast as $t \to \infty$ due to the fact that $\text{Re}(i\theta)(\xi,p) < 0$ and $\text{Re}(i\theta)(\xi,\bar{p}) > 0$ throughout the interval $(-\infty,v_o)$. Thus, the leading-order asymptotics for $p \in D_2^-$ and $\xi \in (-\infty,v_o)$ is the same with the one of the trap regime, i.e. it is described by the plane wave (2.13).

For $v_o < \xi < \widetilde{v}_s$, the phase function switches from θ to h via transformation (4.76) and we eventually arrive at Riemann–Hilbert problem (4.88). Moreover, we still have $\text{Re}(ih)(\xi,p) < 0$ and $\text{Re}(ih)(\xi,\bar{p}) > 0$, thus the jumps along $\partial D_p^{\varepsilon}$ and $\partial D_{\bar{p}}^{\varepsilon}$ still do not contribute to the leading-order asymptotics, which is described by the modulated elliptic wave (2.21).

At $\xi = \widetilde{v}_s$, we have $\text{Re}(ih)(\widetilde{v}_s, p) = \text{Re}(ih)(\widetilde{v}_s, \bar{p}) = 0$. Thus, as explained in Sect. 5.3, the jumps along $\partial D_p^{\varepsilon}$ and $\partial D_{\bar{p}}^{\varepsilon}$ now contribute to the leading-order asymptotics, which is described by (2.22) as the soliton (2.23) on top of the modulated elliptic wave (2.21) evaluated at \widetilde{v}_s .

The range $\widetilde{v}_s < \xi < v_w$, which is not present in the trap regime since v_w does not arise there, requires a modification of the first four deformations. Specifically, while the first stage of the first deformation remains the same (compare Fig. 25 with Fig. 14), the poles p and \bar{p} now lie on the right of the branch cut \widetilde{B} . We emphasize that this is the defining difference between the trap/wake regime $p \in D_2^-$ and the trap regime $p \in D_2^+$, since in the latter case the poles are always on the left of \widetilde{B} for $\xi > \widetilde{v}_s$ (see also Fig. 7). Thus, for $\widetilde{v}_s < \xi < v_w$ in the trap/wake regime, in order to lift the jump along $[k_0, 0]$ away from the real axis and onto \widetilde{B} , the remaining stages of the first deformation

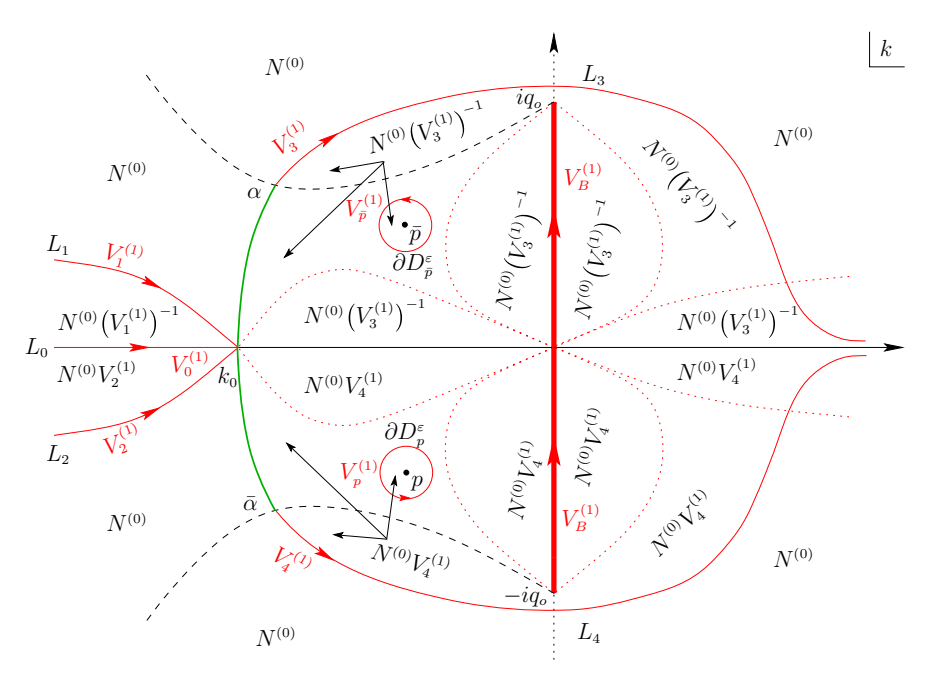


Fig. 26. Modulated elliptic wave in the trap/wake $(p \in D_2^-)$ and transmission/wake $(p \in D_3)$ regimes in the ranges $\widetilde{v}_s < \xi < v_w$ (for $p \in D_2^-$) and $v_o < \xi < v_w$ (for $p \in D_3$): the final stage of the first deformation. The jumps along $\partial D_p^{\varepsilon}$ and $\partial D_p^{\varepsilon}$ have now changed

are adjusted from those of the trap regime to the factorization shown in Fig. 26. Then, applying the second deformation (4.3) with δ given by (4.69) and the third deformation as shown in Fig. 13 but with the disks D_p^{ε} and $D_{\bar{p}}^{\varepsilon}$ now lying *between* the contours L_3 and L_4 , we obtain the analogue of Fig. 15, the only difference now being that the poles p and \bar{p} lie on the *right* of B. Subsequently, proceeding as in Sect. 4.4, we eventually arrive at the deformed Riemann–Hilbert problem of Fig. 27, which can be handled in the same way with Riemann–Hilbert problem (4.104). Indeed, since $\text{Re}(ih)(\xi, p) > 0$ and $\text{Re}(ih)(\xi, \bar{p}) < 0$, the jumps along $\partial D_p^{\varepsilon}$ and $\partial D_{\bar{p}}^{\varepsilon}$ are not significant at leading order and the corresponding asymptotics is given by (2.18) as the modulated elliptic wave (2.19) with a phase shift of $\text{4arg}[p + \lambda(p)]$.

For $v_w < \xi < 0$, the poles p and \bar{p} lie on the left of \widetilde{B} and, therefore, the analysis is identical to the one for the trap regime in the range $\widetilde{v}_s < \xi < 0$, leading once again to the asymptotics (2.18).

It remains to analyze the case $\xi=v_w$, which corresponds to the crossing of the poles p and \bar{p} by the branch cut \widetilde{B} of h (green contour connecting α and $\bar{\alpha}$ in Fig. 25) as the latter sweeps the region to its right en route to collapsing onto B as $\xi\to 0^-$. Since \widetilde{B} is also a zero-contour of $\mathrm{Re}(ih)$, this is the mechanism giving rise to the second solution of Eq. (4.80) when $p\in D_2^-$, since $\mathrm{Re}(ih)(\xi,k)$ vanishes along \widetilde{B} for all ξ and hence $\mathrm{Re}(ih)(v_w,p)=0$. As previously emphasized, the crossing of p and p by p occurs for $p\in D_2^+$ but not for $p\in D_2^+$, since in the latter case the poles are always on the left of p in the range p is p0.

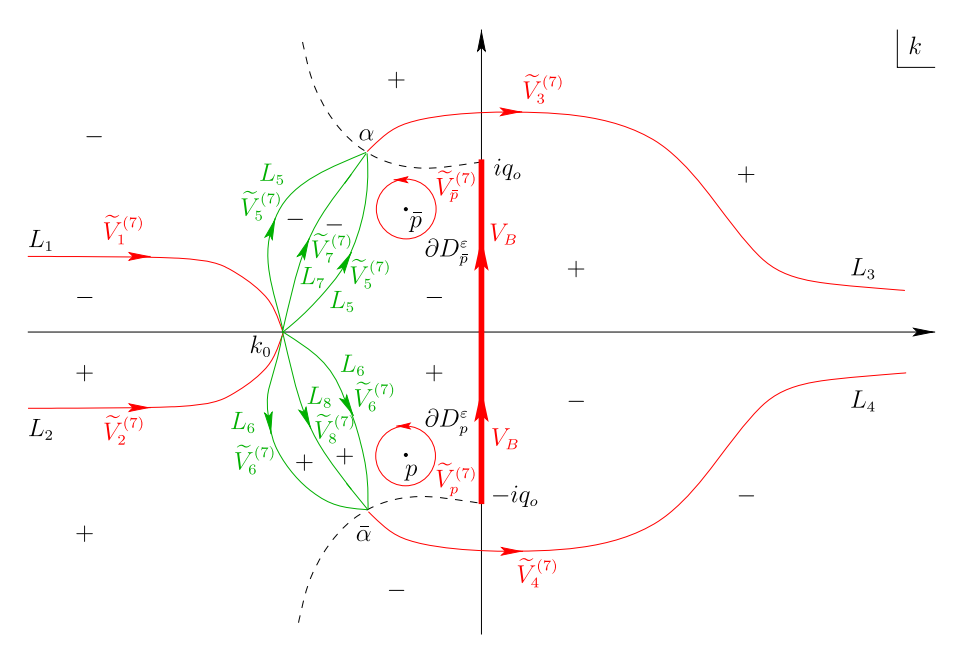


Fig. 27. Modulated elliptic wave in the trap/wake $(p \in D_2^-)$ and transmission/wake regimes $(p \in D_3)$: the jumps of the Riemann–Hilbert problem (4.104), the final problem in the ranges $\xi \in (\widetilde{v}_s, v_w) \cup (v_w, 0)$ (for $p \in D_2^-$) and $\xi \in (v_o, v_w) \cup (v_w, 0)$ (for $p \in D_3$)

The case $\xi = v_w$: soliton wake For this value of ξ , the poles p and \bar{p} lie on \widetilde{B} (depicted in green in Fig. 25), which is both a zero-contour for Re(ih) and a branch cut for h (along with the branch cut $B = i[-q_o, q_o]$). For this reason, in view of the fifth deformation of Riemann–Hilbert problem (3.16) (see (4.76)), it is convenient to switch from h to a function h_w which does not have a branch cut along \widetilde{B} but which is such that Re (ih_w) still vanishes along \widetilde{B} . More specifically, we define

$$h_w(k) = \begin{cases} h(v_w, k), & k \in \mathbb{C} \setminus \overline{\mathcal{R}}, \\ \Omega(v_w) - h(v_w, k), & k \in \mathcal{R}, \end{cases}$$
(6.1)

where the real constant $\Omega(v_w)$ is given by (4.133) and \mathcal{R} is the finite region enclosed by \widetilde{B} and the contour \widetilde{B}_w shown in blue in Fig. 28. It is straightforward to see that the function h_w (i) has branch cuts along B and \widetilde{B}_w , and (ii) is continuous along \widetilde{B} . Indeed, recall (see (4.74b)) that along \widetilde{B} we have $h^+ + h^- = \Omega(v_w)$. Hence, according to the definition (6.1) of h_w , along \widetilde{B} we have $h^+_w = (\Omega(v_w) - h)^+ = \Omega(v_w) - h^+ = h^- = h^-_w$, i.e. h_w is continuous along \widetilde{B} . On the other hand, along the contour \widetilde{B}_w shown in blue in Fig. 28 we have $h^+_w = (\Omega(v_w) - h)^+ = \Omega(v_w) - h = \Omega(v_w) - h^-_w$ (having used the fact that h is continuous along \widetilde{B}_w). Hence, h_w is discontinuous along \widetilde{B}_w with $h^+_w + h^-_w = \Omega(v_w)$. Furthermore, h_w is discontinuous along B since it is equal to B0 not both sides of B1. Therefore, B2 has branch cuts along B3 and B3 and is continuous along B3.

The sign structure of $Re(ih_w)$ is shown in Fig. 28. With this in mind, we perform the first deformation according to Fig. 28 and then deform the contours $L_{3,1}$, $L_{3,2}$ and $L_{4,1}$, $L_{4,2}$ to the contours L_3 and L_4 of Fig. 29, which depicts the final stage of the first deformation. Note that L_3 consists of the upper half of the branch cut \widetilde{B}_w as well as of

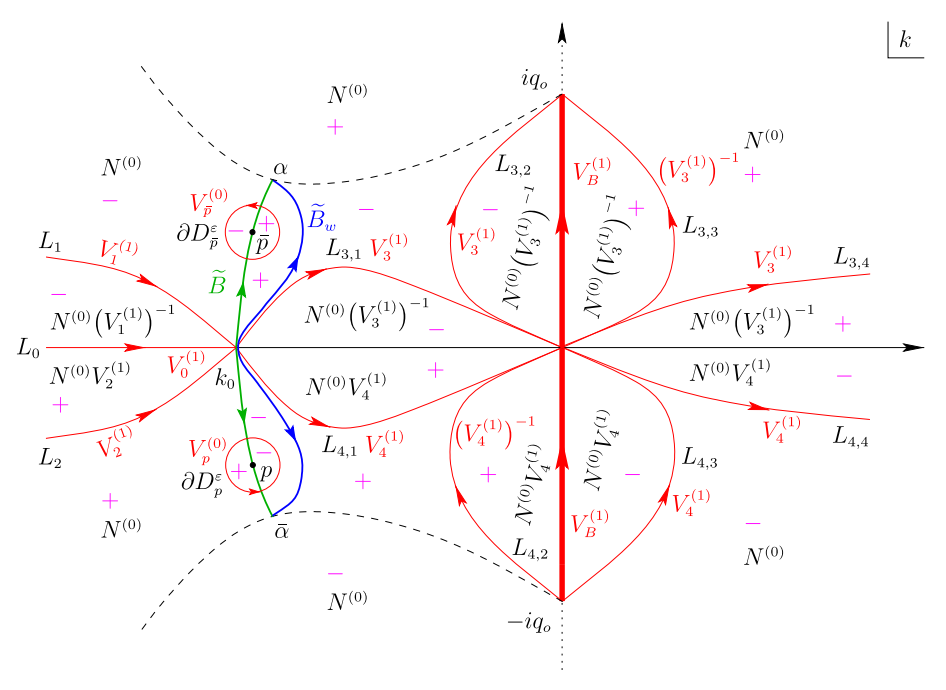


Fig. 28. Modulated elliptic wave in the trap/wake $(p \in D_2^-)$ and transmission/wake $(p \in D_3)$ regimes at $\xi = v_w$: the sign structure of $\operatorname{Re}(ih_w)$ and the initial stage of the first deformation. Note that the jumps along $\partial D_{\tilde{p}}^{\varepsilon}$ and $\partial D_{\tilde{p}}^{\varepsilon}$ are not affected. Furthermore, the branch cut \widetilde{B}_w of the function h_w (blue contour) lies on the right of the zero-contour \widetilde{B} of $\operatorname{Re}(ih_w)$ (green contour) as well as on the right of the circles $\partial D_{\tilde{p}}^{\varepsilon}$ and $\partial D_{\tilde{p}}^{\varepsilon}$. The finite region enclosed by \widetilde{B} and \widetilde{B}_w is denoted by \mathcal{R}

the red contour starting from α and curving around iq_o and down towards the positive real axis. Similarly, L_4 consists of both the lower half of \widetilde{B}_w and the red curve emanating from $\bar{\alpha}$ and directed upwards towards the positive real axis.

The second and third deformations are identical to those performed in the trap regime, leading to Riemann–Hilbert problem (4.68) but with the contours L_j , j=1,2,3,4 as shown in Fig. 29. For the fourth deformation, we use the factorizations (4.70) to "open up the lenses" off the portions of the contours L_3 and L_4 that lie along \widetilde{B}_w as shown in Fig. 30, where the jumps $V_j^{(4)}$, j=5,6,7,8 are given by (4.71). This Fig. provides the analogue of Fig. 16, where the role of the contour \widetilde{B} (which is a branch cut for h and a zero-contour for $\operatorname{Re}(ih)$ and, by definition (6.1), for $\operatorname{Re}(ih_w)$) is now held by the contour \widetilde{B}_w (which is a branch cut for h_w). The difference between Figs. 16 and 30 is that in the latter case the disks $\overline{D_p^\varepsilon}$ and $\overline{D_p^\varepsilon}$ lie between the contours L_6 , L_8 and L_5 , L_7 respectively. This is necessary in order for the contours L_5 and L_6 to lie in regions where the associated jumps $V_5^{(4)}$ and $V_6^{(4)}$ decay to the identity as $t\to\infty$. Hence, in the fourth deformation shown in Fig. 30, $N^{(3)}$ changes to $N^{(3)}V_6^{(4)}$ in D_p^ε and to $N^{(3)}(V_5^{(4)})^{-1}$ in D_p^ε (in Fig. 16, $N^{(3)}$ remains invariant inside the two disks). Consequently, $N^{(4)}$ satisfies the Riemann–Hilbert problem (4.72) but with the jumps along ∂D_p^ε and ∂D_p^ε now given by

$$V_p^{(4)} = (V_6^{(4)})^{-1} V_p^{(3)} V_6^{(4)}, \quad V_{\bar{p}}^{(4)} = V_5^{(4)} V_{\bar{p}}^{(3)} (V_5^{(4)})^{-1}, \tag{6.2}$$

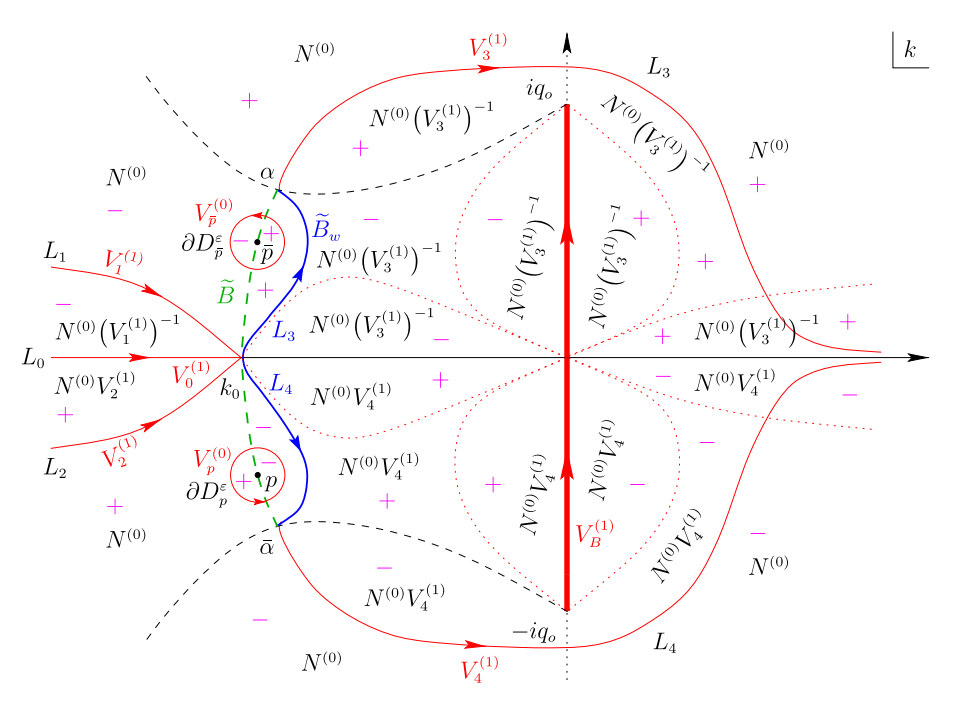


Fig. 29. Modulated elliptic wave in the trap/wake $(p \in D_2^-)$ and transmission/wake $(p \in D_3)$ regimes at $\xi = v_w$: the final stage of the first deformation. The jumps along $\partial D_p^{\varepsilon}$ and $\partial D_{\bar{p}}^{\varepsilon}$ are not affected

where we recall that

$$V_{p}^{(3)} = \begin{pmatrix} 1 - \frac{c_{p} \delta^{2}(v_{w}, k) d(k)}{k - p} e^{2i\theta(v_{w}, p)t} \\ 0 & 1 \end{pmatrix}, \quad V_{\bar{p}}^{(3)} = \begin{pmatrix} 1 & 0 \\ -\frac{c_{\bar{p}} \delta^{-2}(v_{w}, k) d(k)}{k - \bar{p}} e^{-2i\theta(v_{w}, \bar{p})t} 1 \end{pmatrix}$$

$$(6.3)$$

and

$$V_5^{(4)} = \begin{pmatrix} 1 & \frac{\delta^2}{r} e^{2i\theta t} \\ 0 & 1 \end{pmatrix}, \quad V_6^{(4)} = \begin{pmatrix} 1 & 0 \\ \frac{1}{r\delta^2} e^{-2i\theta t} & 1 \end{pmatrix}. \tag{6.4}$$

Next, we switch from $N^{(4)}$ to $N^{(5)}$ via the analogue of transformation (4.76), now involving h_w defined by (6.1) instead of h:

$$N^{(5)}(v_w t, t, k) = N^{(4)}(v_w t, t, k) e^{-i[h_w(k) - \theta(v_w, k)]t\sigma_3}.$$
 (6.5)

This transformation results in the analogue of Riemann–Hilbert problem (4.77), where all relevant jumps are given by (4.78) with h replaced by h_w except for the jumps along $\partial D_p^{\varepsilon}$ and $\partial D_{\bar{p}}^{\varepsilon}$, which are equal to

$$V_p^{(5)} = e^{i(h_w - \theta)t\sigma_3} (V_6^{(4)})^{-1} V_p^{(3)} V_6^{(4)} e^{-i(h_w - \theta)t\sigma_3}, \tag{6.6a}$$

$$V_{\bar{p}}^{(5)} = e^{i(h_w - \theta)t\sigma_3} V_5^{(4)} V_{\bar{p}}^{(3)} (V_5^{(4)})^{-1} e^{-i(h_w - \theta)t\sigma_3}.$$
 (6.6b)

Finally, we perform the sixth deformation similarly to (4.81), i.e. we let

$$N^{(6)}(v_w t, t, k) = N^{(5)}(v_w t, t, k)e^{ig_w(k)\sigma_3},$$
(6.7)

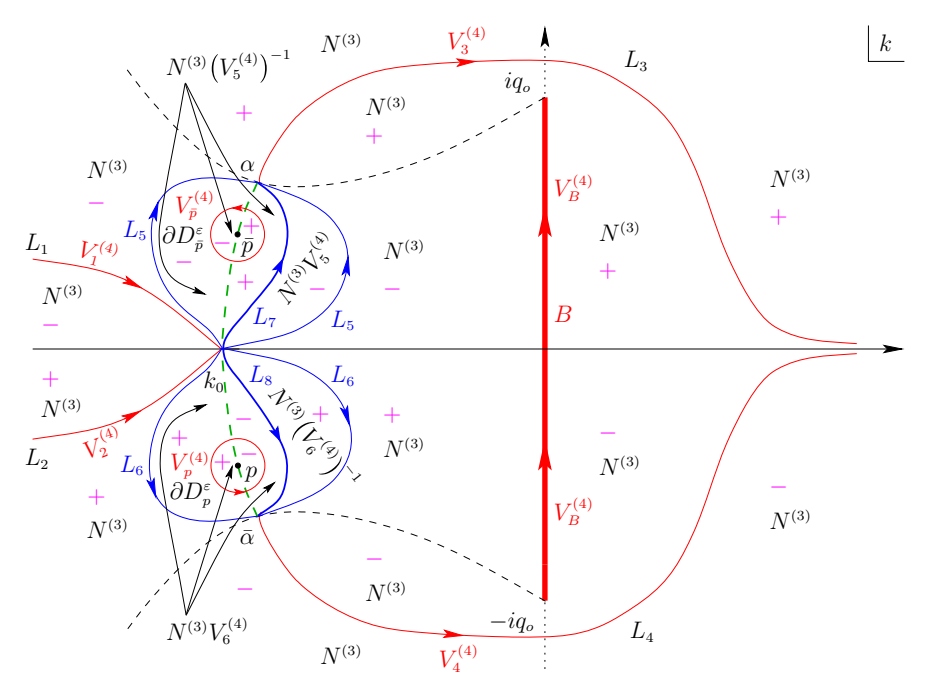


Fig. 30. Modulated elliptic wave in the trap/wake $(p \in D_2^-)$ and transmission/wake $(p \in D_3)$ regimes at $\xi = v_w$: the fourth deformation. We recall that the dashed green contour is the branch cut \widetilde{B} of h, along which $\operatorname{Re}(ih) = \operatorname{Re}(ih_w) = 0$, while the function h_w has branch cuts along $B = i[-q_o, q_o]$ and $\widetilde{B}_w = L_7 \cup (-L_8)$

where the function g_w , which is the analogue of the function g involved in (4.81), is analytic in $\mathbb{C}\setminus (B\cup \widetilde{B}_w)$ and satisfies the following jump conditions:

$$g_w^+ + g_w^- = -i \ln \left(\delta^2 \right), \qquad k \in B,$$
 (6.8a)

$$g_{w}^{+} + g_{w}^{-} = -i \ln \left(\frac{\delta^{2}}{r}\right) + \omega_{w}, \qquad k \in L_{7},$$

$$g_{w}^{+} + g_{w}^{-} = -i \ln \left(\delta^{2}\bar{r}\right) + \omega_{w}, \qquad k \in L_{8},$$
(6.8b)

$$g_w^+ + g_w^- = -i \ln \left(\delta^2 \bar{r}\right) + \omega_w, \qquad k \in L_8, \tag{6.8c}$$

with the contours B, L₇, L₈ as in Fig. 30, the function $\delta(v_w, k)$ given by (4.69) and the real constant ω_w defined by

$$\omega_{w} = i \frac{\int_{B} \frac{\ln \delta^{2}(v_{w}, v)}{\gamma_{w}(v)} dv + \int_{\widetilde{B}_{w}^{+}} \frac{\ln \left[\frac{\delta^{2}(v_{w}, v)}{r(v)}\right]}{\gamma_{w}(v)} dv + \int_{\widetilde{B}_{w}^{-}} \frac{\ln \left[\delta^{2}(v_{w}, v) \bar{r}(v)\right]}{\gamma_{w}(v)} dv}{\int_{\widetilde{B}_{w}} \frac{dv}{\gamma_{w}(v)}},$$
(6.9)

where

$$\widetilde{B}_w^{\pm} := \widetilde{B}_w \cap \mathbb{C}^{\pm} \tag{6.10}$$

and the function γ_w is defined in terms of the function γ (see (2.9)) by

$$\gamma_w(k) = \begin{cases} \gamma(v_w, k), & k \in \mathbb{C} \backslash \overline{\mathcal{R}}, \\ -\gamma(v_w, k), & k \in \mathcal{R}, \end{cases}$$
(6.11)

where we recall that \mathcal{R} is the finite region enclosed by \widetilde{B} and \widetilde{B}_w (see Fig. 28). Recalling further that γ is analytic in $\mathbb{C} \setminus B \cup \widetilde{B}$ and changes sign as k crosses B and \widetilde{B} , we deduce that γ_w has branch cuts along B and \widetilde{B}_w , across which it changes sign, but is continuous as k crosses \widetilde{B} . Dividing the jumps of problem (6.8) by γ_w and using Plemelj's formulae, we obtain

$$g_{w}(k) = \frac{\gamma_{w}(k)}{2\pi} \left[\int_{B} \frac{\ln \delta^{2}(v_{w}, v)}{\gamma_{w}(v)(v - k)} dv + \int_{L_{7}} \frac{\ln \left[\frac{\delta^{2}(v_{w}, v)}{r(v)} \right] + i\omega_{w}}{\gamma_{w}(v)(v - k)} dv - \int_{L_{8}} \frac{\ln \left[\delta^{2}(v_{w}, v) \bar{r}(v) \right] + i\omega_{w}}{\gamma_{w}(v)(v - k)} dv \right].$$

$$(6.12)$$

We note that the presence of ω_w in the above formula ensures that $g_w(k) = g_{w,\infty} + O\left(\frac{1}{k}\right)$ as $k \to \infty$ with the real constant $g_{w,\infty}$ given by

$$g_{w,\infty} = -\frac{1}{2\pi} \left[\int_{B} \frac{\ln \delta^{2}(v_{w}, v)}{\gamma_{w}(v)} v dv + \int_{\widetilde{B}_{w}^{+}} \frac{\ln \left[\frac{\delta^{2}(v_{w}, v)}{r(v)} \right] + i\omega_{w}}{\gamma_{w}(v)} v dv + \int_{\widetilde{B}_{w}^{-}} \frac{\ln \left[\delta^{2}(v_{w}, v) \, \bar{r}(v) \right] + i\omega_{w}}{\gamma_{w}(v)} v dv \right]. \tag{6.13}$$

Transformation (6.7) results in the analogue of Riemann–Hilbert problem (4.88), i.e.

$$N^{(6)+} = N^{(6)-}V_B, k \in B, (6.14a)$$

$$N^{(6)+} = N^{(6)-}V_{\widetilde{B}_w}^{(6)}, \qquad k \in \widetilde{B}_w, \tag{6.14b}$$

$$N^{(6)+} = N^{(6)-}V_j^{(6)},$$
 $k \in L_j, j = 1, ..., 6,$ (6.14c)

$$N^{(6)+} = N^{(6)-}V_p^{(6)}, k \in \partial D_p^{\varepsilon}, (6.14d)$$

$$N^{(6)+} = N^{(6)-}V_{\bar{p}}^{(6)}, \qquad k \in \partial D_{\bar{p}}^{\varepsilon}, \tag{6.14e}$$

$$N^{(6)} = \left[I + O\left(\frac{1}{k}\right)\right] e^{i\left[g_{w,\infty} - G_{\infty}(v_w)t\right]\sigma_3}, \qquad k \to \infty, \tag{6.14f}$$

where the jump along B is given by (4.2), the jump along \widetilde{B}_w is equal to

$$V_{\widetilde{B}_w}^{(6)} = \begin{pmatrix} 0 & -e^{i(\Omega(v_w)t - \omega_w)} \\ e^{-i(\Omega(v_w)t - \omega_w)} & 0 \end{pmatrix}$$
(6.15)

with the real constants $\Omega(v_w)$ and ω_w given by (4.133) and (6.9) respectively, the jumps along the contours L_i of Fig. 30 are equal to

$$V_1^{(6)} = \begin{pmatrix} 1 & \frac{\bar{r} \, \delta^2 e^{-2igw}}{1 + r\bar{r}} \, e^{2ih_w t} \\ 0 & 1 \end{pmatrix}, \qquad V_2^{(6)} = \begin{pmatrix} 1 & 0 \\ \frac{r\delta^{-2} e^{2igw}}{1 + r\bar{r}} \, e^{-2ih_w t} \, 1 \end{pmatrix}, \tag{6.16a}$$

$$V_3^{(6)} = \begin{pmatrix} 1 & 0 \\ r\delta^{-2}e^{2ig_w}e^{-2ih_wt} & 1 \end{pmatrix}, \qquad V_4^{(6)} = \begin{pmatrix} 1 & \bar{r}\delta^2e^{-2ig_w}e^{2ih_wt} \\ 0 & 1 \end{pmatrix}, \qquad (6.16b)$$

$$V_5^{(6)} = \begin{pmatrix} 1 & \frac{\delta^2 e^{-2ig_w}}{r} e^{2ih_w t} \\ 0 & 1 \end{pmatrix}, \qquad V_6^{(6)} = \begin{pmatrix} 1 & 0 \\ \frac{\delta^{-2} e^{2ig_w}}{r} e^{-2ih_w t} & 1 \end{pmatrix}, \qquad (6.16c)$$

the jumps along $\partial D_p^{\varepsilon}$ and $\partial D_{\bar{p}}^{\varepsilon}$ are given by

$$V_{p}^{(6)} = \begin{pmatrix} 1 - \frac{c_{p}d(k)}{\bar{r}(k)(k-p)} e^{-2i[\theta(v_{w},k) - \theta(v_{w},p)]t} & -\frac{c_{p}\delta^{2}(v_{w},k)d(k)e^{-2ig_{w}(k)}}{k-p} e^{2i[h_{w}(k) - \theta(v_{w},k) + \theta(v_{w},p)]t} \\ \frac{c_{p}d(k)e^{2ig_{w}(k)}}{\bar{r}^{2}(k)\delta^{2}(v_{w},k)(k-p)} e^{-2i[h_{w}(k) + \theta(v_{w},k) - \theta(v_{w},p)]t} & 1 + \frac{c_{p}d(k)}{\bar{r}(k)(k-p)} e^{-2i[\theta(v_{w},k) - \theta(v_{w},p)]t} \end{pmatrix},$$

$$(6.17a)$$

$$V_{\bar{p}}^{(6)} = \begin{pmatrix} 1 - \frac{c_{\bar{p}}d(k)}{r(k)(k-\bar{p})} e^{2i[\theta(v_w,k) - \theta(v_w,\bar{p})]t} & \frac{c_{\bar{p}}\delta^2(v_w,k)d(k)e^{-2ig_w(k)}}{r^2(k)(k-\bar{p})} e^{2i[h_w(k) + \theta(v_w,k) - \theta(v_w,\bar{p})]t} \\ - \frac{c_{\bar{p}}\delta^{-2}(v_w,k)d(k)e^{2ig_w(k)}}{k-\bar{p}} e^{-2i[h_w(k) - \theta(v_w,k) + \theta(v_w,\bar{p})]t} & 1 + \frac{c_{\bar{p}}d(k)}{r(k)(k-\bar{p})} e^{2i[\theta(v_w,k) - \theta(v_w,\bar{p})]t} \end{pmatrix}, \tag{6.17b}$$

and the real constants $G_{\infty}(v_w)$ and $g_{w,\infty}$ are given by (4.79) and (6.13) respectively.

The sign structure of $Re(ih_w)$ shown in Fig. 30 indicates that the leading-order contribution to the solution of problem (6.14) in the limit $t \to \infty$ comes from the jumps along B, \tilde{B}_w , $\partial D_p^{\varepsilon}$ and $\partial D_{\tilde{p}}^{\varepsilon}$. Indeed, observe that while the jumps along the contours L_j , $j=1,\ldots,6$, decay to the identity exponentially fast as $t\to\infty$, those along B and \widetilde{B}_w are purely oscillatory. Furthermore, noting that the jumps along $\partial D_p^{\varepsilon}$ and $\partial D_{\bar{p}}^{\varepsilon}$ will eventually be transformed to residue conditions at p and \bar{p} respectively, we see that the contributions of these jumps are also purely oscillatory as $t \to \infty$ since $\operatorname{Re}(ih_w)(p) = \operatorname{Re}(ih_w)(\bar{p}) = 0$ (recall that p and \bar{p} lie on the dashed green contour \widetilde{B} of Fig. 30, along which $Re(ih_w)$ vanishes). This analysis motivates a decomposition of $N^{(6)}$ entirely analogous to (5.7) and eventually leads to the asymptotic formula (5.14),

$$q(x,t) = -2i \lim_{k \to \infty} k N_{12}^{\text{dom}}(v_w t, t, k) e^{i \left[g_{w,\infty} - G_{\infty}(v_w)t\right]} + O\left(t^{-\frac{1}{2}}\right), \quad t \to \infty, \quad (6.18)$$

where N^{dom} is the solution of the dominant component of Riemann–Hilbert problem (6.14), i.e.

$$N^{\text{dom+}} = N^{\text{dom-}} V_B, \qquad k \in B, \qquad (6.19a)$$

$$\begin{split} N^{\mathrm{dom+}} &= N^{\mathrm{dom-}} V_B, & k \in B, \\ N^{\mathrm{dom+}} &= N^{\mathrm{dom-}} V_{\widetilde{B}_w}^{(6)}, & k \in \widetilde{B}_w, \\ N^{\mathrm{dom+}} &= N^{\mathrm{dom-}} V_p^{(6)}, & k \in \partial D_p^{\varepsilon}, \\ \end{split} \tag{6.19a}$$

$$N^{\text{dom+}} = N^{\text{dom-}} V_p^{(6)}, \qquad k \in \partial D_p^{\varepsilon}, \tag{6.19c}$$

$$N^{\text{dom+}} = N^{\text{dom-}} V_{\bar{p}}^{(6)}, \qquad k \in \partial D_{\bar{p}}^{\varepsilon}, \tag{6.19d}$$

$$N^{\text{dom}} = \left[I + O\left(\frac{1}{k}\right)\right] e^{i\left[g_{w,\infty} - G_{\infty}(v_w)t\right]\sigma_3}, \qquad k \to \infty.$$
 (6.19e)

The transformation

$$M^{\text{dom}} = \begin{cases} N^{\text{dom}}(V_p^{(6)})^{-1}, & k \in D_p^{\varepsilon}, \\ N^{\text{dom}}, & k \in \mathbb{C}^- \setminus (B^- \cup \widetilde{B}_w^- \cup \overline{D}_p^{\varepsilon}), \\ N^{\text{dom}}(V_{\overline{p}}^{(6)})^{-1}, & k \in D_{\overline{p}}^{\varepsilon}, \\ N^{\text{dom}}, & k \in \mathbb{C}^+ \setminus (B^+ \cup \widetilde{B}_w^+ \cup \overline{D}_{\overline{p}}^{\varepsilon}), \end{cases}$$
(6.20)

which is the analogue of transformation (5.15), allows us to turn the jumps of N^{dom} along D_p^{ε} and $D_{\bar{p}}^{\varepsilon}$ into residue conditions for M^{dom} at p and \bar{p} . In particular, note that $V_p^{(6)}$ and $V_{\bar{p}}^{(6)}$ are meromorphic inside the disks D_p^{ε} and $D_{\bar{p}}^{\varepsilon}$, their only singularities being simple poles at p and \bar{p} respectively. Furthermore, since $a(p) = \bar{a}(\bar{p}) = 0$, it follows from the definition (3.9) of the reflection coefficient r(k) that $\frac{1}{\bar{r}(p)} = \frac{1}{r(\bar{p})} = 0$. Thus, the singularity at k=p is removable from all elements of the matrix $V_p^{(6)}$ except for the 12-element. Similarly, the singularity at $k=\bar{p}$ is removable from all elements of the matrix $V_{\bar{p}}^{(6)}$ except for the 21-element. Therefore, employing transformation (6.20), we convert problem (6.19) for N^{dom} to the following problem for M^{dom} :

$$M^{\text{dom+}} = M^{\text{dom-}} V_B, \qquad k \in B, \tag{6.21a}$$

$$M^{\text{dom+}} = M^{\text{dom-}} \widetilde{V}_{\widetilde{B}_w}^{(6)}, \qquad k \in \widetilde{B}_w, \tag{6.21b}$$

$$M^{\text{dom}} = \left[I + O\left(\frac{1}{k}\right)\right] e^{i\left[g_{w,\infty} - G_{\infty}(v_w)t\right]\sigma_3}, \qquad k \to \infty, \tag{6.21c}$$

$$\operatorname{Res}_{k=p} M^{\operatorname{dom}} = \left(0, \rho_{p_w} M_2^{\operatorname{dom}}(p)\right), \tag{6.21d}$$

$$\operatorname{Res}_{k=\bar{p}} M^{\operatorname{dom}} = \left(\rho_{\bar{p}_w} M_1^{\operatorname{dom}}(\bar{p}), 0 \right), \tag{6.21e}$$

where M_1^{dom} , M_2^{dom} denote the two columns of M^{dom} and

$$\rho_{p_w} = c_p \delta^2(v_w, p) d(p) e^{2i[h_w(p)t - g_w(p)]}, \quad \rho_{\bar{p}_w} = c_{\bar{p}} \delta^{-2}(v_w, \bar{p}) d(\bar{p}) e^{-2i[h_w(\bar{p})t - g_w(\bar{p})]},$$
(6.22)

which similarly to (5.18) can be expressed in the form

$$\rho_{p_w} = R_{p_w} e^{2ih_w(p)t}, \quad \rho_{\bar{p}_w} = -\overline{R_{p_w}} e^{-2ih(p)t}, \quad R_{p_w} := C_p \frac{\delta^2(v_w, p)e^{-2ig_w(p)}}{a'(p)}, \quad (6.23)$$

revealing that $\rho_{\bar{p}_w} = -\overline{\rho_{p_w}}$.

Similarly to the previous sections, we solve problem (6.21) by employing the factorization

$$M^{\text{dom}} = \mathcal{M}^{\text{dom}} W_w, \tag{6.24}$$

where W_w is the solution of the continuous spectrum component of problem (6.21), i.e.

$$W_w^+ = W_w^- V_B, \qquad k \in B,$$
 (6.25a)

$$W_w = W_w V_B^{(6)},$$
 $k \in B,$ (6.25a)
 $W_w^+ = W_w^- V_{\widetilde{B}_w}^{(6)},$ $k \in \widetilde{B}_w,$ (6.25b)

$$W_w = \left[I + O\left(\frac{1}{k}\right)\right] e^{i\left[g_{w,\infty} - G_{\infty}(v_w)t\right]\sigma_3}, \qquad k \to \infty, \tag{6.25c}$$

and \mathcal{M}^{dom} solves the discrete spectrum component of problem (6.21), i.e. \mathcal{M}^{dom} is analytic in $\mathbb{C}\setminus\{p,\bar{p}\}$ and satisfies the residue conditions

$$\operatorname{Res}_{k=p} \mathcal{M}_{1}^{\text{dom}} = -W_{w21}(p)\rho_{p_{w}} M_{1}^{\text{dom}}(p), \qquad \operatorname{Res}_{k=p} \mathcal{M}_{2}^{\text{dom}} = W_{w11}(p)\rho_{p_{w}} M_{1}^{\text{dom}}(p),$$
(6.26a)

$$\operatorname{Res}_{k=\bar{p}} \mathcal{M}_{1}^{\text{dom}} = W_{w22}(\bar{p}) \rho_{\bar{p}_{w}} M_{2}^{\text{dom}}(\bar{p}), \qquad \operatorname{Res}_{k=\bar{p}} \mathcal{M}_{2}^{\text{dom}} = -W_{w12}(\bar{p}) \rho_{\bar{p}_{w}} M_{2}^{\text{dom}}(\bar{p}),$$
(6.26b)

and the asymptotic condition

$$\mathcal{M}^{\text{dom}} = I + O\left(\frac{1}{k}\right), \quad k \to \infty.$$
 (6.26c)

Problem (6.25) is entirely analogous to problem (5.20). In fact, similarly to problem (5.20), since the jump $V_{\widetilde{B}_w}^{(6)}$ is independent of k, the jump contour \widetilde{B}_w in problem (6.25) can be deformed to the straight line segment B' connecting $\bar{\alpha}$ to α (see Fig. 21). The solution of this deformed problem is then given by the analogue of formula (5.21), i.e.

$$W_w = e^{i[g_{w,\infty} - G_{\infty}(v_w)t]\sigma_3} \mathcal{N}_w^{-1}(\infty, c) \,\mathcal{N}_w(k, c), \tag{6.27}$$

where \mathcal{N}_w is defined similarly to (5.4) by

$$\mathcal{N}_{w}(k,c) = \frac{1}{2} \begin{pmatrix} \left[\eta(k) + \eta^{-1}(k) \right] N_{w1}(k,c) & i \left[\eta(k) - \eta^{-1}(k) \right] N_{w2}(k,c) \\ -i \left[\eta(k) - \eta^{-1}(k) \right] N_{w1}(k,-c) \left[\eta(k) + \eta^{-1}(k) \right] N_{w2}(k,-c) \end{pmatrix}$$
(6.28)

and

$$\mathcal{N}_w(\infty, c) := \lim_{k \to \infty} \mathcal{N}_w(k, c) \tag{6.29}$$

with η defined by (4.118) and with N_{w1} and N_{w2} denoting the first and second column of the vector-valued function

$$N_{w}(k,c) = \left(\frac{\Theta\left(-\frac{\Omega(v_{w})t}{2\pi} + \frac{\omega_{w}}{2\pi} + \frac{i\ln\left(\frac{\bar{q}_{-}}{iq_{o}}\right)}{2\pi} + \nu(k) + c\right)}{\sqrt{\frac{\bar{i}q_{o}}{\bar{q}_{-}}}\Theta\left(\nu(k) + c\right)}, \frac{\Theta\left(-\frac{\Omega(v_{w})t}{2\pi} + \frac{\omega_{w}}{2\pi} + \frac{i\ln\left(\frac{\bar{q}_{-}}{iq_{o}}\right)}{2\pi} - \nu(k) + c\right)}{\sqrt{\frac{\bar{q}_{-}}{iq_{o}}}\Theta\left(-\nu(k) + c\right)}\right),$$

$$(6.30)$$

where $c = c(v_w)$ and $v(k) = v(v_w, k)$ are given by formulae (4.123) and (4.124) evaluated at $\xi = v_w$.

Furthermore, arguing as in Sect. 4.2, we infer that the solution of problem (6.26) takes the form

$$\mathcal{M}^{\text{dom}} = I + \frac{\underset{k=p}{\text{Res } \mathcal{M}^{\text{dom}}}}{k-p} + \frac{\underset{k=\bar{p}}{\text{Res } \mathcal{M}^{\text{dom}}}}{k-\bar{p}}.$$
 (6.31)

In addition, we compute

$$M_1^{\text{dom}}(p) = \frac{-\mathcal{B}_w \rho_{\bar{p}_w} W_{w2}(\bar{p}) + (1 + \mathcal{C}_w \rho_{\bar{p}_w}) W_{w1}(p)}{\mathcal{B}_w^2 \rho_{p_w} \rho_{\bar{p}_w} + (1 + \mathcal{C}_w \rho_{\bar{p}_w}) (1 + \mathcal{A}_w \rho_{p_w})},$$
(6.32a)

$$M_{2}^{\text{dom}}(\bar{p}) = \frac{\mathcal{B}_{w} \rho_{p_{w}} W_{w1}(p) + (1 + \mathcal{A}_{w} \rho_{p_{w}}) W_{w2}(\bar{p})}{\mathcal{B}_{w}^{2} \rho_{p_{w}} \rho_{\bar{p}_{w}} + (1 + \mathcal{C}_{w} \rho_{\bar{p}_{w}}) (1 + \mathcal{A}_{w} \rho_{p_{w}})},$$
(6.32b)

where

$$A_w = W_{w11}'(p)W_{w21}(p) - W_{w11}(p)W_{w21}'(p), \tag{6.33a}$$

$$\mathcal{B}_{w} = \frac{W_{w21}(p)W_{w12}(\bar{p}) - W_{w11}(p)W_{w22}(\bar{p})}{p - \bar{p}},$$
(6.33b)

$$C_w = W_{w'2}(\bar{p})W_{w12}(\bar{p}) - W_{w'12}(\bar{p})W_{w22}(\bar{p}). \tag{6.33c}$$

Combining expressions (6.26) and (6.32), we obtain \mathcal{M}^{dom} through the representation (6.31). In turn, proceeding as in Sect. 5.3 we obtain the leading-order asymptotics for the focusing NLS IVP (1.5) at $\xi = v_w$ in the form (2.24)–(2.25). Finally, similarly to Remark 5.1, we note that the overall dependence of the asymptotic solution (2.24) on $g_{w,\infty}$ and $G_{\infty}(v_w)$ is expressed by a factor of $e^{2i\left[g_{w,\infty}-G_{\infty}(v_w)t\right]}$.

The proof of Theorem 2.3 for the leading-order asymptotics in the trap/wake regime $p \in D_2^-$ is complete.

Remark 6.1 (Soliton vs. soliton wake). We recall that the soliton arising at $\xi = \widetilde{v}_s$ induces a phase shift in the asymptotics for $\widetilde{v}_s < \xi < 0$. This is because in the transition from \widetilde{v}_s^- to \widetilde{v}_s^+ the quantity $\operatorname{Re}(ih)$ switches sign from negative (Fig. 23) to positive (Fig. 27) along ∂D_p^ε . Hence, in the latter case the additional transformation (4.92) must be employed in order to convert growth into decay in the jump along ∂D_p^ε . On the other hand, the soliton wake arising at $\xi = v_w$ does not cause a phase shift in the asymptotics for $v_w < \xi < 0$. To see this, recall that the wake is created at $\xi = v_w$ because at that value of ξ the contour \widetilde{B} , along which $\operatorname{Re}(ih)$ vanishes for all ξ , crosses the pole p. Hence, $\operatorname{Re}(ih)(v_w, p) = \operatorname{Re}(ih_w)(p) = 0$ and the jump along ∂D_p^ε contributes to the leading-order asymptotics. However, the quantity $\operatorname{Re}(ih)$ is positive along ∂D_p^ε both right before and right after the crossing with \widetilde{B} (see Fig. 27). Consequently, the jump along ∂D_p^ε remains bounded in the transition from v_w^- to v_w^+ (recall that transformation (4.92) has already been applied for $\xi > \widetilde{v}_s$) and hence no further transformations are required for $v_w < \xi < 0$.

Remark 6.2 (h vs. h_w). Although the case $\xi = v_w$ was analyzed by switching from the phase function h (used for all $\xi \neq v_w$) to the phase h_w defined by (6.1), it would have still been possible to obtain the asymptotic result (2.24)–(2.25) by adhering to h. However, the fact that for $\xi = v_w$ the poles p and \bar{p} lie along the branch cut \tilde{B} of h would have made the analysis significantly more complicated. In particular, even the very first step of the analysis, namely, transformation (3.14) which converts the residue conditions at p and \bar{p} to jumps along the circles ∂D_p^ε and $\partial D_{\bar{p}}^\varepsilon$, would have resulted in additional jump conditions inside the disks D_p^ε and $D_{\bar{p}}^\varepsilon$ due to fact that for $\xi = v_w$ these disks are crossed by the branch cut \tilde{B} of h. Switching from h to h_w , whose branch cut \tilde{B}_w does not intersect with D_p^ε and $D_{\bar{p}}^\varepsilon$, significantly simplifies the analysis for the case $\xi = v_w$. Of course, for all $\xi \neq v_w$ the poles are away from \tilde{B} and hence the switch from h to h_w is not necessary.

6.2. The transmission/wake regime. Recall that for $p \in D_3$ we have $v_s < v_o$ and, furthermore, the integral Eq. (4.80) possesses a unique solution v_w in the interval $(v_o, 0)$, which corresponds to the crossing of the pole p by the branch cut \widetilde{B} .

For $\xi < v_o$, performing the deformations of Sect. 4.1 of the transmission regime, we obtain Riemann–Hilbert problem (4.14). Then, like in the transmission regime, since $\text{Re}(i\theta)(\xi,p) < 0$ throughout the interval $(-\infty,v_s)$ the leading-order asymptotics is described by the plane wave (2.13). At $\xi = v_s$, we have $\text{Re}(i\theta)(v_s,p) = 0$. Hence, Riemann–Hilbert problem (4.14) can be analyzed like in Sect. 4.2 to yield the asymptotics in the form (2.15) as the soliton (2.16) on top of the plane wave (2.14) evaluated at v_s . For $v_s < \xi < v_o$, the fact that $p \in D_3$ means that $p_{\text{re}} > k_2$, as opposed to $p_{\text{re}} < k_1$ of the case $p \in D_1$. That is, if $p \in D_3$ then p is crossed by the portion of the curve $\text{Re}(i\theta) = 0$ that goes through $\pm iq_o$ and k_2 (as opposed to the one going through k_1). Hence, after the crossing p lies inside the finite region enclosed by the curve $\text{Re}(i\theta) = 0$ and the branch cut B (see Fig. 31) as opposed to the unbounded region on the left of $\text{Re}(i\theta) = 0$ and k_1 . For this reason, the analysis of Sect. 4.3 for $p \in D_1$ now needs to be modified as described below.

First deformation (Figs. 31, 32, 33 and 34). Choose the contours $L_{4,1}$, $L_{4,2}$ and $L_{3,1}$, $L_{3,2}$ so that they do not intersect with the disks $\overline{D_p^{\varepsilon}}$ and $\overline{D_p^{\varepsilon}}$. Then, as shown in Figs. 31, 32 and 33, in order to deform L_4 outside the bounded region of "wrong" (i.e. positive) sign,

we eventually need to set $N^{(1)} = N^{(0)} V_4^{(1)}$ inside the disk D_p^{ε} , as opposed to the regime $p \in D_1$ in which the fact that $p_{\rm re} < k_1$ allows us to always have $N^{(1)} = N^{(0)}$ in D_p^{ε} (see Figs. 8, 9, 10 and 11). The situation is analogous for the disk $D_{\bar{p}}^{\varepsilon}$. Therefore, for $p \in D_3$ the Riemann–Hilbert problem for $N^{(1)}$ reads

$$N^{(1)+} = N^{(1)-}V_p^{(1)}, k \in B, (6.34a)$$

$$N^{(1)+} = N^{(1)-}V_i^{(1)}, \qquad k \in L_j, \ j = 1, 2, 3, 4,$$
 (6.34b)

$$N^{(1)+} = N^{(1)-}V_p^{(1)}, \qquad k \in \partial D_p^{\varepsilon},$$
 (6.34c)

$$N^{(1)+} = N^{(1)-} V_{\bar{p}}^{(1)}, \qquad k \in \partial D_{\bar{p}}^{\varepsilon},$$
 (6.34d)

$$N^{(1)} = I + O\left(\frac{1}{k}\right), \qquad k \to \infty, \tag{6.34e}$$

where the matrices $V_B^{(1)}$ and $V_j^{(1)}$, j=1,2,3,4, are defined as in (4.2) but the matrices $V_p^{(1)}$ and $V_{\bar{p}}^{(1)}$ are given instead by

$$V_p^{(1)} = (V_4^{(1)})^{-1} V_p^{(0)} V_4^{(1)} = \begin{pmatrix} 1 - \frac{c_p d(k)}{k - p} e^{2i\theta(\xi, p)t} \\ 0 & 1 \end{pmatrix}, \tag{6.35}$$

$$V_{\bar{p}}^{(1)} = V_3^{(1)} V_{\bar{p}}^{(0)} (V_3^{(1)})^{-1} = \begin{pmatrix} 1 & 0 \\ -\frac{c_{\bar{p}} d(k)}{k - \bar{p}} e^{-2i\theta(\xi, \bar{p})t} & 1 \end{pmatrix}.$$
(6.36)

Second deformation This deformation is identical to (4.3) of Sect. 4.1 and results in the Riemann–Hilbert problem

$$N^{(2)+} = N^{(2)-}V_R^{(2)}, \qquad k \in B, \tag{6.37a}$$

$$N^{(2)+} = N^{(2)-}V_i^{(2)}, \qquad k \in L_i, \ j = 1, 2, 3, 4,$$
 (6.37b)

$$N^{(2)+} = N^{(2)-}V_n^{(2)}, \qquad k \in \partial D_n^{\varepsilon},$$
 (6.37c)

$$N^{(2)+} = N^{(2)-}V_{\bar{p}}^{(2)}, \qquad k \in \partial D_{\bar{p}}^{\varepsilon},$$
 (6.37d)

$$N^{(2)} = I + O\left(\frac{1}{k}\right), \qquad k \to \infty, \tag{6.37e}$$

with $V_B^{(2)}$ and $V_j^{(2)}$, j = 1, 2, 3, 4, as in (4.6) but with

$$V_p^{(2)} = \delta^{\sigma_3} V_p^{(1)} \delta^{-\sigma_3} = \begin{pmatrix} 1 - \frac{c_p \, \delta^2(\xi, k) d(k)}{k - p} \, e^{2i\theta(\xi, p)t} \\ 0 & 1 \end{pmatrix}, \tag{6.38a}$$

$$V_{\bar{p}}^{(2)} = \delta^{\sigma_3} V_{\bar{p}}^{(0)} \delta^{-\sigma_3} = \begin{pmatrix} 1 & 0 \\ -\frac{c_{\bar{p}}}{\delta^{-2}(\xi, k)d(k)} e^{-2i\theta(\xi, \bar{p})t} & 1 \end{pmatrix}.$$
(6.38b)

Third deformation (Fig. 35). This deformation is different than the one of Fig. 13 in that the disks $\overline{D_p^{\varepsilon}}$ and $\overline{D_p^{\varepsilon}}$ now lie between the contours L_4 and L_3 and hence inside these disks we have $N^{(3)} = N^{(2)}$. Thus, the jumps (6.38) now remain invariant while the remaining jumps of problem (6.37) are modified as in the second deformation (4.3)

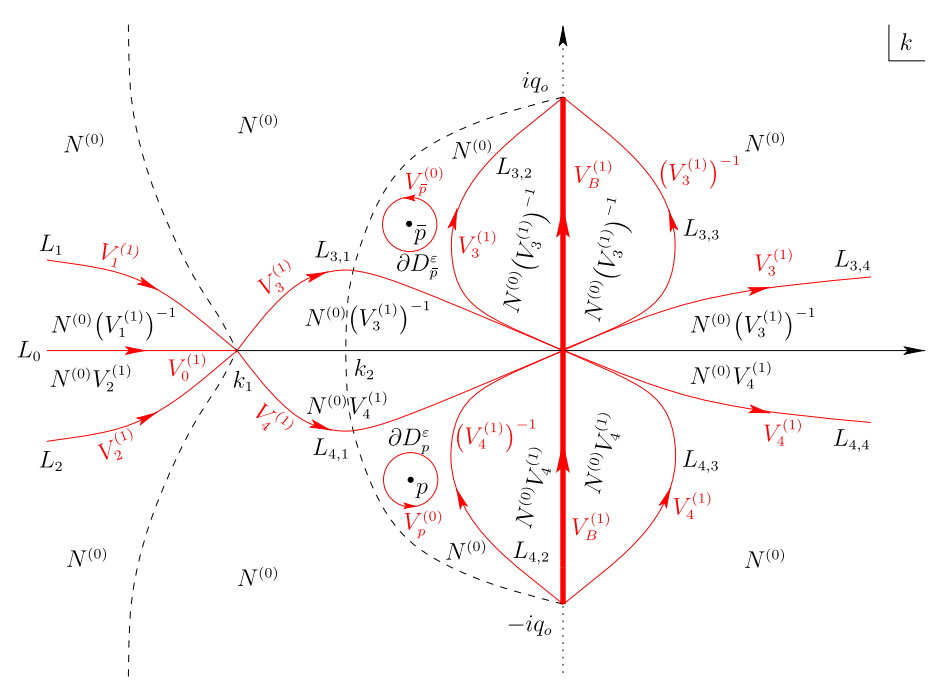


Fig. 31. Plane wave in the transmission/wake regime $(p \in D_3)$ for $v_s < \xi < v_o$: the first stage of the first deformation. The jumps along $\partial D_p^{\varepsilon}$ and $\partial D_{\bar{p}}^{\varepsilon}$ are unaffected

but with $d^{\frac{1}{2}}$ now holding the role of δ . Eventually, we find that $N^{(3)}$ satisfies the same problem as in Sect. 4.1.

Fourth deformation This is identical to (4.10), leading to Riemann–Hilbert problem (4.14).

In summary, in the range $v_s < \xi < v_o$ the original Riemann–Hilbert problem (3.16) can be deformed to Riemann–Hilbert problem (4.14) both for $p \in D_1$ and for $p \in D_3$. Thus, performing the analysis of Sect. 4.3, we obtain once again the phase-shifted plane wave (2.17).

For $v_o < \xi < 0$, the phase function changes from θ to h. Recall that for $p \in D_1$ the asymptotics is given by the phase-shifted modulated elliptic wave (2.18) throughout the range $(v_o,0)$. Now, however, $p \in D_3$ and hence, as noted in the relevant discussion of Sect. 4.4, there is a value $v_w \in (v_o,0)$ for which the contour \widetilde{B} crosses the pole p en route to collapsing onto B. Indeed, this value is the unique solution of Eq. (4.80) in the interval $(v_o,0)$. Thus, similarly to the case $p \in D_2^-$, a soliton wake arises from the dominant component of Riemann–Hilbert problem (4.104) at $\xi = v_w$. In fact, the dominant problem is precisely that of Sect. 6.1. Therefore, at $\xi = v_w$ the leading-order asymptotics is characterized by (2.24) as the soliton wake (2.25) on top of the modulated elliptic wave $q_{\text{mew},w}(t)$. Finally, for $v_o < \xi < v_w$ and $v_w < \xi < 0$ the jumps along ∂D_p^ε and ∂D_p^ε are not part of the dominant problem and, like in the transmission regime, the leading-order asymptotics is given by the phase-shifted modulated elliptic wave (2.18). We note that, like in the trap/wake regime (see Remark 6.1), the soliton at v_s induces a phase shift of 4 arg $[p + \lambda(p)]$ in the asymptotics but no phase shift is generated by the soliton wake at v_w .

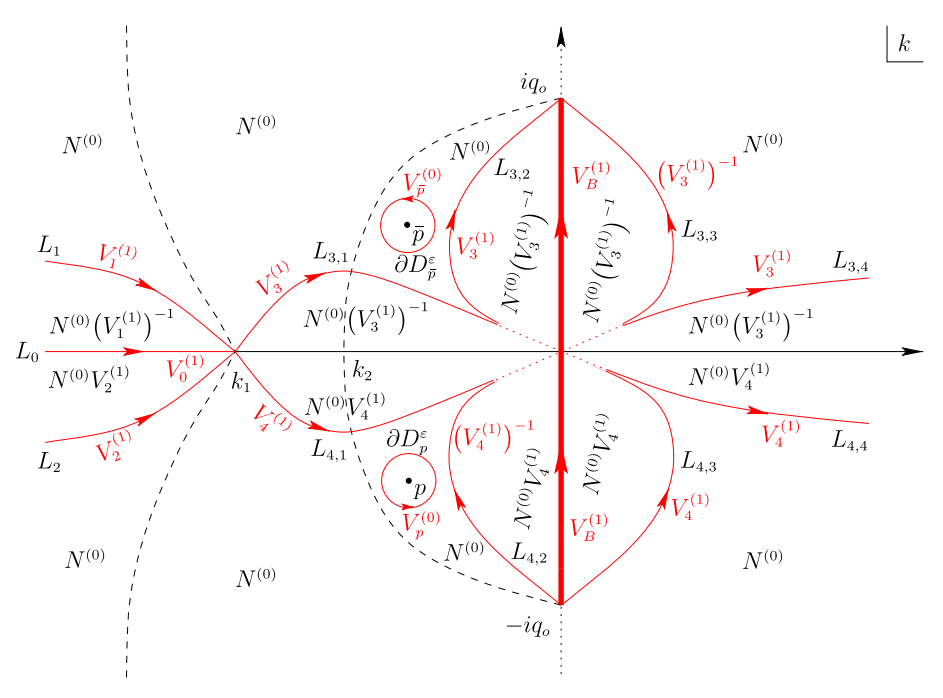


Fig. 32. Plane wave in the transmission/wake regime $(p \in D_3)$ for $v_s < \xi < v_o$: the second stage of the first deformation. The overlapping portions of the contours $L_{3,1}$ and $L_{3,2}$, as well as of the contours $L_{4,1}$ and $L_{4,2}$, have been removed since by definition $N^{(1)}$ does not have a jump there. Hence, the contours $L_{3,1}$, $L_{3,2}$, $L_{4,1}$, $L_{4,2}$ have been lifted away from the origin. The jumps along $\partial D_{\vec{p}}^{\rho}$ and $\partial D_{\vec{p}}^{\rho}$ remain unchanged

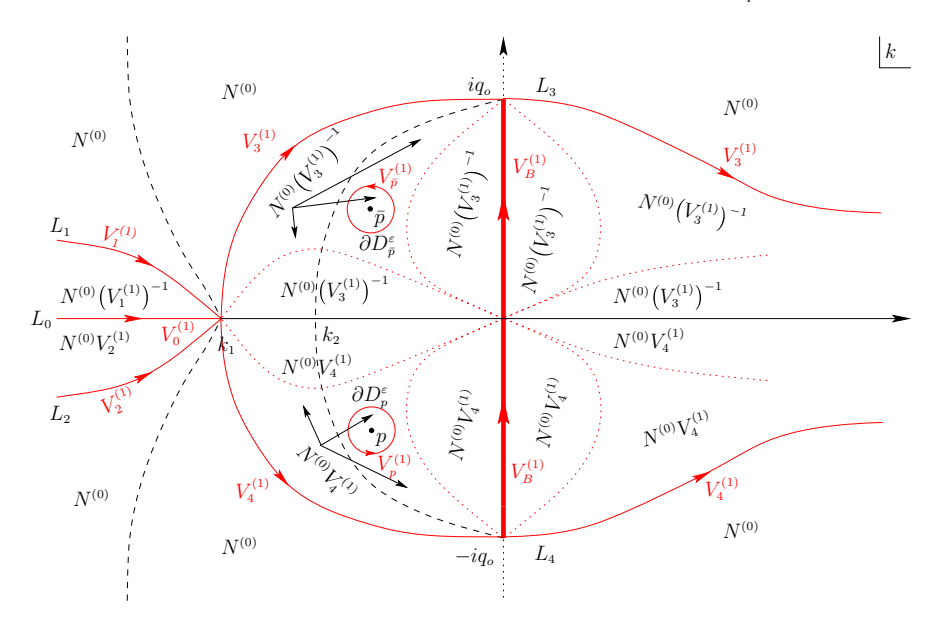


Fig. 33. Plane wave in the transmission/wake regime ($p \in D_3$) for $v_s < \xi < v_o$: the third stage of the first deformation. The jumps along $\partial D_p^{\varepsilon}$ and $\partial D_{\bar{p}}^{\varepsilon}$ have now changed

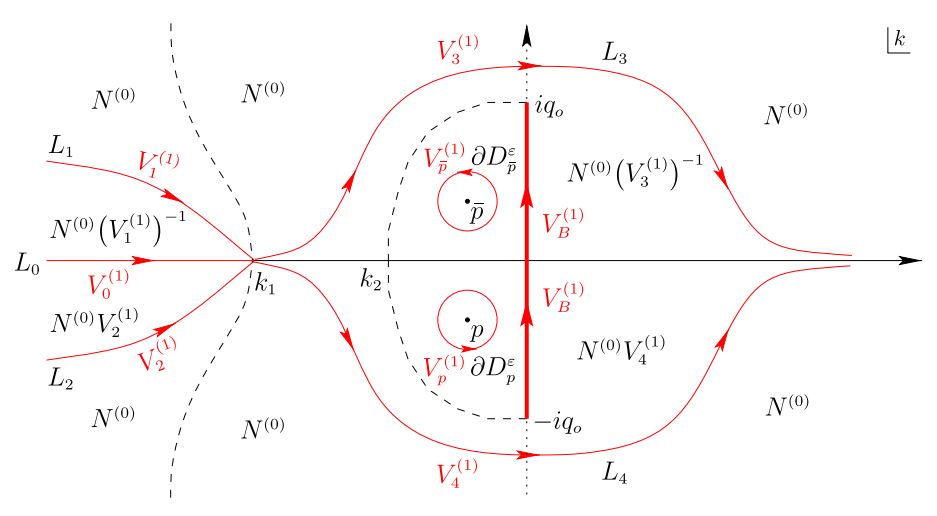


Fig. 34. Plane wave in the transmission/wake regime $(p \in D_3)$ for $v_s < \xi < v_o$: the fourth and final stage of the first deformation. The jump contours L_3 and L_4 have been lifted away from the branch points $\pm iq_o$ similarly to [BM2]

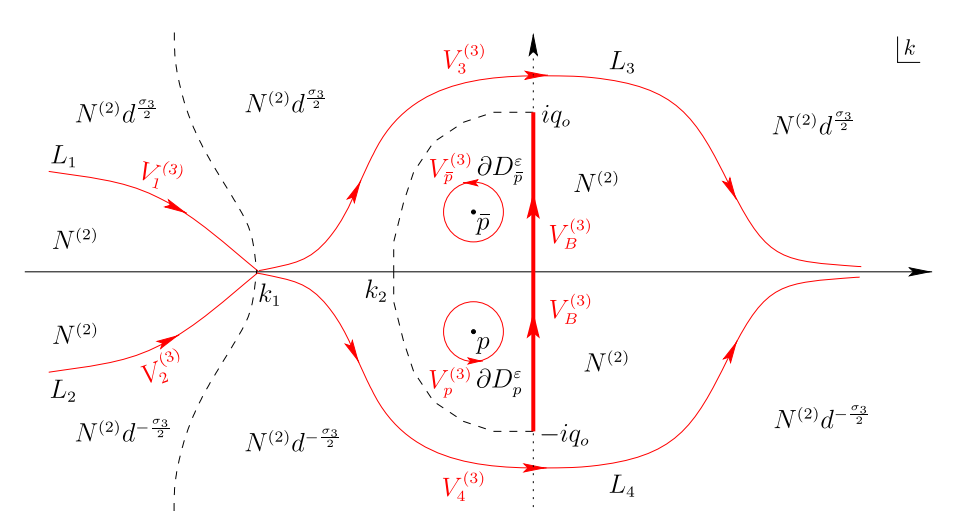


Fig. 35. Plane wave in the transmission/wake regime $(p \in D_3)$ for $v_s < \xi < v_o$: the third deformation

The proof of Theorem 2.4 for the leading-order asymptotics in the transmission/wake regime $p \in D_3$ is complete.

7. Conclusions

In summary, we have characterized the interactions between solitons and localized disturbances in focusing media governed by the NLS equation. We reiterate that the main points of novelty of the results are on one hand the existence of a trapping regime, in which the velocity of the soliton differs from that of the case without radiation, and on the other hand the existence of mixed transmission/wake and trap/wake regimes, in which

a single discrete eigenvalue gives rise to O(1) contributions at two different velocities in the long-time asymptotics.

The applicability of the deformations used in the present work requires that one can extend the reflection coefficient into the complex plane. As in [BM2], this can be done as long as the potential decays to background sufficiently rapidly [according to (1.3)] so as to ensure the existence of a Bargmann strip of analyticity.

Regarding the wake formulae, we note that the expression for the solution at the wake coincides formally with that of a soliton on top of an elliptic background. On the other hand, crossing the wake does not result in an additional phase shift for the solution, while crossing a soliton does (cf. Remark 2.3). We also emphasize that the asymptotic expressions for the solution are not uniform with respect to ξ , as one can see by taking the limit of the various expressions as $\xi \to v_s$, $\xi \to \widetilde{v}_s$ and $\xi \to v_w$.

We should mention that there exists previous literature on the interaction of solitons and the radiation on a nonzero background for integrable systems by the Riemann–Hilbert approach. See, for example, [KT] for the case of the Toda lattice and [AELT] for the case of the KdV equation. To the best of our knowledge, however, none of the previous cases studied in the literature give rise to the phenomena presented here, in which a localized disturbance results in a change of the soliton velocity and/or the production of a wake.

We believe that the asymptotic formulae giving rise to a soliton on top of an elliptic wave should be a limiting reduction of 3-phase solutions of the focusing NLS equation. In this regard, we should mention that, in [BBEIM], the authors consider elliptic solutions of the focusing NLS equation as well as solutions corresponding to a nonlinear superposition of a soliton and hyperelliptic solutions. (We also note that reductions of 2-phase solutions of the focusing NLS equations, which give rise to solitons on a constant background, were studied in [BG].) The authors of [BBEIM] show that, in the genus-1 reduction, their solution reduces to the cnoidal wave solution of focusing NLS, namely (4.5.1) in [BBEIM]. Importantly, however, the dn solution is not the most general periodic solution of the focusing NLS equation (e.g., see [K1,K2,DS]). More precisely, the dn solution is just one of the special cases corresponding to a trivial phase. It is also the case that the modulate elliptic waves arising in the long-time asymptotics are not simply dn solutions. Therefore, it is doubtful that the formulae for the soliton on top of an elliptic wave in our work reduce to those in [BBEIM].

The asymptotic expressions in our work remain valid in the limit $\xi \to 0$. As shown in [BLM1], in this limit $m \to 1$ and the solution reduces to the well-known sech-shaped soliton solution of the focusing NLS equation. However, some details of the derivation are different in this case and hence we omit the details for brevity. It is also the case that the asymptotic formulae remain valid in the limit $p_{\rm re} \to 0$, i.e. when the discrete eigenvalue lies on the imaginary axis. In this case, the velocity v_s is zero (cf. (2.10)). Thus, one does not see the soliton in the plane wave region. Moreover, when $\xi = 0$, the points α , $\bar{\alpha}$ and k_o in the definition (2.5) of h collapse to iq_o , $-iq_o$ and 0, respectively, and hence $h(0, k) = -2(k^2 + q_o^2)$. Thus, for $p_{\rm re} = 0$ we have ${\rm Im}(h)(0, p) = 0$, i.e. for $p_{\rm re} = 0$ the imaginary parts of both θ and h are zero at $\xi = 0$. Therefore, in this case the velocity \tilde{v}_s of the trapped soliton coincides with the unperturbed velocity v_s .

Another interesting special case is that of a pole p lying on the branch cut $i[-q_o, q_o]$, which gives rise to an Akhmediev breather. There are four different considerations: (i) Akhmediev breathers are periodic in x, and are therefore outside the class of initial conditions for which the inverse scattering transform formalism of [BK,BM2] applies (namely, constant nonzero boundary conditions); (ii) Neglecting the direct problem in

the inverse scattering transform, one could still consider the Riemann–Hilbert problem with a pole in the branch cut and ask what happens then. Nonetheless, even the simple formulation of a Riemann–Hilbert problem with a pole in the branch cut requires some care; (iii) Akhmediev breathers are homoclinic in t (i.e. they decay to the background as $t \to \pm \infty$) and hence they do not appear in the long-time asymptotics. However, one can still see the result of their presence in the phase difference of the background before/after the breather; (iv) Indeed, one can look at the case of a pole p on the branch cut as a limit of the case of $p \in D_3$. Therefore, the case of an Akhmediev breather can be viewed as a limit of the trap/wake scenario. Then, the analysis shows that one will see a wake located at $\xi = 0$ (for the same reasons as those outlined in the previous paragraphs).

As usual, the inverse scattering transform is formulated under the assumption of existence and uniqueness of solutions. The well-posedness of IVP (1.1) for short times with initial conditions in suitable Sobolev spaces was recently proved in [Mu]. The question of global well-posedness for initial conditions in the space (1.3) is still open. In general, the issue of existence and uniqueness of solutions of the Riemann–Hilbert problems associated with the inverse scattering transform for integrable nonlinear partial differential equations is a nontrivial one [BDT,Z,TO]. Therefore, since this issue is peripheral to the main thrust of this work, we do not consider it here. However, we note that the asymptotic results provide an explicit solution of the Riemann–Hilbert problem (and hence of the IVP) modulo the solution of the error Riemann–Hilbert problem, which is a small-norm problem and, therefore, is expected to have a unique solution. On the other hand, whether the corresponding solution of the NLS equation belongs to the same function space (1.3) remains an interesting open question. We note that proving well-posedness of an IVP in a given function space through the inverse scattering transform is in general a nontrivial problem.

Acknowledgements. We would like to thank M. Ablowitz, G. El and P. Miller for many insightful discussions. This work was partially supported by the National Science Foundation under Grant No. DMS-1614623. Finally, we are indebted to the anonymous referees whose constructive criticism led to the improvement of our paper.

Publisher's Note Springer Nature remains neutral with regard to jurisdictional claims in published maps and institutional affiliations.

A. Appendix: Soliton Solutions

The pure one-soliton solution of the focusing NLS IVP (1.5) can be derived by solving Riemann–Hilbert problem (3.7) together with the residue conditions (3.12) in the case of a zero reflection coefficient, i.e. by solving the problem

$$M^+(x,t,k) = M^-(x,t,k)V_{1,0}(k),$$
 $k \in \mathbb{R},$ (A.1a)

$$M^+(x,t,k) = M^-(x,t,k)V_{2,0}(k),$$
 $k \in B^+,$ (A.1b)

$$M^+(x,t,k) = M^-(x,t,k)V_{3,0}(k),$$
 $k \in B^-,$ (A.1c)

$$M(x, t, k) = I + O\left(\frac{1}{k}\right),$$
 $k \to \infty,$ (A.1d)

$$\operatorname{Res}_{k=p} M(x,t,k) = \left(0, c_p \, e^{2i\vartheta(x,t,p)} M_1(x,t,p)\right), \qquad x,t \in \mathbb{R},$$
 (A.1e)

$$\operatorname{Res}_{k=\bar{p}} M(x,t,k) = \left(c_{\bar{p}} e^{-2i\vartheta(x,t,\bar{p})} M_2(x,t,\bar{p}), 0 \right), \qquad x,t \in \mathbb{R},$$
 (A.1f)

where the relevant jump matrices are given by

$$V_{1,0}(k) = \begin{pmatrix} \frac{1}{d(k)} & 0\\ 0 & d(k) \end{pmatrix}, \ V_{2,0}(k) = \begin{pmatrix} 0 & \frac{2\lambda(k)}{i\bar{q}_-}\\ \frac{\bar{q}_-}{2i\lambda(k)} & 0 \end{pmatrix}, \ V_{3,0}(k) = \begin{pmatrix} 0 & \frac{q_-}{2i\lambda(k)}\\ \frac{2\lambda(k)}{iq_-} & 0 \end{pmatrix}$$
(A.2)

with the functions λ and d defined by (2.2) and (3.4), and where the phase function ϑ is defined as

$$\vartheta(x,t,k) := \lambda(k) (x - 2kt) \tag{A.3}$$

with M_1 and M_2 denoting the first and second column of M respectively. The jump $V_{1,0}$ of problem (A.1) along \mathbb{R} can be eliminated via the transformation

$$M^{(1)} = \begin{cases} M \begin{pmatrix} d^{\frac{1}{2}} & 0\\ 0 & d^{-\frac{1}{2}} \end{pmatrix} k \in \mathbb{C}^+ \backslash B^+, \\ M \begin{pmatrix} d^{-\frac{1}{2}} & 0\\ 0 & d^{\frac{1}{2}} \end{pmatrix} k \in \mathbb{C}^- \backslash B^-, \end{cases}$$
(A.4)

which implies the following Riemann–Hilbert problem for $M^{(1)}$:

$$M^{(1)+} = M^{(1)-}V_B, k \in B, (A.5a)$$

$$M^{(1)} = I + O\left(\frac{1}{k}\right), \qquad k \to \infty, \qquad (A.5b)$$

$$\operatorname{Res}_{k=p} M^{(1)}(x, t, k) = \left(0, \varrho_p(x, t) M_1^{(1)}(x, t, p)\right), \qquad x, t \in \mathbb{R},$$
 (A.5c)

$$\operatorname{Res}_{k=\bar{p}} M^{(1)}(x,t,k) = \left(-\overline{\varrho_p(x,t)} M_2^{(1)}(x,t,\bar{p}), 0 \right), \qquad x,t \in \mathbb{R},$$
 (A.5d)

where the jump matrix V_B is defined in (4.2) and, recalling the definitions (3.11) and the symmetry (4.33), we have introduced the quantity

$$\varrho_p(x,t) := \frac{C_p}{a'(p)} e^{2i\vartheta(x,t,p)}.$$
 (A.6)

Problem (A.5) can be solved by using the factorization

$$M^{(1)} = M^{(2)}W, (A.7)$$

where W is the solution of the continuous spectrum component of problem (A.5), i.e.

$$W^+ = W^- V_B, \qquad k \in B, \tag{A.8a}$$

$$W = I + O\left(\frac{1}{k}\right), \qquad k \to \infty, \tag{A.8b}$$

and, similarly to problem (4.36), is given by the explicit formula

$$W = \frac{1}{2} \begin{pmatrix} \Lambda(k) + \Lambda^{-1}(k) & -\frac{q_o}{\bar{q}_-} \left[\Lambda(k) - \Lambda^{-1}(k) \right] \\ -\frac{q_o}{q_-} \left[\Lambda(k) - \Lambda^{-1}(k) \right] & \Lambda(k) + \Lambda^{-1}(k) \end{pmatrix}$$
(A.9)

with $\Lambda(k)$ defined by (4.20).

In turn, $M^{(2)}$ is the solution of the discrete spectrum component of problem (A.5), i.e. $M^{(2)}$ is analytic for all $k \in \mathbb{C}$ apart from the poles p and \bar{p} , where it satisfies the residue conditions

$$\operatorname{Res}_{k=p} M_{1}^{(2)} = -W_{21}(p)c_{p} d(p)M_{1}^{(1)}(p), \qquad \operatorname{Res}_{k=p} M_{2}^{(2)} = W_{11}(p)c_{p} d(p)M_{1}^{(1)}(p),$$

$$(A.10a)$$

$$\operatorname{Res}_{k=\bar{p}} M_{1}^{(2)} = W_{22}(\bar{p})c_{\bar{p}} d(\bar{p})M_{2}^{(1)}(\bar{p}), \qquad \operatorname{Res}_{k=\bar{p}} M_{2}^{(2)} = -W_{12}(\bar{p})c_{\bar{p}} d(\bar{p})M_{2}^{(1)}(\bar{p}).$$

$$(A.10b)$$

Furthermore, $M^{(2)}$ satisfies the asymptotic condition

$$M^{(2)} = I + O\left(\frac{1}{k}\right), \quad k \to \infty. \tag{A.11}$$

Therefore, similarly to Sect. 4.2, we infer that $M^{(2)}$ is of the form

$$M^{(2)} = I + \frac{\text{Res } M^{(2)}}{k - p} + \frac{\text{Res } M^{(2)}}{k - \bar{p}}.$$
 (A.12)

Expressions (A.7), (A.9), (A.10) and (A.12) yield

$$M_1^{\text{dom}}(p) = \frac{-\mathcal{B}\overline{\varrho_p}W_2(\bar{p}) + \left(1 + \overline{\mathcal{A}\varrho_p}\right)W_1(p)}{\left(1 + \overline{\mathcal{A}\varrho_p}\right)\left(1 + \mathcal{A}\varrho_p\right) - \mathcal{B}^2|\varrho_p|^2},\tag{A.13a}$$

$$M_2^{\text{dom}}(\bar{p}) = \frac{\left(1 + \mathcal{A}\varrho_p\right)W_2(\bar{p}) - \mathcal{B}\varrho_pW_1(p)}{\left(1 + \overline{\mathcal{A}\varrho_p}\right)\left(1 + \mathcal{A}\varrho_p\right) - \mathcal{B}^2|\varrho_p|^2}$$
(A.13b)

with the constants A, B given by (4.47). Hence, in view of (A.12) and (A.10), the function $M^{(2)}$ has been determined.

Then, reverting the transformations (A.7) and (A.4) we obtain the solution M of problem (A.1) which, combined with the reconstruction formula (3.13), yields the pure one-soliton solution of IVP (1.5) for the focusing NLS equation in the form

$$\begin{split} q(x,t) &= q_{-} - \frac{i}{2} \left\{ \left[1 + \overline{\mathcal{A}\varrho_{p}(x,t)} \right] \left[1 + \mathcal{A}\varrho_{p}(x,t) \right] - \mathcal{B}^{2} \left| \varrho_{p}(x,t) \right|^{2} \right\}^{-1} \\ &\cdot \left\{ \left[1 + \overline{\mathcal{A}\varrho_{p}(x,t)} \right] \varrho_{p}(x,t) \left[\Lambda(p) + \Lambda^{-1}(p) \right]^{2} \right. \\ &\left. + \left[1 + \mathcal{A}\varrho_{p}(x,t) \right] \overline{\varrho_{p}}(x,t) \frac{q_{-}}{\bar{q}_{-}} \left[\overline{\Lambda(p) - \Lambda^{-1}(p)} \right]^{2} \right. \\ &\left. - 2\mathcal{B} \left| \varrho_{p}(x,t) \right|^{2} \frac{q_{o}}{\bar{q}_{-}} \left[\Lambda(p) + \Lambda^{-1}(p) \right] \left[\overline{\Lambda(p) - \Lambda^{-1}(p)} \right] \right\}. \end{split}$$
 (A.14)

Actually, letting

$$\chi(x,t) := -2\operatorname{Im} \left[\vartheta(x,t,p)\right] + \ln \left|\frac{C_p}{a'(p)}\right|, \quad \psi(x,t) := 2\operatorname{Re} \left[\vartheta(x,t,p)\right] + \operatorname{arg}\left(\frac{C_p}{a'(p)}\right) \tag{A.15}$$

allows us to express the quantity ϱ_p defined by (A.6) as

$$\varrho_p(x,t) = e^{\chi(x,t) + i\psi(x,t)}.$$
(A.16)

In turn, formula (A.14) takes the more compact form

$$q(x,t) = q_{-} + \frac{e^{\chi(x,t)} \left(\bar{\mathcal{A}} \Lambda_{1}^{2} \bar{q}_{-} + \mathcal{A} \Lambda_{2}^{2} q_{-} - 2\mathcal{B} \Lambda_{1} \Lambda_{2} q_{o} \right) + e^{i\psi(x,t)} \Lambda_{1}^{2} \bar{q}_{-} + e^{-i\psi(x,t)} \Lambda_{2}^{2} q_{-}}{4i \bar{q}_{-} \left[\sqrt{|\mathcal{A}|^{2} - \mathcal{B}^{2}} \cosh\left(\chi(x,t) + \ln \sqrt{|\mathcal{A}|^{2} - \mathcal{B}^{2}}\right) + \operatorname{Re}\left(\mathcal{A} e^{i\psi(x,t)}\right) \right]}$$
(A.17)

with the constants Λ_1 and Λ_2 given by (4.55). It now becomes evident that the pure one-soliton is localized along the line $\chi(x,t) + \ln \sqrt{|\mathcal{A}|^2 - \mathcal{B}^2} = 0$ which in view of (A.15) is equivalent to

$$\operatorname{Im}\left[\vartheta(x,t,p)\right] = \frac{1}{2}\left(\ln\left|\frac{C_p}{a'(p)}\right| + \ln\sqrt{|\mathcal{A}|^2 - \mathcal{B}^2}\right). \tag{A.18}$$

Expressing the pure one-soliton in the non-standard form (A.17) allows us to compare it against the leading-order asymptotics (2.15), since both expressions involve two portions: the background (first term) and a traveling wave part (second term). To perform this comparison, we calculate the long-time asymptotics of (A.17). The pure one-soliton propagates along the line specified by Eq. (A.18). Noting that $\vartheta(x,t,k) = \theta(\xi,k)t$ [cf. definitions (A.3) and (2.3)], we infer that a necessary condition for Eq. (A.18) to hold in the limit $t \to \infty$ is that $\text{Im}[\theta(\xi,p)] = 0$. This last equation, however, amounts to $\xi = v_s$ [recall (2.10)–(2.11)]. Thus, we consider three cases: $\xi < v_s$ (left of soliton); $\xi > v_s$ (right of soliton); $\xi = v_s$.

If $\xi < v_s$ then $\text{Im}[\theta(\xi, p)] > 0$ (recall Fig. 6). Hence, as $t \to \infty$ we have $\chi(x, t) \to -\infty$ and, in turn, $e^{\chi(x,t)} \to 0$ and $\cosh(\chi(x,t) + \ln\sqrt{|\mathcal{A}|^2 - \mathcal{B}^2}) \to \infty$. Therefore, for $\xi < v_s$ we obtain

$$q(x,t) = q_- + o(1), \quad t \to \infty,$$
 (A.19)

in agreement with the asymptotics (2.13) apart from the real constant phase $g_{\infty}(\xi)$, which originates from the radiation of Riemann–Hilbert problem (3.7), (3.12) and which vanishes once the reflection coefficient in this problem is set to zero.

If $\xi > v_s$ then $\operatorname{Im}[\theta(\xi, p)] < 0$. Hence, as $t \to \infty$ we have $\chi(x, t) \to \infty$ and, therefore, $e^{\chi(x,t)} \to \infty$ and $\cosh(\chi(x,t) + \ln\sqrt{|\mathcal{A}|^2 - \mathcal{B}^2}) \to \infty$. Thus, expressing cosh in exponential form we obtain

$$q(x,t) = q_{-} + \frac{\bar{\mathcal{A}}\Lambda_{1}^{2}\bar{q}_{-} + \mathcal{A}\Lambda_{2}^{2}q_{-} - 2\mathcal{B}\Lambda_{1}\Lambda_{2}q_{o}}{2i\bar{q}_{-}\left(|\mathcal{A}|^{2} - \mathcal{B}^{2}\right)} + o(1), \quad t \to \infty.$$
 (A.20)

Through algebraic manipulations, it can be shown that the leading-order term of (A.20) is equal to q_+ , which is consistent with the fact that propagation along speeds $\xi > v_s$ always remains to the right of the soliton at $\xi = v_s$.

Finally, if $\xi = v_s$ then $\text{Im}[\theta(\xi, p)] = 0$ and hence $\text{Im}[\vartheta(x, t, p)] = 0$, which implies

$$\chi(v_s t, t) = \ln |\mathcal{R}_p|, \quad \psi(v_s t, t) = 2\theta(v_s, p)t + \arg (\mathcal{R}_p), \quad \mathcal{R}_p := \frac{C_p}{a'(p)}.$$

Then, (A.17) becomes

 $q(v_s t, t)$

$$=q_{-}+\frac{\left|\mathcal{R}_{p}\right|\left(\bar{\mathcal{A}}\Lambda_{1}^{2}\bar{q}_{-}+\mathcal{A}\Lambda_{2}^{2}q_{-}-2\mathcal{B}\Lambda_{1}\Lambda_{2}q_{o}\right)+e^{i\left[2\theta\left(v_{s},p\right)t+\arg\left(\mathcal{R}_{p}\right)\right]}\Lambda_{1}^{2}\bar{q}_{-}+e^{-i\left[2\theta\left(v_{s},p\right)t+\arg\left(\mathcal{R}_{p}\right)\right]}\Lambda_{2}^{2}q_{-}}{4i\bar{q}_{-}\left\{\sqrt{|\mathcal{A}|^{2}-\mathcal{B}^{2}}\cosh\left[\ln\left(|\mathcal{R}_{p}|\sqrt{|\mathcal{A}|^{2}-\mathcal{B}^{2}}\right)\right]+\operatorname{Re}\left(\mathcal{A}e^{i\left[2\theta\left(v_{s},p\right)t+\arg\left(\mathcal{R}_{p}\right)\right]}\right)\right\}}$$

$$(A.21)$$

The exact one-soliton solution (A.21) is the same with the leading-order asymptotics (2.15) except for three points: (i) the background, which is q_- in (A.21) and $q_-e^{2ig_\infty(v_s)}$ in (2.15); (ii) an overall phase of $e^{2ig_\infty(v_s)}$, which is present in (2.15) but not in (A.21); (iii) the quantity \mathcal{R}_p in (A.21), which is replaced by R_p in (2.15), where $R_p = \mathcal{R}_p \delta^2(v_s, p) e^{-2ig(v_s, p)}$. However, this variation is exclusively due to the presence of radiation in IVP (1.5). Indeed, setting the reflection coefficient equal to zero in the definitions (4.5), (4.13) and (4.16) of δ , g and g_∞ yields $\delta(v_s, p) = g(v_s, p) = g_\infty(v_s) = 0$, i.e. in the absence of radiation (2.15) would be identical to (A.21).

References

- [AS] Ablowitz, M., Segur, H.: Solitons and the Inverse Scattering Transform. SIAM, New Delhi (1981)
- [AK] Akhmediev, N., Korneev, V.: Modulational instability and periodic solutions of the nonlinear Schrödinger equation. Theor. Math. Phys. 69, 1089–1093 (1987)
- [AELT] Andreiev, K., Egorova, I., Lange, T., Teschl, G.: Rarefaction waves of the Korteweg–de Vries equation via nonlinear steepest descent. J. Differ. Equ. 261, 5371–5410 (2016)
- [BDT] Beals, R., Deift, P., Tomei, C.: Direct and Inverse Scattering on the Line. American Mathematical Society, Providence (1988)
- [BBEIM] Belokolos, E., Bobenko, A., Enol'ski, V., Its, A., Matveev, V.: Algebro-Geometric Approach to Nonlinear Integrable Equations. Springer, Berlin (1994)
- [BF] Benjamin, T., Feir, J.: The disintegration of wave trains on deep water. J. Fluid Mech. 27, 417–430 (1967)
- [BG] Bertola, M., Giavedoni, P.: A degeneration of two-phase solutions of the focusing nonlinear Schrödinger equation via Riemann–Hilbert problems. J. Math. Phys. 56, 061507 (2015)
- [BMi] Bilman, D., Miller, P.: A robust inverse scattering transform for the focusing nonlinear Schrödinger equation. arXiv:1710.06568, to appear in Commun. Pure Appl. Math
- [BF] Biondini, G., Fagerstrom, E.: The integrable nature of modulational instability. SIAM J. Appl. Math. 75, 136–163 (2015)
- [BK] Biondini, G., Kovačič, G.: Inverse scattering transform for the focusing nonlinear Schrödinger equation with nonzero boundary conditions. J. Math. Phys. **55**, 031506 (2014)
- [BLM1] Biondini, G., Li, S., Mantzavinos, D.: Oscillation structure of localized perturbations in modulationally unstable media. Phys. Rev. E **94**, 060201(R) (2016)
- [BLM2] Biondini, G., Li, S., Mantzavinos, D.: Soliton trapping, transmission and wake in modulationally unstable media. Phys. Rev. E 98, 042211 (2018)
- [BLMT] Biondini, G., Li, S., Mantzavinos, D., Trillo, S.: Universal behavior of modulationally unstable media. SIAM Rev. 60, 888–908 (2018)
- [BM1] Biondini, G., Mantzavinos, D.: Universal nature of the nonlinear stage of modulational instability. Phys. Rev. Lett. 116, 043902 (2016)
- [BM2] Biondini, G., Mantzavinos, D.: Long-time asymptotics for the focusing nonlinear Schrödinger equation with nonzero boundary conditions at infinity and asymptotic stage of modulational instability. Commun. Pure Appl. Math. 70, 2300–2365 (2017)
- [BKS] Boutet de Monvel, A., Kotlyarov, V., Shepelsky, D.: Focusing NLS equation: long-time dynamics of step-like initial data. Int. Math. Res. Not. 2011, 1613–1653 (2011)
- [BV] Buckingham, R., Venakides, S.: Long-time asymptotics of the nonlinear Schrödinger equation shock problem. Commun. Pure Appl. Math. 60, 1349–1414 (2007)
- [DS] Deconinck, B., Segal, B.: The stability spectrum for elliptic solutions to the focusing NLS equation. Phys. D 346, 1–19 (2017)
- [DKKZ] Deift, P., Kamvissis, S., Kriecherbauer, T., Zhou, X.: The Toda rarefaction problem. Commun. Pure Appl. Math. 49, 35–83 (1996)

- [DZ1] Deift, P., Zhou, X.: A steepest descent method for oscillatory Riemann–Hilbert problems. Asymptotics for the mKdV equation. Ann. Math. 137, 295–370 (1993)
- [DZ2] Deift, P., Zhou, X.: Long-time behavior of the non-focusing nonlinear Schrödinger equation—a case study. New Series, Lectures in Mathematical Sciences, 5, University of Tokyo (1995)
- [DVZ1] Deift, P., Venakides, S., Zhou, X.: The collisionless shock region for the long-time behavior of solutions of the KdV equation. Commun. Pure Appl. Math. 47, 199–206 (1994)
- [DVZ2] Deift, P., Venakides, S., Zhou, X.: An extension of the steepest descent method for Riemann–Hilbert problems: the small dispersion limit of the Korteweg–de Vries (KdV) equation. Proc. Natl. Acad. Sci. USA **95**, 450–454 (1998)
- [DPVV] Demontis, F., Prinari, B., van der Mee, C., Vitale, F.: The inverse scattering transform for the focusing nonlinear Schrödinger equation with asymmetric boundary conditions. J. Math. Phys. **55**, 101505 (2014)
- [EGKK] El, G., Gurevich, A., Khodorovskii, V., Krylov, A.: Modulational instability and formation of a nonlinear oscillatory structure in a focusing medium. Phys. Lett. A 177, 357–361 (1993)
- [FL] Forest, M., Lee, J.-E.: Geometry and modulation theory for periodic nonlinear Schrödinger equation, in Oscillation theory, computation and methods of compensated compactness, IMA Vol. Math. Appl. 2, C. Dafermos, J. Ericksen, D. Kinderlehrer, and M. Slemrod, Eds., Springer, New York (1986)
- [GZ] Gelash, A., Zakharov, V.: Superregular solitonic solutions: a novel scenario for the nonlinear stage of modulation instability. Nonlinearity 27, R1–R39 (2014)
- [JM] Jenkins, R., McLaughlin, K.D.T.-R.: Semiclassical limit of focusing NLS for a family of square barrier initial data. Commun. Pure Appl. Math. 67, 246–320 (2013)
- [K1] Kamchatnov, A.: Nonlinear Periodic Waves and Their Modulations. World Scientific, Singapore (2000)
- [K2] Kamchatnov, A.: On improving the effectiveness of periodic solutions of the NLS and DNLS equations. J. Phys. A 23, 2945–2960 (1990)
- [KMM] Kamvissis, S., McLaughlin, K.D.T.-R., Miller, P.: Semiclassical Soliton Ensembles for the Focusing Nonlinear SchröDinger Equation. Princeton University Press, Princeton (2003)
- [KSER] Kraych, A., Suret, P., El, G., Randoux, S.: Nonlinear evolution of the locally induced modulational instability in fiber optics. Phys. Rev. Lett. 122, 054101 (2019)
- [KT] Kruger, H., Teschl, G.: Stability of the periodic Toda lattice in the soliton region. Int. Math. Res. Not. 2009, 3996–4031 (2009)
- [Ma] Ma, Y.-C.: The perturbed plane-wave solutions of the cubic Schrödinger equation. Stud. Appl. Math. 60, 43–58 (1979)
- [Mi] Miller, P.: Riemann-Hilbert problems with lots of discrete spectrum. Contemp. Math. 458, 163–181 (2008)
- [Mu] Muñoz, C.: Instability in nonlinear Schrödinger breathers. Proyecc. J. Math. 36, 653–683 (2017)
- [PV] Prinari, B., Vitale, F.: Inverse scattering transform for the focusing nonlinear Schrödinger equation with one-sided nonzero boundary conditions. Contemp. Math. **652**, 157–194 (2015)
- [SA1] Segur, H., Ablowitz, M.: Asymptotic solutions and conservation laws for the nonlinear Schrödinger equation. I. J. Math. Phys. 17, 710–713 (1976)
- [SA2] Segur, H., Ablowitz, M.: Asymptotic solutions and conservation laws for the nonlinear Schrödinger equation. II. J. Math. Phys. 17, 714–716 (1976)
- [TW] Trillo, S., Wabnitz, S.: Dynamics of the nonlinear modulational instability in optical fibers. Opt. Lett. 16, 986–988 (1991)
- [TO] Trogdon, T., Olver, S.: Riemann–Hilbert problems, their numerical solution, and the computation of nonlinear special functions. SIAM, University City (2016)
- [W] Whitham, G.: Linear and Nonlinear Waves. Wiley, Hoboken (1974)
- [ZM] Zakharov, V., Manakov, S.: Asymptotic behavior of nonlinear waves systems integrated by the inverse scattering method. Sov. Phys. JETP 44, 106–112 (1976)
- [ZG] Zakharov, V., Gelash, A.: Nonlinear stage of modulation instability. Phys. Rev. Lett. 111, 054101 (2013)
- [ZO] Zakharov, V., Ostrovsky, L.: Modulational instability: the beginning. Phys. D 238, 540–548 (2009)
- [ZS] Zakharov, V., Shabat, A.: Exact theory of two-dimensional self-focusing and one-dimensional self-modulation of waves in nonlinear media. Sov. Phys. JETP 34, 63–69 (1972)
- [Z] Zhou, X.: The Riemann–Hilbert problem and inverse scattering. SIAM J. Math. Anal. 20, 966–986 (1989)